Alterations of cellular electrophysiology and Ca^{2+}-handling in patients with different forms of atrial fibrillation

Inaugural-Dissertation

zur

Erlangung des Doktorgrades

Dr. rer. nat.

der Fakultät für Biologie

an der

Universität Duisburg-Essen

vorgelegt von

Azinwi Phina Muna geb. Khan

aus Mankon-Bamenda, Kamerun

März 2017

Die der vorliegenden Arbeit zugrunde liegenden Experimente wurden am Institut für Pharmakologie des Universitätsklinikums Essen und der Universität Duisburg-Essen durchgeführt.

1. Gutachter: Univ.-Prof. Dr. med. Dobromir Dobrev
2. Gutachter: Univ.-Prof. Dr. rer. nat. Gero Hilken
3. Gutachter: Univ.-Prof. Dr. med. Ali El-Armouche

Vorsitzender des Prüfungsausschusses: -Prof. Dr. med. Joachim Fandrey

Tag der mündlichen Prüfung: 25.09.2017

Efforts triumph all difficulties (dedicated to my Mum and Dad)

Summary

Atrial Fibrillation (AF) is the most common clinical arrhythmia. When AF occurs after (cardiac) surgery it is referred to as postoperative AF (poAF). Though usually self-limiting, uncontrolled poAF can cause debilitating strokes and prolong hospital stay. A multifactorial pathophysiology involving triggered activity has been hypothesized, but the cellular and molecular mechanisms underlying poAF remain unknown and were the subject of the first part of this study. The second part of this study focused on inward-rectifier K^+ currents like I_{K1}, which stabilize the resting membrane potential. It has been suggested to contribute to the shorter action potentials that promote reentry in chronic AF (cAF). However, the exact magnitude of I_{K1} in cAF is unknown and was investigated. Membrane currents (whole-cell voltage clamp) and $[Ca^{2+}]_i$ (Fluo-3) epifluorescence were measured in right-atrial cardiomyocytes from patients with sinus-rhythm (Ctl, n=58), poAF (n=46) or cAF (n=6). Protein expression was quantified by immunoblot. Amplitude of L-type Ca^{2+} current was unchanged, whereas the L-type Ca^{2+} current-triggered $[Ca^{2+}]_i$ transient amplitude was reduced by ~35% in poAF vs Ctl, likely contributing to the ~44% reduction in fractional cell shortening. Sarcoplasmic reticulum (SR) Ca^{2+} content, calculated by integrating Na^+-Ca^{2+} exchange current during caffeine (10 mM)-induced SR Ca^{2+} release, was unchanged, consistent with the unaltered protein expression of the SR Ca^{2+} ATPase type-2a and its regulator phospholamban. When challenged with interleukin-1β as a postoperative trigger the frequency of potentially proarrhythmic spontaneous SR Ca^{2+} release events was increased, likely due to hyperphosphorylation of ryanodine receptor channels at Ser2014 (~34%), whereas protein expression of the ryanodine receptor channel regulators triadin, junctin, junctophilin-2 and calsequestrin was unaltered. In cAF, basal inward-rectifier K^+ current was increased, whereas the major effector of vagal nerve stimulation, the acetylcholine-activated K^+ current $I_{K,ACh}$, was reduced compared to Ctl patients. Application of the selective I_{K1}-inbititor PA-6 (200 nM) to basal inward-rectifier K^+ current unmasked a larger "pure" I_{K1} in cAF compared to Ctl patients. In summary, we discovered that poAF is associated with Ca^{2+}-handling abnormalities that predispose patients to cellular triggered activity underlying poAF. We could demonstrate using PA-6; a novel inhibitor of I_{K1}, that "pure" I_{K1} is larger in cAF. Our data improve our understanding of atrial cellular arrhythmogenic mechanisms in AF in general and in poAF in particular, potentially facilitating the development of improved therapeutic anti-AF strategies.

Zusammenfassung

Vorhofflimmern (VHF) ist die häufigste klinische Arrhythmie. Wenn es nach herzchirurgischen Eingriffen auftritt, wird es als postoperatives VHF (poVHF) bezeichnet. Wenngleich normalerweise selbstlimitierend, kann unkontrolliertes poVHF Schlaganfälle und einen verlängerten Krankenhausaufenthalt verursachen. PoVHF liegt vermutlich eine multifaktorielle Pathophysiologie zugrunde, wobei der „getriggerten" Aktivität eine zentrale Rolle zukommen könnte. Die genauen zellulären Mechanismen des poVHF sind unbekannt und waren Gegenstand des ersten Teils dieser Arbeit. Der zweite Teil der Arbeit befasste sich mit einwärtsgleichrichtenden K^+-Strömen wie dem I_{K1}, die das negative Ruhemembranpotential aufrechterhalten. Es wird vermutet, dass diese zur Verkürzung der Aktionspotentiale beitragen und die Entstehung kreisender Erregungen („Reentry") bei chronischem VHF (cVHF) begünstigen, wobei die genaue Größe des I_{K1} bei cVHF bisher unbekannt war. Membranströme („whole-cell voltage clamp") und $[Ca^{2+}]_i$ (Fluo-3) Epifluoreszenz wurden in rechtsatrialen Kardiomyozyten von Patienten mit Sinusrhythmus (Ktr, n=58), mit poVHF (n=46) oder mit cVHF (n=6) registriert. Die Proteinexpression wurde mittels Immunoblot quantifiziert. Die Amplitude des L-Typ Ca^{2+}-Stromes war unverändert, während die L-Typ Ca^{2+}-Strom ausgelöste $[Ca^{2+}]_i$-Transientamplitude beim poVHF um ~35% reduziert war. Entsprechend war die relative Zellverkürzung um ~44% vermindert. Der Ca^{2+}-Gehalt im sarkoplasmatischen Retikulum (SR), der durch Integration des Na^+-Ca^{2+}-Austauschstroms während der Koffein (10 mM)-ausgelösten Ca^{2+}-Freisetzung aus dem SR berechnet wurde, war unverändert. Dies stimmte mit der unveränderten Proteinexpression der SR Ca^{2+}-ATPase Typ-2a und dessen Regulator Phospholamban überein. Der Einsatz von Interleukin-1β als postoperativer Trigger steigerte die Frequenz spontaner proarrhythmischer Ca^{2+}-Freisetzungen aus dem SR, möglicherweise aufgrund der Zunahme der Ser2014-Hyperphosphorylierung der Ryanodin-Rezeptorkanäle (~34%). Die Proteinexpression der Ryanodin-Rezeptorkanal-Regulatoren Triadin, Junctin, Junctophilin-2 und Calsequestrin blieb dagegen unverändert. Beim cVHF war der basale einwärtsgleichrichtende K^+-Strom erhöht, während der Haupteffektor einer Stimulation von Nervus vagus, der Acetylcholin-aktivierte K^+-Strom $I_{K,ACh}$, reduziert war. Die Applikation des selektiven I_{K1}-Inhibitors PA-6 (200 nM) beim cVHF konnte einen größeren "reinen" I_{K1} aufdecken. Zusammenfassend konnten wir nachweisen, dass poVHF mit Störungen der Ca^{2+}-Homöostase assoziiert ist. Letzteres könnte das Auftreten von „getriggerter" Aktivität als Auslöser von poVHF begünstigen. Wir konnten außerdem zeigen, dass PA-6; ein neuartiger Inhibitor von $I_{K1,}$ einen erhöhten I_{K1} beim cVHF demaskierte. Unsere Daten verbessern unser Verständnis der zellulären Mechanismen von

VHF, insbesondere von poVHF, und könnten zur Entwicklung von neuen therapeutischen Strategien für VHF führen.

Table of Contents

Abbreviations

ACE	Angiotensin-converting enzyme
AF	Atrial fibrillation
AP	Action potential
APD	Action potential duration
AT_1	Angiotensin-II receptor type-1
AVN	Atrioventricular node
AVD	Aortic valve disease
BCA	Bicinchoninic acid
CAD	Coronary artery disease
cAF	Chronic atrial fibrillation
CaMKII	Ca^{2+}/calmodulin-dependent protein kinase-II
CCh	Carbachol
CS	Cell shortening
CICR	Calcium-induced calcium release
DADs	Delayed afterdepolarizations (DADs)
EADs	Early afterdepolarizations (EADs)
ECC	Excitation-contraction coupling
ECG	Electrocardiogram
ERP	Effective refractory period
E_K	Reversal potential of potassium
I_{K1}	Inward-rectifier K^+ current
$I_{K,ACh}$	ACh-activated K^+ current
I_{K2P}	Two-pore-domain K^+ current
I_{Ks}	Slow delayed-rectifier K^+ current
I_{Kr}	Rapid delayed-rectifier K^+ current
I_{Kur}	Ultra-rapid delayed-rectifier K^+ current
$I_{Ca,L}$	L-type calcium current
LVEF	Left ventricular ejection fraction
MVD	Mitral valve disease
NCX1	Type-1 Na^+/Ca^{2+}-exchanger
pAF	Paroxysmal atrial fibrillation
PMCA	Plasma membrane Ca^{2+}-ATPase
poAF	Post-operative atrial fibrillation

RyR2	Ryanodine receptor channel type-2
RT	Room temperature
RMP	Resting membrane potential
SAN	Sinoatrial node
SCaEs	Spontaneous diastolic SR Ca^{2+}-release events
SDS-PAGE	Sodium dodecyl sulfate polyacrylamide gel electrophoresis
SERCA	Sarcoplasmic reticulum Ca^{2+}-ATPase
TMC	Time-matched control
QSS	Quasi-Steady-State

List of figures

List of tables

1 Introduction

The heart is a pump consisting of four primary chambers: the right atrium, left atrium, right ventricle, and left ventricle. The atria are smaller and have thinner, less muscular walls than the ventricles. The atria are connected to the veins that carry blood to the heart and act as receiving chambers for blood. The ventricles are connected to the arteries that carry blood away from the heart and pump blood to the rest of the body. The function of the heart is tightly regulated via its electrical activity. The process by which electrical stimuli induce a mechanical response is called Excitation-Contraction Coupling (ECC). The heart coordinates its own rhythm by generating electrical impulses and conducting them throughout the heart to produce a synchronous activation and contraction. The cardiac electrical activity is also conducted through the body and can be measured at the body surface as the electrocardiogram (ECG). Disturbances in the electrical properties of the heart are associated with many types of cardiac arrhythmias, which have a significant impact on quality of life, morbidity and mortality of millions of people (Bers 2008).

The origin and propagation of electrical activity across the different chambers of the heart, as well as the consequent contractile response, originate at the cellular level in cardiomyocytes organized by ion channels, Ca^{2+}-handling proteins and the contractile machinery. These fundamental processes can be studied using the patch-clamp technique and other physiological techniques, which allow the investigation of electrical properties at the (sub)-cellular level.

This introductory chapter will describe the foundation of cardiac electrical activity, the history and development of the ECG, as well as the fundamental processes driving contraction at the cellular level. In addition, we will discuss their role in the normal functioning of the heart and in atrial fibrillation (AF), which is the most common sustained arrhythmia. Finally, the goals of this thesis will be presented.

1.1 Cardiac electrophysiology

The heart muscles (myocardium) consist of two main types of cells, cardiomyocytes and fibroblasts. Cardiomyocyte properties are different throughout the heart, having developed specialized properties to ensure precise control of cardiac function. The pacemaker cells located in the sinoatrial node (SAN) in the right atrium are one example of such specialized function. The cardiac cycle begins with electrical impulses initiated by the spontaneous activity of these pacemaker cells. This property of the pacemaker cells is known as automaticity (Antzelevitch & Burashnikov 2011). The electrical impulses, known as action

potentials (APs), propagate as a wave front across the different chambers of the heart through a defined route, which is shown in **Figure 1.** From the SAN, the excitation wave spreads-out first across the atria, causing the atria to contract and pump blood to the ventricles. It then conducts through the atrioventricular node (AVN) to the bundle of His. At the AVN, the impulse is briefly delayed to allow complete contraction of the atria and movement of blood from the atria to the ventricles. From the bundle of His the electrical activity then quickly travels through the Purkinje system, resulting in a coordinated activation of the ventricular myocardium, initiating contraction of the ventricles.

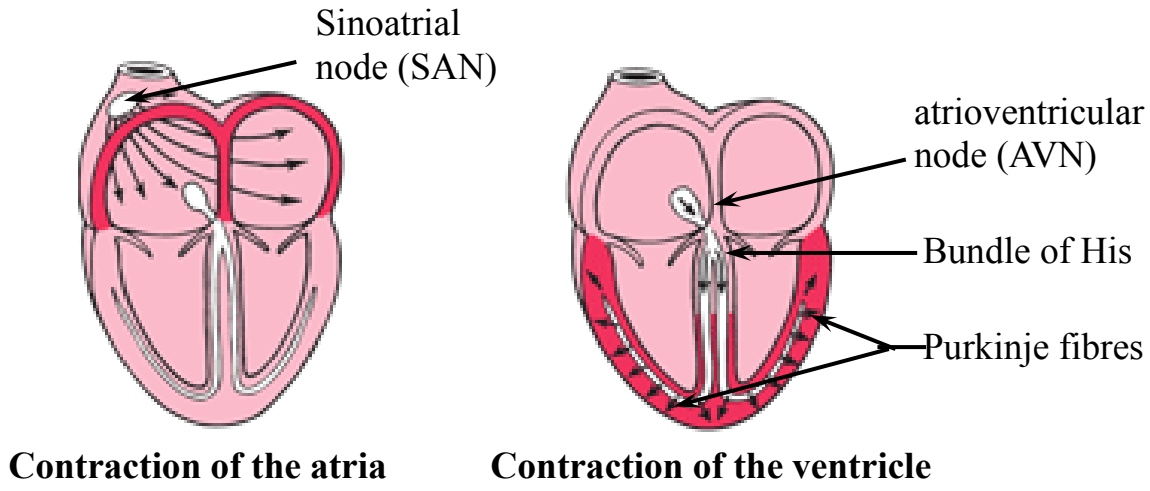

Figure 1: Route of excitation propagation in the heart.
Electrical impulses are generated in the sinoatrial node (SAN) and conducted across the atria to the atrioventricular node (AVN) and then through the bundle of His to the Purkinje fibers, resulting in synchronous activation of the ventricles. Adapted from Interpreting ECG. (n.d.). *The Biology Corner Web site*.

1.2 The electrocardiogram

Changes in the electrical activity during a heartbeat propagate to the body surface and can be recorded via electrodes placed on the surface of the skin as the electrocardiogram (ECG) (**Figure 2**). The pattern of the ECG comprises three major components: the P wave, QRS complex, and the T wave.

The ECG plays a major role in clinical practice in the detection and characterization of arrhythmias based on alterations in the shape, duration or frequency of the three ECG components (**Figure 2, right**). The presence of P waves before every QRS complex is a key characteristic to determine whether a patient has a normal heart rhythm (sinus rhythm). In the absence of clear P waves, emphasis is placed on the morphologies of the QRS complexes, particularly whether they are wide or narrow, regular or irregular. The absence of P waves and an irregular, narrow QRS complex are the ECG hallmarks of AF. The ECG provides a fast,

reliable, non-invasive diagnostic tool that remains the cornerstone of modern cardiology (Fye 1994).

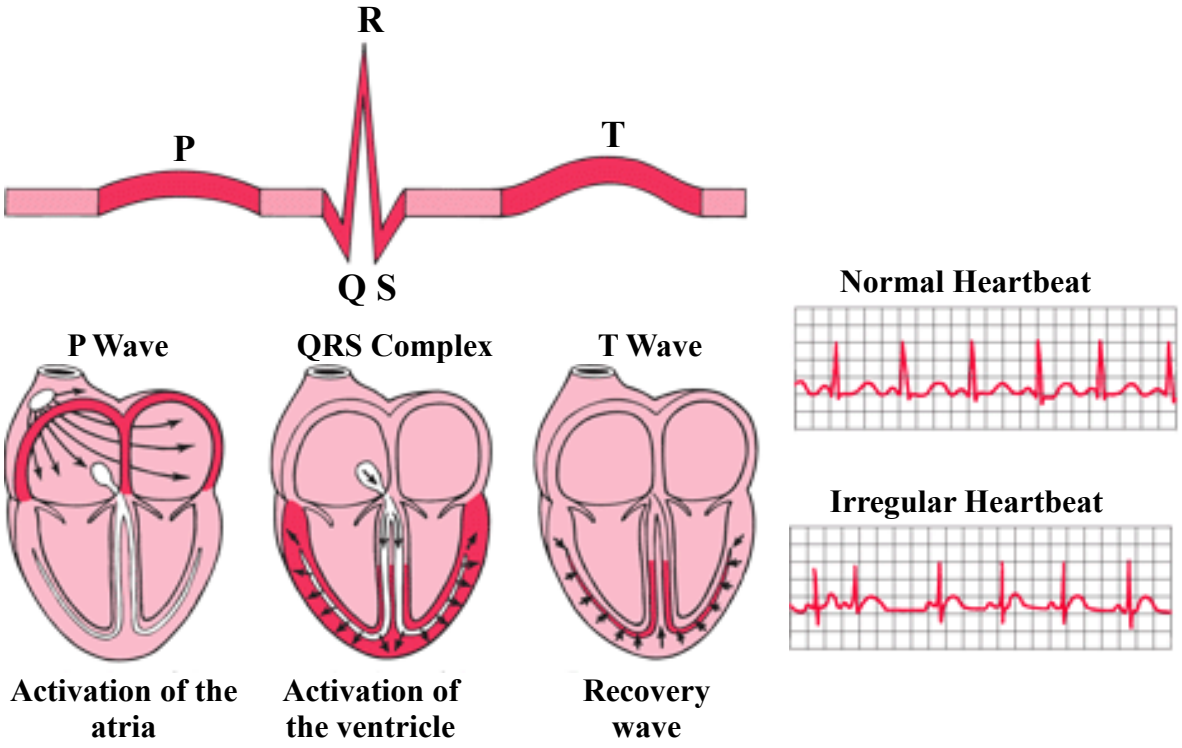

Figure 2: Schematic representation of the electrocardiogram.

The ECG of a specific lead reflects the electrical activity along a specific vector / in a specific direction. On the ECG, the first little hump is the P wave which reflects depolarization of the atria. The next three waves form the QRS complex and represent the depolarization of the ventricles. Finally, the T wave represents the electrical recovery (repolarization) of the ventricles. Adapted from Interpreting ECG. (n.d.). *The Biology Corner Web site*.

1.2.1 Ionic currents and the cardiac action potential

When excited, cardiomyocytes generate a typical electrical response consisting of rapid depolarization and slow repolarization, which is propagated to neighboring cells. This so-called AP is the result of a highly orchestrated sequence of different ionic currents that play an important role for coordinating the heartbeat. The shape and duration of the AP vary in the different chambers of the heart (e.g., in atrium versus ventricle). These regional AP differences result in large part from heterogeneities in the expression of ion channels, transporters, signaling pathway components and tissue structures (Molina et al. 2016; Goette et al. 2016). In this section, we will focus on the human atrial AP.

In a typical atrial cardiomyocyte, the AP is composed of five phases, beginning with phase 0 and ending with phase 4 (**Figure 3**). An atrial cardiomyocyte in a quiescent state has a resting transmembrane potential (RMP) of around -75 mV. This is maintained due to substantial K^+ conductance, mainly through the basal inward-rectifier K^+ current (I_{K1}) while the Na^+ and

Ca^{2+} channels are closed. When an AP is triggered in a neighboring cardiomyocyte, electrotonic interactions between cardiomyocytes through gap-junctions lead to a rise in RMP. This depolarization causes opening of fast Na^+ channels, allowing influx of Na^+ into the cell and generating an inward Na^+ current (I_{Na}) that rapidly depolarizes the cell (phase 0). Because these fast Na^+ channels are both voltage- and time-dependent, they quickly close, limiting the upstroke to a few milliseconds. When the depolarization is greater than -40 mV, the L-type Ca^{2+} channels open and initiate a small but steady depolarizing Ca^{2+} current ($I_{Ca,L}$), which is critical for the ECC process described below. When the membrane potential becomes slightly positive, transient-outward K^+ channels open, producing a repolarizing K^+ current (I_{to}) which returns the membrane potential to approximately 0 mV. This is termed the early repolarization phase (phase 1). During the subsequent plateau phase (phase 2), the L-type Ca^{2+} channels are still open, allowing a constant influx of Ca^{2+}. Simultaneously, there is also efflux of K^+ through the ultra-rapid, rapid and slow delayed-rectifier K^+ channels. The resulting currents (I_{Kur}, I_{Kr}, and I_{Ks}, respectively) electrically counter-balance the depolarizing currents, maintaining the membrane potential at a plateau just below 0 mV throughout this phase 2.

During the final repolarization (phase 3), L-type Ca^{2+} channels gradually inactivate and progressive activation of K^+ currents surpasses depolarizing $I_{Ca,L}$, returning the AP to levels where I_{K1} is activated, promoting repolarization to the resting RMP of approximately -75 mV (phase 4) and preparing the cell for a new cycle of depolarization (Roden et al. 2002; Grant 2009).

Homeostasis of transmembrane ionic concentration gradients is achieved by extrusion of Ca^{2+} to the extracellular space and Ca^{2+} reuptake in the intracellular stores of the sarcoplasmic reticulum (SR), the main intracellular Ca^{2+} store. As well as pumping Na^+ to extracellular space and K^+ to the interior of the cell. The transport mechanisms involved in this intricate process are the plasma membrane Ca^{2+}-ATPase (PMCA), sarcolemmal Na^+-Ca^{2+} exchanger type-1 (NCX1), SR Ca^{2+}-ATPase type-2a (SERCA2a) and Na^+-K^+-ATPase. **Figure 3** shows the structure of the atrial AP with the different phases elaborated above.

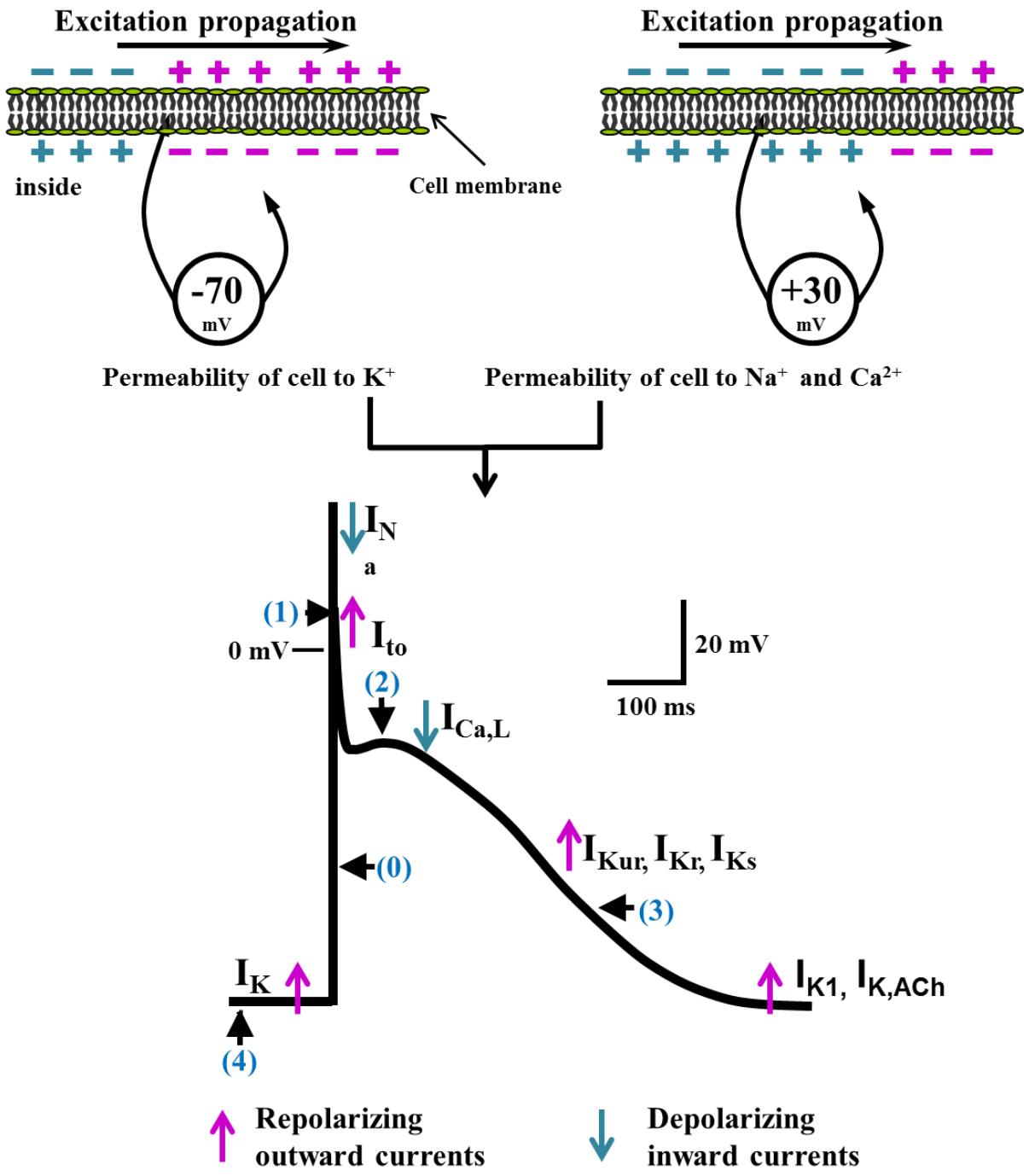

Figure 3: How an action potential is formed.

A representative atrial action potential (AP), showing the different phases of an AP. The AP is formed by fluxes of different ions in and out of the cell and is separated into the resting phase (4), the upstroke or depolarization phase (0), the early repolarization (1), the plateau (2), and the final repolarization (3). Each phase is characterized by particular ion currents as shown.

The family of inward-rectifier K^+ channels play an important role in cardiac function by setting the RMP, which largely determines the upstroke velocity of the AP and the conduction velocity of electrical impulses between cardiomyocytes. In addition, these channels carry a small but significant outward current during late stages of the AP, thereby contributing greatly

to the final repolarization of the AP (phase 3). Under experimental conditions, these channels conduct less outward K^+ current compared to the current in the inward direction, a property which is known as inward-rectification and which gives this family of K^+ channels its name (Lu 2004). There are several inward-rectifier K^+ currents that have been identified in the heart (**Figure 4**) (Anumonwo & Lopatin 2010). The most important of them is I_{K1}, which is instantaneously active in cardiac cells and can be measured under basal conditions. In previous publications, we have shown that I_{K1} is increased in patients with paroxysmal atrial fibrillation (pAF) and chronic AF (cAF).These contribute to the shortening of the AP duration (APD), thereby supporting the formation of AF-promoting reentrant mechanisms (Dobrev et al. 2001; Dobrev et al. 2002; Voigt, et al. 2010; Heijman, et al. 2014).

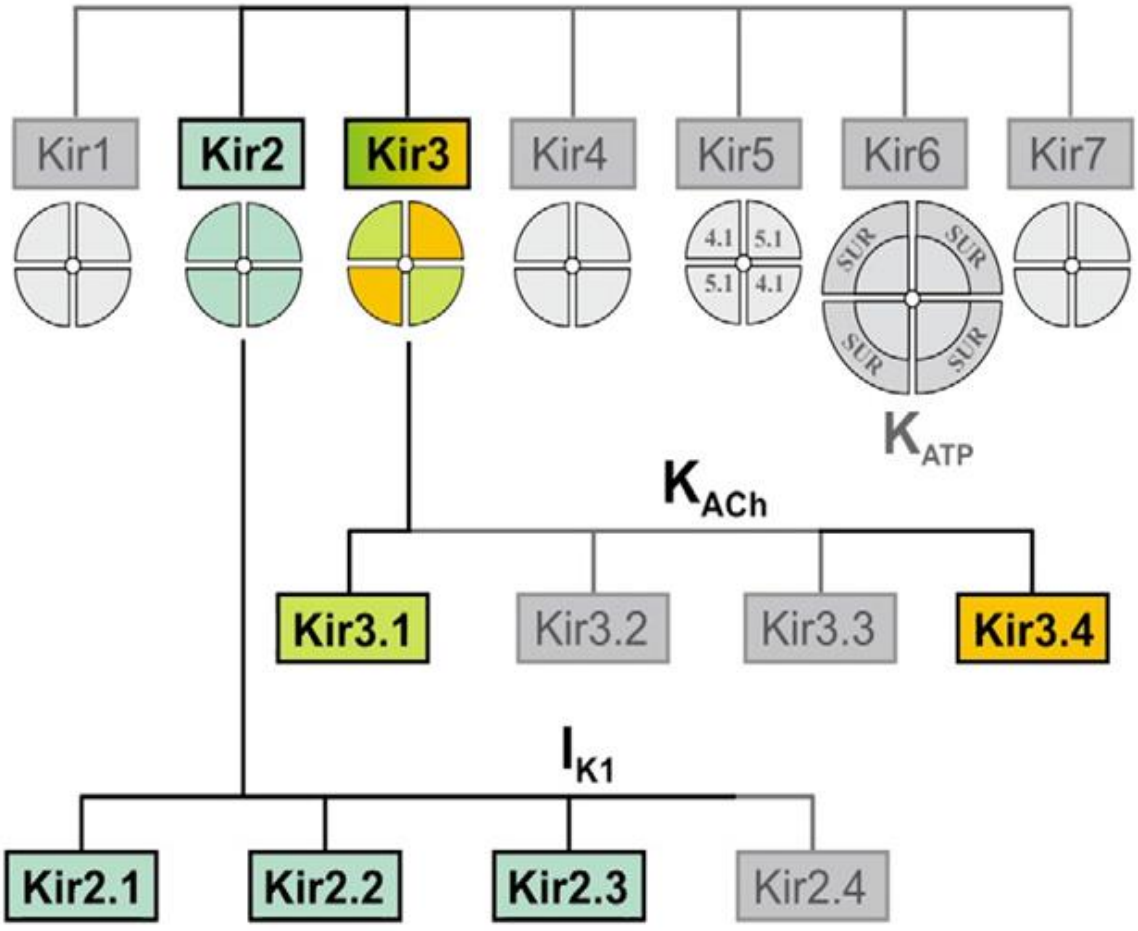

Figure 4: Inward-rectifier K^+ currents (K_{IR}).

The diagram shows the different inward-rectifier K^+ currents identified in cardiac tissue. All members of this family share significant structural similarity, but only Kir2 and Kir3 subfamilies represent channels carrying classical strongly rectifying current. Adapted from Anumonwo & Lopatin 2010.

I_{K1} and $I_{K,ACh}$ are the major K^+ currents displaying classical strong inward rectification (**Figure 5**), a distinct property that is critical for their roles in cardiac excitability. Rectification profiles are distinct in different K_{IR} channels. When current amplitudes are normalized at far negative membrane potentials the outward currents are the smallest for $K_{IR}2.2$ and the largest for $K_{IR}3.1/K_{IR}3.4$ channels (Anumonwo & Lopatin 2010)

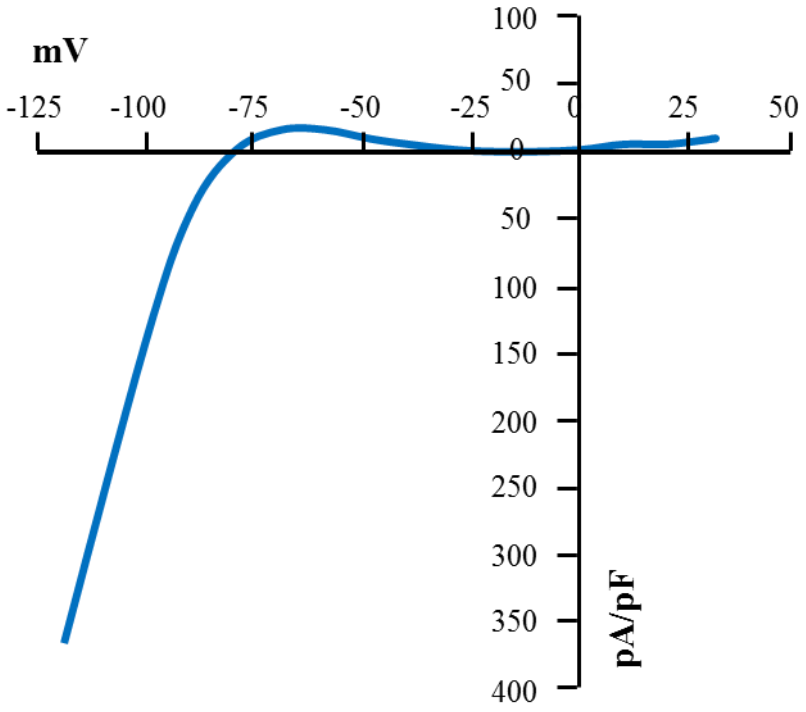

Figure 5: Schematics of rectification properties of inward-rectifier K^+ currents.

A typical current-voltage (I-V) relationship with a small outward but large inward current component.

1.2.2 Mechanism of excitation-contraction coupling.

ECC is a complex system regulating cardiomyocyte contraction in response to its electrical activation (**Figure 6**). L-type Ca^{2+} channels are voltage-dependent and are activated in response to membrane depolarization during an AP, allowing influx of Ca^{2+} (El Khoury et al. 2014). This influx of Ca^{2+} in the cytosol triggers a much larger Ca^{2+} release from the SR through a mechanism called Ca^{2+}-induced Ca^{2+} release (CICR), which is the major determinant of the contractile performance of the heart (Fabiato 1983; Bers 2002). The Ca^{2+} is released from the SR through the Ca^{2+}-sensitive ryanodine receptor channels type-2 (RyR2). Part of the extruded Ca^{2+} then binds to the actin/myosin complex, initiating contraction. In the resting phase of the cell (diastole), the Ca^{2+} is pumped back into the SR by SERCA2a, whereas the Ca^{2+} that entered through the L-type Ca^{2+} channel is extruded by NCX1. NCX1 is

electrogenic because of asymmetric transport of Na^+ and Ca^{2+} ions. In particular, in the forward mode, three Na^+ ions enter the cell for every Ca^{2+} that is extruded, resulting in a net gain of one positive charge (i.e., producing a depolarizing current) (Bers 2002; Bers 2008). Consequently, the electrical equilibrium that results from the ion currents in cardiomyocytes throughout the heart is essential for the rhythmic mechanical contraction of the heart. Therefore, an imbalance in the electrical activation can produce arrhythmias, which can severely disturb the function of the heart (Voigt, et al. 2012).

Since Ca^{2+}-handling abnormalities appear to play a central role in cardiac arrhythmogenesis, Ca^{2+}-handling proteins may represent potential therapeutic targets for the development of new antiarrhythmic drugs (Heijman et al. 2015).

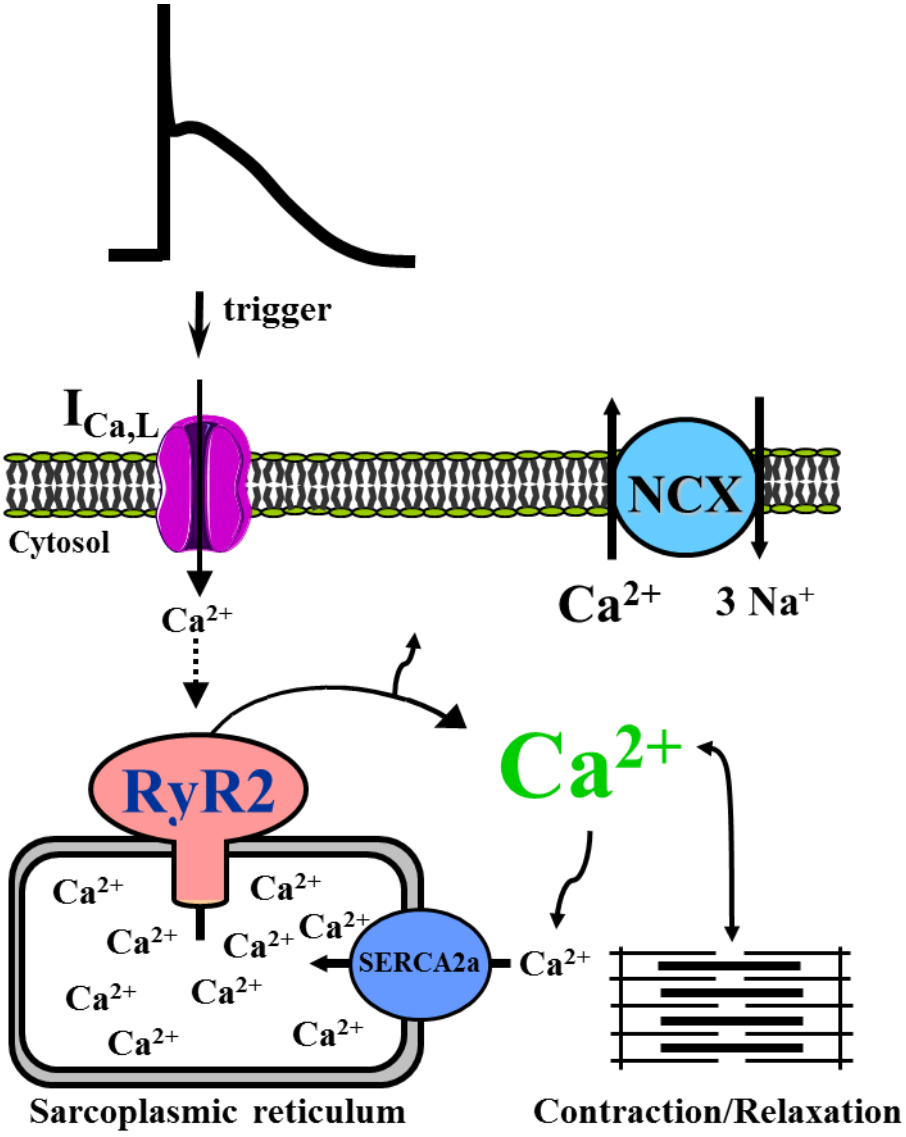

Figure 6: Mechanism of excitation-contraction coupling (ECC)

The process from electrical excitation of a cardiomyocyte to the contraction of the heart. See text for further details.

1.3 Atrial fibrillation

Atrial fibrillation (AF) is the most common sustained clinical arrhythmia occurring in 1-2% of the general population (Kirchhof et al. 2016). It is reported that over 33 million people worldwide suffer from AF (Chugh et al. 2014). The incidence and prevalence of AF are predicted to rise with ageing of the population. AF is associated with increased morbidity and mortality, predominantly because of progressive ventricular dysfunction (e.g., worsening heart failure), and thromboembolic complications (Andrade et al. 2014). AF is promoted by age and a wide range of cardiac and non-cardiac pathologies (Andrade et al. 2014). In the clinical setting, AF is characterized by rapid, disorganized electrical activity of the atria, resulting in impaired atrial contractility.

After the first diagnosed episode of AF, AF can be classified into different patterns based on the duration of episodes. pAF involves recurrent episodes of AF, which spontaneously self-terminate back to sinus rhythm within 7 days of onset and can progress to persistent forms leading to cAF (Heijman et al. 2014). Finally if no further attempts are made to restore normal sinus rhythm, this is defined as permanent AF. Several proposals for more mechanistic classifications of AF have been made (Fabritz et al. 2015), but these have generally not found widespread application. Post-operative AF (poAF), which develops after surgery, is another form of AF which increases the duration of hospital stay, and increases risk for stroke, morbidity and mortality (Maesen et al. 2012). Details of the classification of AF were elaborated in a recent paper (Kirchhof et al. 2016) and are helpful in organizing the thinking about the management of this highly variable arrhythmia.

Conceptually, the onset of the different forms of AF can be linked to factors like genetic predisposition, advanced age, sex, environmental factors and by a wide range of cardiac and non-cardiac etiologies (Nishida & Nattel 2014), which produce a substrate for atrial arrhythmogenesis, including focal ectopic (triggered) activity and reentry (Heijman et al. 2016).

1.3.1 Current treatment strategies of AF

Administration of anticoagulants is used to reduce the risk of stroke (Nattel 2016). Thereafter, the treatment of arrhythmia can be based on rhythm or rate control. For rate control, negative dromotrop acting drugs (e.g. digitalis glycosides, β-blockers and Ca^{2+}-antagonists like verapamil and diltiazem) are used. With adequate rate control, the atria can stay fibrillating whereas the ventricles can perform at a normal activation rate. If patients remain symptomatic, rhythm control is attempted. For rhythm control, interventional procedures (e.g.

catheter ablation) have success rates that exceed currently available antiarrhythmic drugs (Naccarelli & Gonzalez 2008). However, due to the high cost, duration and the complex nature of the procedure, as well as the incomplete efficacy and high recurrence rates, pharmacological treatment options still remain the mainstream therapy for the majority of AF patients (Heijman et al. 2013; Lüscher 2016). The most common pharmacological rhythm control agents include; class I (e.g., flecainide) and class III (e.g., sotolol or amiodarone) antiarrhythmic drugs (Naccarelli & Gonzalez 2008; Camm et al. 2010; Heijman et al. 2013). The overall clinical outcome is similar regardless of whether drugs for rate or rhythm control are used as AF therapy. This is likely results from the limited efficacy of currently available antiarrhythmic drugs, which maintain only a limited number of patients in sinus rhythm and produce substantial toxicity.

We and others have shown that at the cellular and molecular levels, different mechanisms underlie atrial arrhythmogenesis in pAF (Voigt et al. 2014) and cAF (Voigt et al. 2012) patients. However, very little is known about the molecular and cellular characteristics of the vulnerable atrial substrate that predisposes patients to the development of poAF, which will be one major goal in this work.

Substantial progress in the understanding of AF pathophysiology has been made over the past 20 years (Nishida & Nattel 2014). One important discovery in AF research was the demonstration that AF causes important electrophysiological alterations in the atrium of goats that promotes progression to more sustained forms of AF (Wijffelset al. 1995). This led to the concept of AF-induced remodeling, which has become a central paradigm in the maintenance and progression of AF (Antzelevitch & Burashnikov 2011; Goette et al. 2016; Heijman et al. 2016). Atrial cardiomyopathy which predisposes to AF induction is defined as any complex of structural, architectural, contractile or electrophysiological changes affecting the atria with the potential to produce clinically relevant manifestations (Goette et al. 2016)

1.3.2 Mechanisms of AF maintenance

Abnormalities of impulse generation (i.e. abnormal automaticity or ectopic/triggered activity) and conduction disturbances (i.e. reentry) are considered the predominant conceptual mechanisms of cardiac arrhythmias (**Figure 7**) (Roden et al. 2002; Antzelevitch & Burashnikov 2011; Heijman et al. 2016). Abnormal automaticity comprises reduced and increased automaticity, which causes bradycardia (slower heart rate) and tachycardia respectively. It can originate from abnormalities in the SAN or from cardiomyocytes elsewhere in the atria, notably those in the sleeves of the pulmonary veins (Antzelevitch & Burashnikov 2011). Triggered activity describes the abnormal impulse formation in

cardiomyocytes other than the SAN. Mechanistically, triggered activity is generally a consequence of either early afterdepolarizations (EADs) or of delayed afterdepolarizations (DADs, Heijman et al. 2015). EADs occur during phase 2 or 3 of repolarization of the AP when prolonged repolarization allows L-type Ca^{2+} channels to recover from voltage/Ca^{2+}-dependent inactivation and produce secondary afterdepolarizations before a full AP repolarization. DADs occurs when repolarization is complete and results from spontaneous diastolic SR Ca^{2+} release events (SCaEs) that activate NCX, producing a depolarizing transient-inward current (Heijman et al. 2015). If membrane depolarization is sufficiently large to reach threshold, a triggered AP follows, which can produce focal ectopic firing (Wit & Boyden 2007; Heijman et al. 2016). Triggered activity can initiate reentry within a vulnerable substrate characterized by structural (e.g., fibrosis) and electrical (reduced AP duration [APD] and conduction velocity) remodeling (Heijman et al. 2014; Heijman et al. 2015)

Functional reentry is considered the main mechanism for AF maintenance and can be initiated by different mechanisms, usually explained with the "leading circle" or the "spiral wave" theories. The main factors promoting reentry are shortening of effective refractory period (ERP = APD + post-repolarization refractoriness) and slowing in atrial conduction, both of which would make it more likely that tissue within a re-entrant loop would regain excitability before the arrival of the next impulse, thereby maintaining AF (Heijman et al. 2014; Heijman et al. 2015).

Post-repolarization refractoriness results from voltage-dependent inactivation of Na^+ channels. Atrial Na^+ channels have been suggested to have a more negative half-inactivation voltage compared with ventricular channels, allowing for greater post-repolarization refractoriness, particularly in the presence of Na^+-channel blockers. Conduction velocity is mainly determined by excitatory Na^+ current, cardiomyocyte electric coupling through gap junctions and muscle bundle architecture. Reduced I_{Na} decreased gap junctional coupling and muscle bundle discontinuities resulting from fibrosis, all reduce conduction velocity and promote reentry. Ca^{2+}-handling abnormalities can also promote AF maintenance through conduction slowing. Atrial conduction velocity is reduced in mice with a RyR2 catecholaminergic polymorphic ventricular tachycardia mutation causing increased SR Ca^{2+} leak and in mouse hearts with acutely elevated intracellular Ca^{2+}. The underlying mechanisms seem to involve both acute Ca^{2+}-dependent inhibition of Na^+ channels and chronic down regulation of Nav1.5 expression (Heijman et al. 2014).

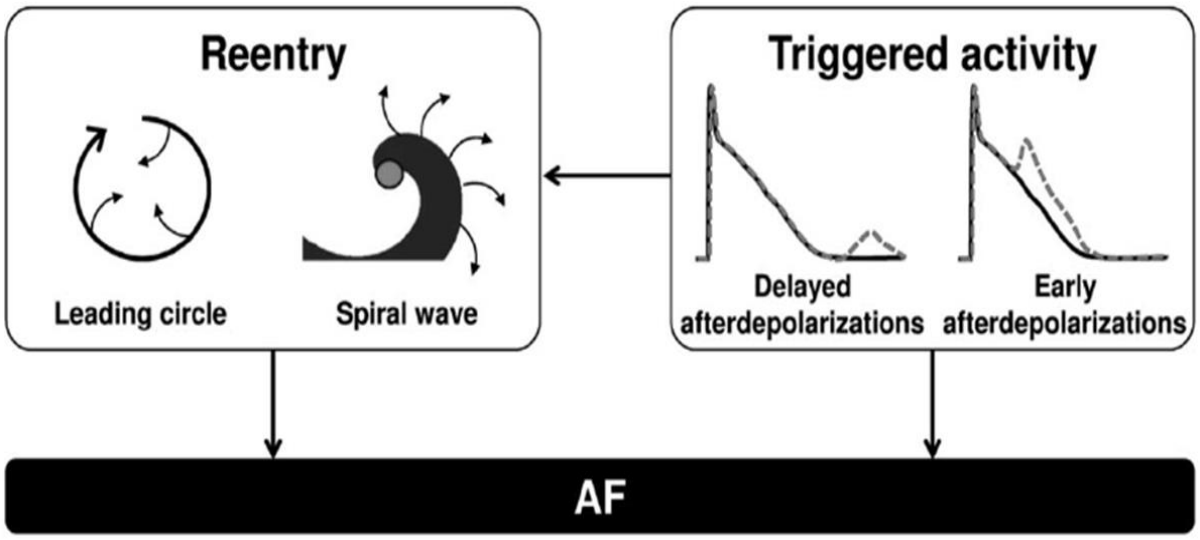

Figure 7: Major mechanisms of AF pathophysiology.

Early or delayed afterdepolarizations can contribute to ectopic activity, which may initiate reentrant excitations in a vulnerable substrate (electrical and structural remodeling), promoting AF maintenance. Ectopic triggers may also maintain AF by themselves when occurring repetitively with high frequencies (Heijman et al. 2015).

1.3.3 Cellular and molecular mechanisms of atrial arrhythmogenesis in cAF

Proper Ca^{2+} homeostasis is maintained through Ca^{2+} reuptake into the SR by SERCA2a and Ca^{2+} extrusion out of the cell via NCX1. SERCA2a is inhibited by dephosphorylated phospholamban (PLB) and sarcolipin, the latter being atrial specific, whereas phosphorylation of PLB at Ser16 (protein kinase A [PKA] site) and Thr17 (Ca^{2+}/calmodulin dependent protein kinase II [CaMKII] site) and phosphorylation of sarcolipin at Thr5 (CaMKII site) disinhibit SERCA2a, increasing SR Ca^{2+} uptake (Heijman et al., 2015). Na^{+} homeostasis is maintained through Na^{+}-K^{+}-ATPase and is closely coupled to atrial Ca^{2+}-handling through NCX1. Different forms of AF have been associated with distinct remodeling patterns, producing altered APs and Ca^{2+}-handling that predispose to AF initiation and maintenance through triggered activity and/or reentry (Heijman et al. 2016).

Triggered activity promoting increased SR Ca^{2+} leak along with enhanced frequency of SCaEs has been observed in both pAF and cAF, notwithstanding their distinct underlying molecular mechanisms (**Figure 8**).

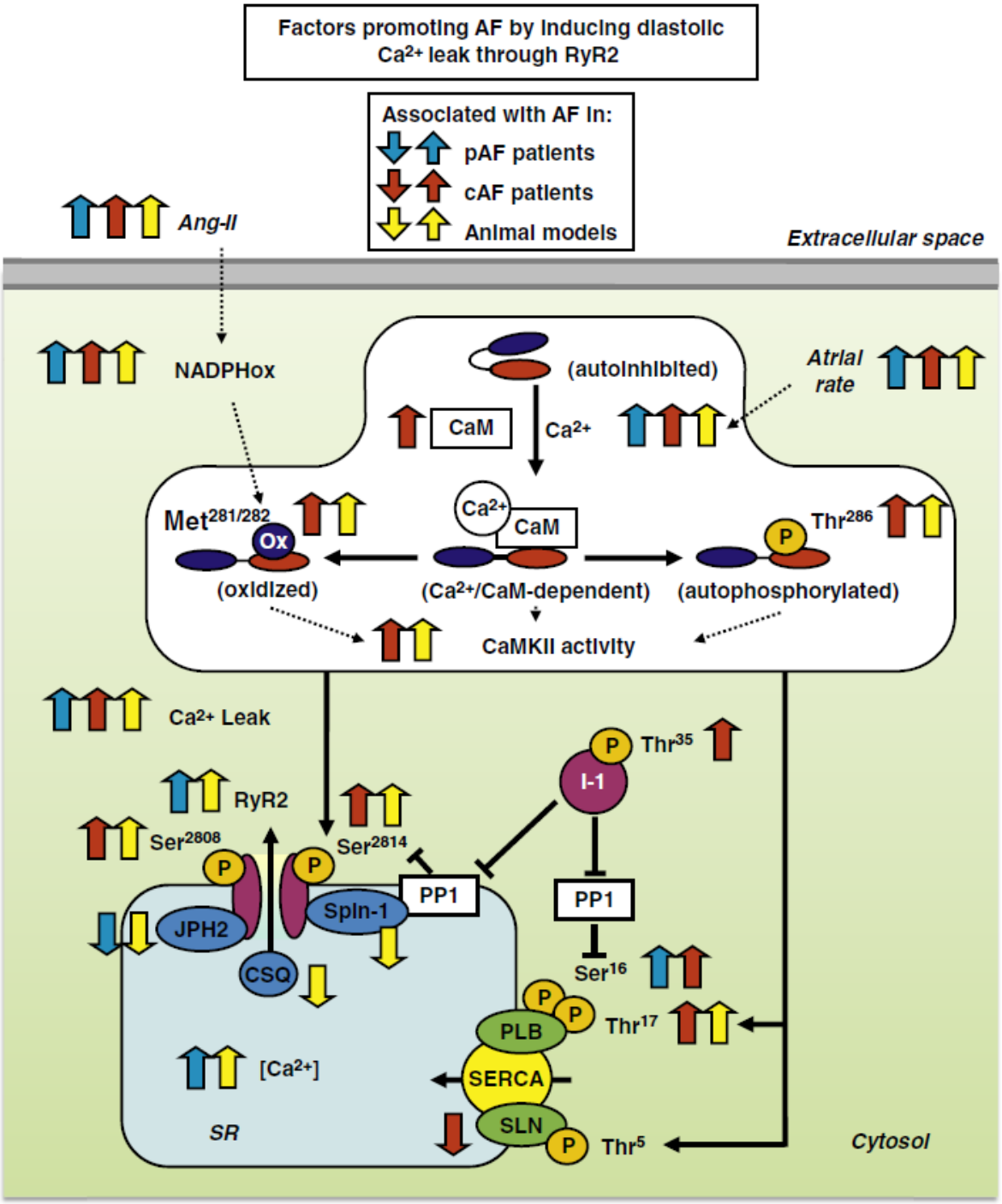

Figure 8: Molecular basis of Ca^{2+}-handling abnormalities in atrial fibrillation.

Ryanodine receptor (RyR) dysfunction is caused by RyR hyperphosphorylation or excess in Ca^{2+} loads. Phospholamban (PLB) inhibits sarcoplasmic reticulum (SR) Ca^{2+}-ATPase (SERCA). PLB hyperphosphorylation removes this inhibitory effect, enhances SERCA function and can lead to Ca^{2+} overload. High atrial rate during atrial fibrillation (AF) enhances cellular Ca^{2+} entry. Increased cell Ca^{2+} promotes Ca^{2+}/calmodulin (CaM) binding Ca^{2+}/calmodulin-dependent protein kinase-II (CaMKII), disinhibiting the catalytic subunit. After CaMKII catalytic subunit activation, oxidation at Met28/282 or phosphorylation at Thr286 causes persistent CaMKII activity. Inhibitor-1 (I-1) suppresses protein phosphatase-1 (PP1) function in the SR and contributes to PLN and RyR phosphorylation. These factors have been associated with AF in samples from paroxysmal AF (pAF) patients (blue arrows), chronic (cAF) patients (red arrows), or animal models (yellow arrows).Reproduced from Nattel et al. 2016.

In both forms of AF proarrythmic DAD-mediated Ca^{2+}-handling abnormalities contribute to triggered activity and increased atrial arrhythmogenesis. In cAF, SCaE-mediated DADs are principally due to RyR2 hyperphosphorylation caused by increased CaMKII-mediated RyR2 phosphoralation at Ser2014 (Voigt et al. 2012). In contrast, CaMKII activity is unchanged in pAF and SCaEs are due to phosphorylation independent RyR2 dysregulation and increased SR Ca^{2+} load resulting from increased SERCA2a activity. RyR2 dysregulation in pAF involves both increased channel open probability and increased RyR2 protein expression levels (Voigt et al. 2014). In cAF, DADs primarily result from intrinsic RyR2 abnormalities due to RyR2 hyperphosphorylation at Ser2014 combined with increased Ca^{2+} sensitivity of NCX (Heijman et al. 2015).

cAF-associated electrical remodeling also involves changes in ionic currents including I_{Na}, $I_{Ca,L}$ I_{to}, I_{Kur}, I_{Kr}, I_{Ks}, I_{K1}, $I_{K,ACh}$ and the two-pore-domain K^+ channels (I_{K2P}; **Figure 9**). Initially no change in the depolarizing I_{Na} or mRNA expression of the Nav1.5 α-subunit was found in cAF patients (Bosch et al. 1999; Brundel et al. 2001). However, reduced peak I_{Na} is likely to contribute to reentry-promoting conduction slowing in cAF (Sossalla et al. 2010). In addition, persistent/late I_{Na} was increased (Sossalla et al. 2010; Wettwer et al. 2013). Although the exact functional consequences are presently unknown, patients with early-onset of lone AF also exhibit a high prevalence of Na^+ channel mutations that increase persistent/late I_{Na} (Heijman et al. 2014).

Decreased APD is a hallmark of atrial cardiomyocytes from cAF patients. Depolarizing $I_{Ca,L}$ is consistently reduced in cAF (Van Wagoner et al. 1999; Christ et al. 2004) likely due to an adaptive mechanism to protect atrial myocytes from toxic Ca^{2+} overload resulting from fast rates. Reduced $I_{Ca,L}$ contributes both to reduced APD, promoting reentry, and the decreased Ca^{2+}-transient amplitude impairs atrial contractility (Van Wagoner & Nerbonne 2000; Workman et al. 2001; Schotten et al. 2001; Voigt et al. 2012; Voigt et al. 2014). Despite reduced APD at full repolarization, APD at 20% repolarization is generally prolonged. This effect is partly because of smaller I_{to} through reduced expression of the underlying Kv4.3 subunit. I_{to} reduction is more pronounced in LA than in RA (Van Wagoner et al. 1997). Similarly, I_{Kur} and Kv1.5 subunits are reduced in cAF (Van Wagoner et al. 1997; Van Wagoner & Nerbonne 2000). Reduced I_{Kur} can promote EADs in the presence of sympathetic stimulation (Van Wagoner & Nerbonne 2000; Heijman et al. 2014). An increase in I_{Ks} and I_{K2P} were also observed in cAF patients (Caballero et al. 2010; Schmidt et al. 2015). Increased inward-rectifier K^+ currents also contribute to APD shortening in cAF. LA I_{K1} is increased in both pAF and cAF (Dobrev et al. 2001; Voigt et al. 2010). Agonist-activated $I_{K,ACh}$ is larger in RA than in LA from patients with sinus rhythm, but is decreased in RA of pAF and cAF

because of a reduction in underlying Kir3.1 and Kir3.4 subunits (Voigt et al. 2010). Kir3.4, but not Kir3.1, is regulated by intracellular [Na^+], resulting in Na^+-dependent increase in agonist-activated $I_{K,ACh}$. This Na^+-dependent regulation is lost in cAF, probably due to a more pronounced reduction of the Na^+-sensitive subunit Kir3.4 than Kir3.1, and further reduces $I_{K,ACh}$ at fast rates with increased intracellular [Na^+]. $I_{K,ACh}$ also develops agonist-independent (constitutive) activity in cAF (Dobrev et al. 2005; Heijman et al. 2014).

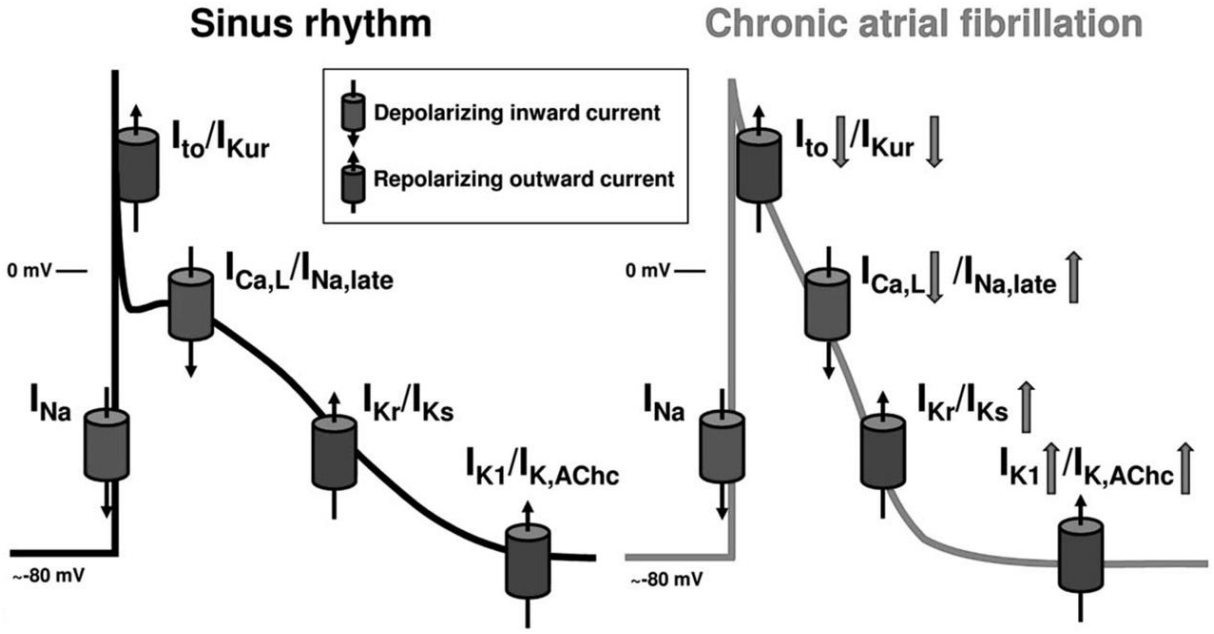

Figure 9: Ionic currents remodeling in cAF.

Typical atrial AP depending on the balanced interaction between depolarizing and repolarizing currents (left). Alterations of ion-channel activities in patients with cAF lead to APD shortening and triangulation (right) (Heijman et al. 2015).

The basal inward-rectifier K^+ current is assumed to be largely mediated by I_{K1}. However, agonist-independent (constitutive) $I_{K,ACh}$ (Dobrev et al. 2005) and I_{K2P} (Schmidt et al., 2015) also contribute to basal inward-rectifier K^+ current making it difficult to dissect the exact contribution of Kir2-carried I_{K1} currents in Ctl compared to AF patients. The recent availability of novel drugs with preferable selectivity to I_{K1} makes it possible for the first time to check the exact contribution of I_{K1} to basal inward-rectifier K^+ current in Ctl and AF patients. In the heart, I_{K1} channels are believed to be homo- and heterotetramers of $K_{IR}2.1$, $K_{IR}2.2$, and $K_{IR}2.3$ subunits. Van der Heyden et al separately expressed the mouse and human forms of these subunits in HEK293 cells (Takanari et al. 2013). They showed a concentration-dependent decrease in expressed currents with PA-6 and the concentration-response curve of

PA-6 showed a comparable potency for the different I_{K1} subunits of both human and mouse. The concentration-response curve reached its maximum effect at about 200 nM (**Figure 10**).

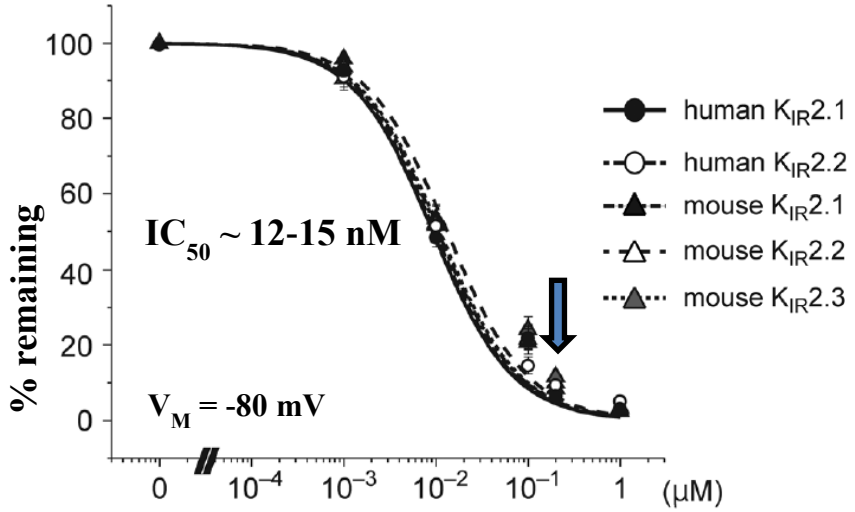

Figure 10: Concentration-response curve of heterologously expressed Kir2.1-2.3 currents to PA-6.

I_{K1} subunits expressed in HEK293 cells, currents measured in the inside out voltage-clamp mode in the presence of different concentrations of PA-6. Adapted from Takanari et al. 2013.

With the elaborate knowledge that cellular and molecular mechanisms differ in pAF and cAF, in particular $I_{Ca,L}$ and cellular Ca^{2+}-mediated proarrhythmic events associated with dysfunctional RyR2 (Voigt et al. 2012; El-Armouche et al. 2006), we aimed to dissect the largely unexplored pathophysiology of poAF in detail.

1.4 Post-operative atrial fibrillation (poAF)

PoAF is a common condition with an incidence rate of between 10% and 60% and predominantly occurring on days 2 and 3 after surgery (**Figure 9**; Mathew et al. 2004; Nattel 2006; Workman et al. 2006; Maesen et al. 2012). Although usually self-limiting, poAF increases length of hospital stay and can cause debilitating strokes (Min et al. 2015). PoAF can occur after non-cardiac surgery, but is more common in patients that undergo cardiac surgery (Maesen et al. 2012; Joshi et al. 2015). It may be defined based on electrocardiogram findings consistent with AF within 30 days post-surgery and requires treatment with rate or rhythm control agents, or requires anticoagulation agents (Frendl et al. 2014; Zaman et al. 2016). Antiarrhythmic agents like amiodarone, sotalol or β-blockers are reported to prevent poAF, however due to their mechanism of action, side effects, and limitations, they are not routinely used in patients undergoing cardiac surgery (Frendl et al. 2014; Ozawa et al. 2015).

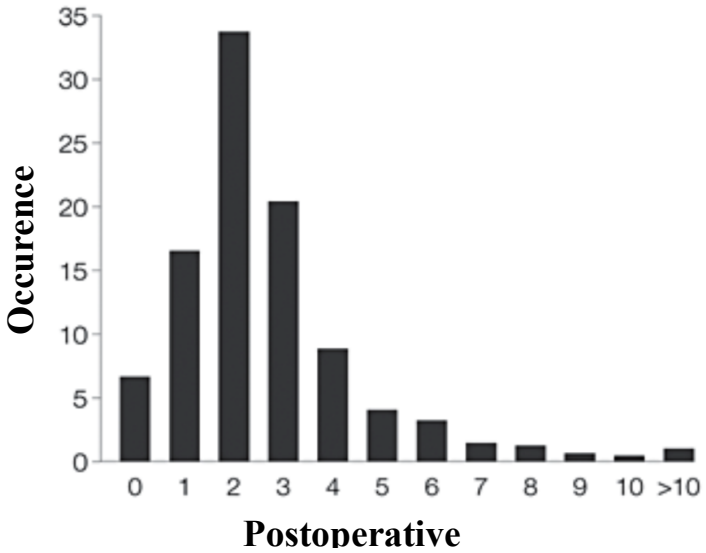

Figure 11: Occurrence of atrial fibrillation post-surgery.

Adapted from Mathew et al. 2004.

Advanced age is an independent predictor of poAF (Verdejo et al. 2015). Older patients (> 75 years) had stiffer LA and an impaired atrial contractile function suggesting that mechanical impairment may provide a substrate for poAF and could be a marker to identify subjects at elevated risk for poAF (Verdejo et al. 2015). However, although initially the incidence of poAF positively correlated with enhanced pre-operative $I_{Ca,L}$ amplitude (Van Wagoner et al. 1999), subsequent work detected no differences in APD and selected ion currents ($I_{Ca,L}$, I_{K1} and $I_{K,ACh}$) in Ctl compared to poAF patients (Dobrev et al. 2001; Workman et al. 2006).

Table 1: Previously published electrophysiological data on poAF.

Papers	Findings in poAF versus Ctl patients	
Van Wagoner et al., Circ Res. 1999	↑	$I_{Ca,L}$
Dobrev et al., Cardiovascular Res. 2002	↔	I_{K1} and $I_{K,ACh}$
Workman et al., J Cardiovasc Electrophysiol. 2006	↔	$I_{Ca,L}$, I_{K1} and I_{to}
	↔	APD components
Brandt et al., JMCC. 2000	↔	I_{to} and I_{Kur}

Arrows indicate increase, decrease or no change in the properties investigated. APD components include APD at 20%, 50%, 90% repolarization, ERP (effective refractory period) and V_{max} (AP maximum phase 0 (upstroke) velocity.

Thus only a limited number of studies about the cellular pathophysiology of poAF are available and the exact mechanisms underlying the development of poAF remain largely unknown. Although the pathophysiology of poAF is likely multifactorial, focal ectopic (triggered) activity has been hypothesized as one major mechanism of poAF (Maesen et al. 2012; Zaman et al. 2016). Perioperative factors like use of catecholamines or increased sympathetic outflow from volume loss/anaemia/pain, metabolic alterations like hypo-/hyperglycaemia and electrolyte disturbances, as well as inflammation resulting from surgery may also promote the development of poAF (Workman et al. 2006; Maesen et al. 2012). Conceptually the initiation and maintenance of poAF likely require both a pre-existing substrate and acute initiators ("triggers") (Frendl et al. 2014), which may be caused by surgical intervention associated alterations (volume, inflammation, metabolic activity and drug) that act on the pre-existing proarrhythmic substrate, initiating AF (**Figure 12**). Although inflammation and sympathetic activation are accepted triggers of poAF development, the underlying cellular and molecular mechanisms by which these factors may predispose to poAF remain unknown. A better understanding of the mechanisms contributing to the development of poAF might lead to more effective and safer therapies (Nattel 2006).

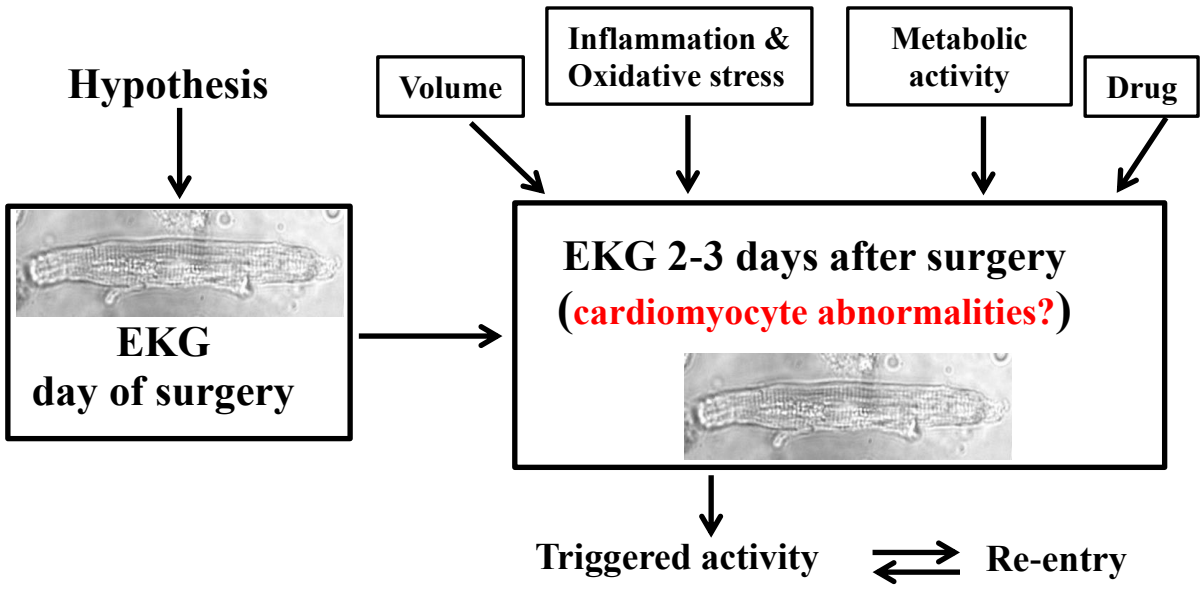

Figure 12: Putative factors contributing to onset of poAF in patients.

We hypothesize that pre-existing vulnerable substrates in atrial cardiomyocytes of patients with sinus rhythm before surgery, encounter post-surgical factors like increase volume, inflammation, oxidative stress, metabolic activity and drugs, thereby promoting the initiation of poAF episodes in predisposed patients.

2 Scope of PhD thesis

The aim of the present work is to investigate the alteration in cellular electrophysiology and Ca^{2+}-handling in patients with different forms of AF. Atrial tissue samples from patients undergoing open-heart surgery are a valuable *in vitro* tool to study the abnormalities in molecular and cellular electrophysiological properties contributing to atrial arrhythmogenesis. These samples represent essential molecular, structural and functional components of the atria, which can be investigated using functional techniques (e.g., patch-clamp), imaging techniques, pharmacological manipulations and biochemistry (Western blot). The principles of these methods are detailed in **Section 3**. Using atrial appendages of patients undergoing open heart surgery, we were able to compare patients with sinus rhythm before cardiac surgery that did not develop AF in the postoperative period (control group) with different patient groups under study (patients that developed AF post-surgery and cAF patients).

In the first part of this thesis (**Section 4.1**), we investigated the underlying pathophysiology and cellular mechanisms of poAF. We performed functional analyses using combined patch-clamp and Ca^{2+}-imaging (epifluorescence techniques). In particular, we I) examined potential Ca^{2+}-handling differences between poAF and control patients before cardiac surgery II) applied proinflammatory cytokins (interleukin 1β) to partially simulate the situation in the postoperative period, thereby providing a putative trigger of poAF; and III) complemented these functional studies with Western blot analysis, investigating key regulatory protein involved in Ca^{2+}-homeostasis at the cellular level. We discovered for the first time that poAF is associated with Ca^{2+}-handling abnormalities that predispose patients to cytokine-induced triggered activity.

In the second part (**Section 4.2**), we focused on increased basal inward-rectifier K^+ current, a well-known hallmark of electrical remodeling in patients with cAF. Increased basal inward-rectifier K^+ current has been suggested to contribute to the shortening of the APD and hyperpolarization of the RMP, which have been implicated in the maintenance of AF by promoting reentry. However the exact contribution of I_{K1} ($K_{IR}2.1$ - $K_{IR}2.3$) in addition to the constitutive $I_{K,ACh}$ and I_{K2P} to the basal inward-rectifier K^+ current is unknown in cAF and was the focus of the second part of this thesis. We performed functional studies and I) compared the basal inward-rectifier K^+ current and $I_{K,ACh}$ in control and cAF patients; II) applied the selective I_{K1} inhibitor PA-6 to both currents in both groups; and III) quantified for the first time the exact magnitude of I_{K1} to the basal inward-rectifier K^+ current in both patient groups.

Finally, the relevance of these studies for our understanding of the pathophysiology of AF is discussed in **Section 5**.

3 Materials and Methods

3.1 Collection of human atrial tissue

Human atrial cardiomyocytes were freshly isolated from right-atrial appendage samples of patients undergoing open-heart surgery for coronary bypass grafting or valve replacement (Voigt et al. 2015). The tip of the right atrial appendage is removed during routine cannulation to extracorporeal circulation through the heart-lung machine (**Figure 13**). After obtaining informed patient consent, we collected the tissue for experimental purposes. Full informed consent was provided by each patient before surgery. The protocols were approved by the local ethics committee of the Medical Faculty, University Duisburg-Essen (No. 12 5268-BO). Atrial cardiomyocytes were isolated as described below and measurements of intracellular Ca^{2+} ($[Ca^{2+}]_i$) and membrane currents were conducted. Only rod-shaped Ca^{2+}-tolerant cells with clear striations were used for the experiments.

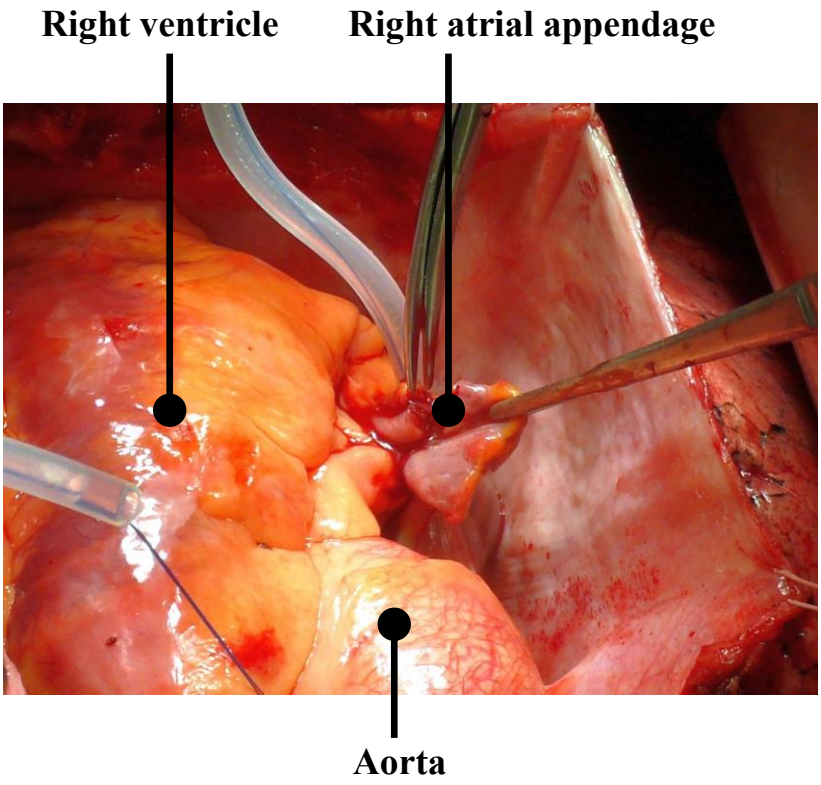

Figure 13: Human right atrial appendage (tissue) procurement.

3.1.1 Tissue transportation

Collected tissue was immediately transferred into a 50 ml Falcon tube with sterile Ca^{2+}-free transport solution (**Table 2**) to protect the tissue from damage by Ca^{2+} overload (Voigt et al. 2013; Voigt et al. 2015). The transport solution contained 2,3-butanedione monoxime (BDM, a non-competitive myosin-II inhibitor, preventing cardiomyocyte contracture). Samples were transferred to the laboratory within 30 - 60 mins for cell isolation. All reagents used are from Sigma Aldrich.

Table 2: Composition of transport solution.

	Substance	**Company**
Transport solution	30 mM BDM	Sigma Aldrich
	20 mM Glucose	Sigma Aldrich
	10 mM KCL	Sigma Aldrich
	1.2 mM KH_2PO_4	Sigma Aldrich
	5 mM $MgSO_4$	Sigma Aldrich
	5 mM MOPS	Sigma Aldrich
	100 mM NaCL	Sigma Aldrich
	50 mM Taurin	Sigma Aldrich

3.1.2 Human atrial cardiomyocyte isolation procedure

Cardiomyocytes used for patch-clamp measurements were prepared following an isolation method that is routinely used in our laboratory (Voigt et al. 2015; **Figure 12**). For the single cardiomyocyte isolation at 37°C, two major phases are critical. Firstly, the washing phase of the tissue with Ca^{2+}-free solution with simultaneous oxygenation which helps to loosen intercellular contacts. Secondly, the enzymatic break-off of the collagen matrix around the cells causes separation of the cells. In the following paragraph, we describe the isolation process in detail.

To start the single cell isolation procedure, a thermocirculator was switched on and the temperature set to about 37°C. Then a jacket beaker was placed on it. To maintain the beaker temperature throughout the isolation procedure at 37°C, it was covered with a glass slide. The tissue sample in the transport solution was then poured into a Petri dish (~10 cm diameter) and fat tissue was cautiously removed using scissors. The rest of the tissue sample was weighed. 200 - 600 mg was a decent amount used for cell isolation, with a small part of it being frozen for biochemical analysis. The weighed tissue was then transferred into a new

Petri dish containing 20 ml Ca^{2+}-free solution at 4°C and chopped into smaller chunks of (~1 mm^3 in size). For washing, the tissue was transferred into the jacketed beaker maintained at 37°C with continuous gassing under 100% O_2. A pipette tip was placed onto the oxygen tube to control the oxygen flow and the pressure was set low enough so as not to generate bubbles. The mixture was stirred for 3 min with the help of a magnetic bar after which the chopped chunks were allowed to settle down for a few seconds and the supernatant was sieved through a nylon mesh (200 µm, **Table 4**). Any chopped chunk on the mesh was returned into the beaker using forceps. The jacked beaker was again refilled with 20 ml Ca^{2+} free solution and this washing procedure was repeated twice.

Two enzymatic steps were used for tissue digestion. In the first enzymatic step, the washed chopped tissue chunks were re-suspended in 20 ml of enzyme solution E1 (**Table 3**) which contained collagenase and protease. It was carefully stirred for 10 min and 40 µl of 10 mM $CaCl_2$-solution was added to obtain a final concentration of 20 µM Ca^{2+}. After 35 min of continuous stirring, the supernatant was carefully sieved through a nylon mesh (200 µm) in a way that most of the tissue chunks remained in the beaker. Tissue chunks that flowed on the mesh were returned into the beaker using forceps. In the second enzymatic step, the tissue chunks were again re-suspended with 20 ml of enzyme solution E2 containing collagenase I only (**Table 3**) with 40 µl of 10 mM $CaCl_2$-solution, immediately to obtain a final concentration of 20 µM Ca^{2+}. In this step, a scissors was used to further chop tissue chunks occasionally. After 5 min, a Pasteur pipette was used to collect sample solution and checked for dissociation of cells. This was repeated every 2-3 min interval until rod-shaped, striated cardiomyocytes was observed. Following observation of the appearance of cardiomyocytes, stirring was stopped and tissue chunks were allowed to settle for about 30 seconds. The supernatant was carefully filtered through a nylon mesh (200 µm) into 50 ml Falcon tube (Tube A) and the retained tissue chunks on the nylon mesh were returned to the beaker. The tissue chunks were again re-suspended with 20 ml storage solution composed of "Feng medium" (**Table 3**). To further dissociate cells, a gentle mechanical resuspension using a 20 ml serological pipette with dispenser was performed slowly for about 30 sec to avoid bubble formation. The supernatant was then carefully filtered again through a nylon mesh (200 µm) into 50 ml Falcon tubes (Tube B).

In the final step, the final concentration of Ca^{2+} was adjusted. First, both falcon tubes A and B was centrifuged at 95 x g for 10 min and the supernatant was carefully removed by means of slow up-pipetting and was discarded. The pellets of both tubes A and B were separately re-suspended in 1.5 ml storage solution, composed of "Feng medium" at room temperature. Into these tubes, 7.5 µl of 10 mM $CaCl_2$ solution is added and incubated for 10 min, this step is

performed twice. After which, 15 µl of 10 mM $CaCl_2$-solution is added to obtain a final Ca^{2+} concentration of 0.2 mM. Cell yield was calculated for each cell preparation.

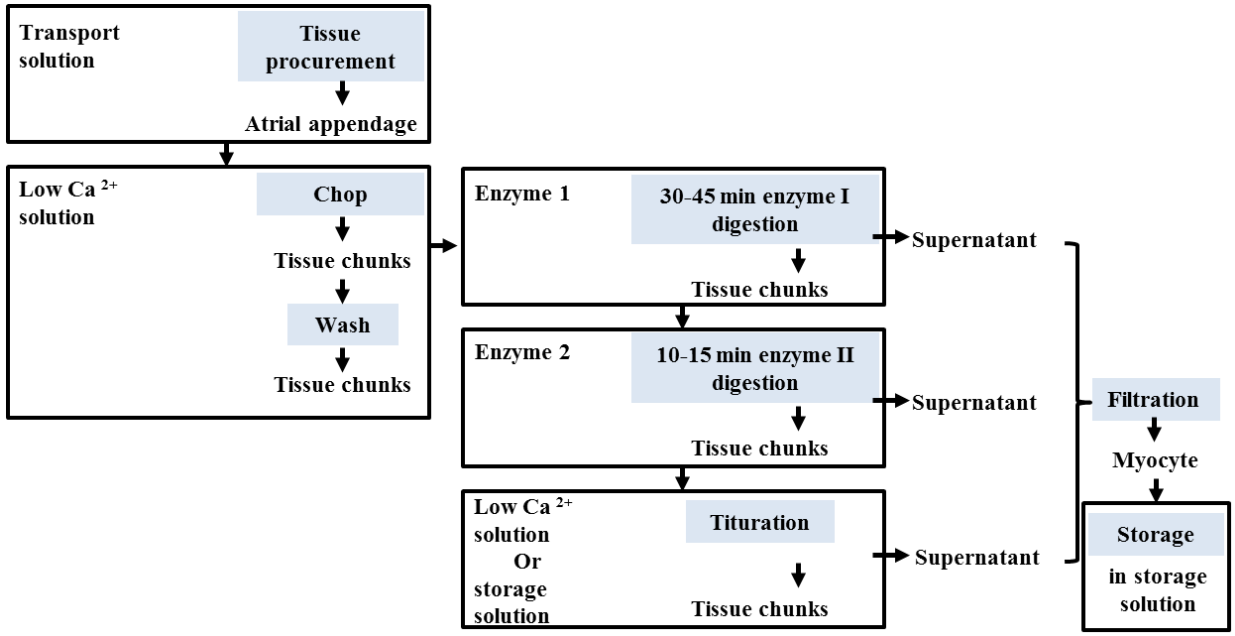

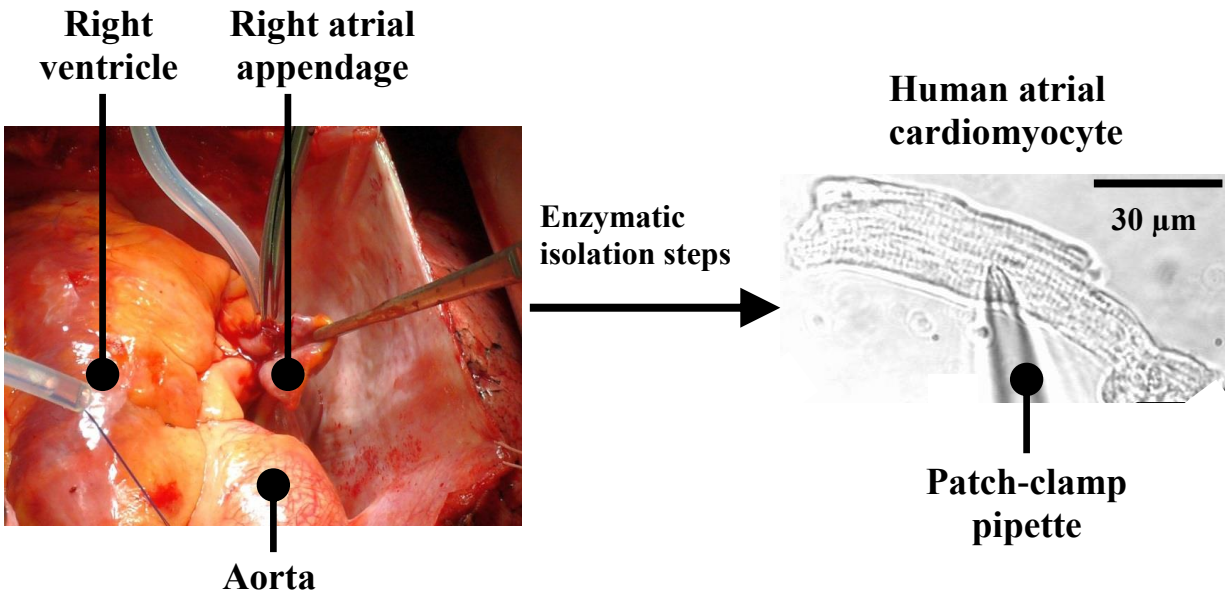

Figure 14: Flowchart of chunk digests method for isolation of human atrial cardiomyocytes.

Table 3: Solutions for human atrial cardiomyocyte isolation.

	Substance	Company
Ca^{2+}-free solution	20 mM Glucose	Sigma Aldrich
	10 mM KCL	Merck
	1.2 mM KH_2PO_4	Sigma Aldrich
	5 mM $MgSO_4$	Sigma Aldrich
	5 mM MOPS	Sigma Aldrich
	100 mM NaCL	Sigma Aldrich
	50 mM Taurin	Sigma Aldrich
Enzyme solution E1 and E2	20 mM Glucose	Sigma Aldrich
	10 mM KCL	Merck
	1.2 mM KH_2PO_4	Sigma Aldrich
	5 mM MgSO4	Sigma Aldrich
	5 mM MOPS	Sigma Aldrich
	100 mM NaCL	Sigma Aldrich
	50 mM Taurin	Sigma Aldrich
	286 U/ml Collagenase I	Worthington
	5 U/ ml Protease XXIV *****	Sigma Aldrich
Storage Solution „Feng medium“	1% Albumin	Sigma Aldrich
	10 mM Glucose	Sigma Aldrich
	10 mM DL-β-hydroxybutyric acid	Sigma Aldrich
	70 mM L-Glutamic acid	Sigma Aldrich
	20 mM KCL	Merck
	10 mM KH_2PO_4	Sigma Aldrich
	10 mM Taurin	Sigma Aldrich

* Protease XXIV is included only in the Enzyme solution E1

pH is adjusted to 7 for all solution with 1 M NaOH, except storage solution, where 1 M KOH is used.

Table 4: Specific equipment for cell isolation.

Equipment	Company	Catalogue number
Nylon Mesh	VWR	510-9527
Jacketed reaction beaker	VWR	KT317000-0050

3.2 The patch-clamp technique

3.2.1 The history of patch-clamp technique

The origin and development of electrophysiology to the patch-clamp technique can be traced back to the very pioneers of electrophysiology described by (Verkhratsky et al. 2006). In the 1660`s, Jan Swammerdam, the Dutch microscopist and natural scientist discovered contraction upon initial stimulation of the nerve of a large muscle he separated from a frog thigh. He called this "irritation". Eighty years later, the story of ion channels began with the work of Luigi Galvani, an Italian physician and physicist. In his book, "DE Viribus Electricitatis in Motu Musculari Commentarius" he described his observations on over 10 years on contraction of isolated frog nerve-muscle preparations. He identified electrical excitation of the nerve-muscle preparation and found the relationship between stimulus intensity and muscle contraction. His breakthrough was in the period of 1794 - 1797, where he used two frog legs of his preparation and showed that stimulation of the nerve of the first preparation induced contraction of the second preparation when both nerves came in contact. Based on his work, the theory of electrical excitation was developed. He hypothesized that "animal electricity" resulted from positive and negative charges accumulating on external and internal surfaces of muscle or nerve fibers. Later, in the 19th century, it was suggested that cells have a conductive cytoplasm, surrounded by a membrane composed of lipids that were hardly electrically conductive, but were permeable to water and many low molecular weight substances.

In the 1930`s, Kenneth Cole and Howard Curtis developed the principle of voltage clamp and independent of Alan Hodgkin and Andrew Huxley, they used this principle to measure the AP of a squid axon using external electrodes for the first time (Hodgkin & Huxley 1939; Curtis & Cole 1942). In 1949 Cole and Marmont designed the voltage-clamp technique which was used by Hodgkin and Huxley to develop the ionic theory of membrane excitation, which was published in a series of landmark publications (Hodgkin et al. 1952a; Hodgkin & Huxley 1952b; Hodgkin & Huxley 1952c; Hodgkin & Huxley 1952d; Hodgkin & Huxley 1990). This theory stated that membrane excitability is determined by passive ion fluxes according to their electro-chemical gradients, which implied existence of transmembrane aqueous pathways. They interpreted membrane permeability as the selective opening and closing of ion channels and in 1963, they were awarded the Nobel Prize in Physiology or Medicine for their work.

In the 20th century, the first recordings of single ion channel currents of isolated membrane patch by Erwin Neher and Bert Sakmann (Neher & Sakmann 1976) with the help of microelectrodes and voltage clamp and the discovery of the high resistance (giga-ohm) seal

between very thin smooth micropipette tips and surface cell membranes (the so-called giga-seal) (Hamill et al. 1981) led to the invention of the patch-clamp technique. For this work, another Nobel Prize was awarded in Physiology or Medicine in 1991. The different configuration, whole-cell- and the cell-attached configuration as well as the inside-out- and the outside-out-configuration are described in detail in the seminal work of Hamill et al (Hamill et al. 1981).

3.2.2 The principle of patch-clamp technique

Studies of the electrical properties of biological membranes, particularly of excitable cells such as neurons, cardiomyocytes and muscle fibers can be sub grouped into roughly two categories: those that employ extracellular recording techniques and those that employ intracellular recording techniques. Intracellular recordings measure the difference in voltage or current across a cell membrane (the patch-clamp technique), whereas extracellular recordings measure differences in these parameters within the extracellular space. Intracellular recording of transmembrane currents while holding transmembrane voltage at a known value is referred to as voltage-clamp method, whereas measurement of transmembrane voltage while holding transmembrane current constant is referred to as current-clamp technique (Kornreich 2007).

The principle of the patch-clamp recording technique usually makes use of a small glass pipette (with microelectrode) containing a conductive salt solution that allows the investigation of one side of a membrane (the intracellular space) for comparison to a reference electrode placed on the other side of the membrane (the extracellular space). Depending on the configuration, a set of ion channels on the whole-cell membrane or just single ion channels on a cell membrane can be investigated.

An ion channel can conduct up to 10 million ions per second. This however, generates only a few picoamperes of current and recording this current at such low magnitude is quite challenging. In principle, a pipette (with microelectrode) attached to cell is coupled to amplifiers as shown below (**Figure 15**). Descriptively, suction is applied through the pipette to aid the development of a high-resistance seal in the giga-ohm (GΩ) range with the cell membrane. This tight seal isolates the membrane patch electrically, creating a continuous electrical field between the membrane (all ions fluxing the membrane) and the pipette. These electrical properties are recorded by a chlorinated silver electrode connected to a highly-sensitive electronic amplifier system, with a bath electrode used to set the zero level. Alterations in the membrane potential are prevented with a compensating current generated

by the amplifier as a negative feedback mechanism that counteracts the current that is flowing through the membrane.

The membrane potential of the cell is measured and compared to the command potential (**Figure 15**). If differences occur, a current will be injected (compensation current) in a voltage-clamp configuration. This compensation current is recorded and reflects the time and voltage dependent changes of membrane conductance. Manipulation of the membrane potential allows for the investigation of the current-voltage relationships of membrane channels of isolated tissue preparations, single cells and reconstituted lipid bilayers. By holding the membrane potential constant, the time- and voltage dependence of changes in membrane conductivity (and of individual membrane current such as $I_{Ca,L}$) can be studied. This is the "new" concept which Cole and Moore and more extensively Hodgkin and Huxley used to describe time and voltage dependence of Na^+ and K^+ currents. This current work focuses primarily on the use of voltage-clamp techniques to characterize the behavior of specific ion channels in isolated atrial cardiomyocytes.

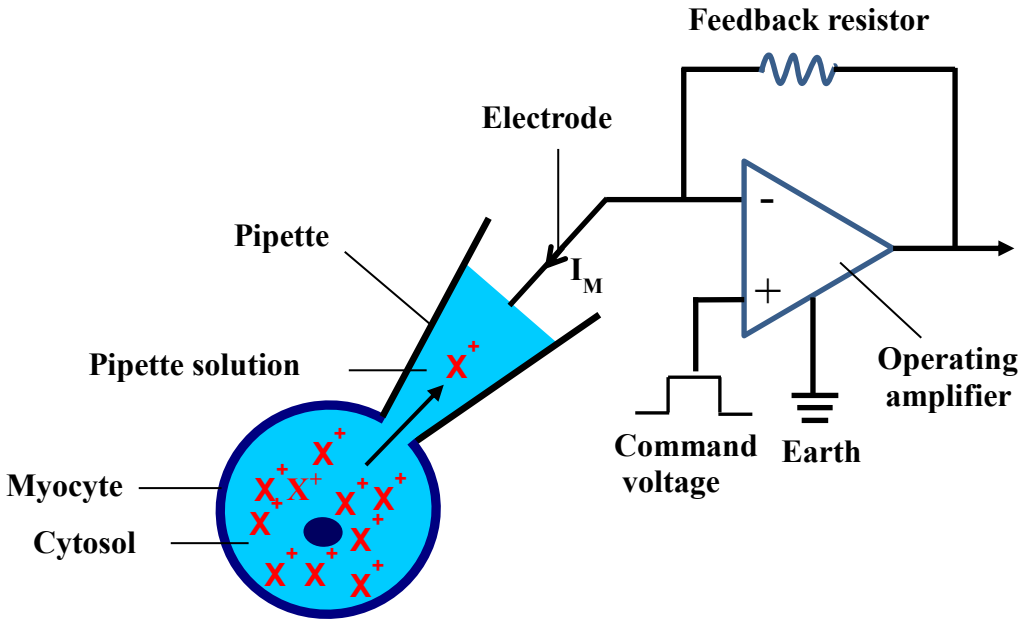

Figure 15: General principle of patch-clamp recordings.

A glass pipette containing pipette solution is tightly sealed onto the cell membrane. The ruptured membrane patch is isolated electrically. Currents fluxing through the channels in the membrane flow into the pipette and can be recorded by an electrode that is connected to a highly-sensitive differential amplifier. In the voltage-clamp configuration, a current is injected into the cell via a negative feedback loop to compensate changes in membrane potential. Recording this current allows conclusions about the membrane conductance.

3.2.3 The patch-clamp setup

The patch-clamp setup can be divided into components that influence the extracellular milieu, such as measuring chamber, perfusion system and the quick solution chamber. Other components include instruments that serve for the actual measurement of membrane channels (amplifier, software), optical devices (microscope and video imaging) and mechanical (vibration damped table) and electrical shield (Faraday cage). For better understanding, a picture of the used patch-clamp setup is shown on **Figure 16** (other details given in **Table 5**).

A measuring chamber made of a Plexiglas (RC-24E, Warner Instruments), was used to conduct recordings. The chamber has 3 wells, 2 interconnected and one solo well and can contain up to a volume of 150 µL. The floor is decked with a cover glass slide (22 x 40 mm, Warner Instruments), using Vaseline for adhesion. For continuous perfusion of the chamber, some solution from the solution changer arm was perfused out of the chamber through a side-mounted cannula in a hose tube connected to a vacuum pump system (Scientific instruments) which allows even suction of the solution. An agar bridge was mounted in an adjacent well, inter-connecting all wells in the chamber through a reference electrode solution. This created a circuit between all wells in the measuring chamber.

To study the electrical activity of a membrane patch, patch pipettes filled with pipette solution were used to electrically isolate the membrane patch. In the whole-cell patch configuration (see below), the pipette solution diffuses into the interior of the cell, as such should have a similar composition to the intracellular content of the cell. A thin chlorinated silver wire was put into a pulled pipette which was later filled with pipette solution (see below). Silver/silver chloride electrodes were made using 3 M KCl and an electronically controlled current source (version ACL-0, Npi electronics, Germany). The pipette holder, with the glass pipette was attached directly on the pre-amplifier, creating an electrical connection of the electrode to the amplifier. The hydraulic micromanipulator was connected to the preamplifier attached to the pipette holder. This allowed for three-dimensional mobility of the pipette in chamber well containing cells. With this, the pipette could be moved very precisely in all directions and placed on the cell to be measured. Another hose was connected from the patch pipette to a glass syringe, through which a positive or negative pressure could be applied to the patch pipette. The glass pipettes were prepared as described below for each experiment. All components are placed on a vibration-damped table (TMC, GIMBAL PISTON™, AMETEK Ultra Precision Technologies), which was itself inside a Faraday cage. The vibration-damped table minimizes mechanical disturbances induced by environmental factors. The Faraday cage is made of thin aluminum (~2mm) with shielded electrical background noise, in particular, from the 50 Hz-hum caused by public voltage grid. The Faraday cage was connected through

a cable to the ground input of the amplifier. The manual control unit of the micromanipulator is located outside the vibration-damped table to prevent vibrations through manual manipulations.The preamplifier receives current signals as voltage via a feedback resistor. The signal is then amplified by the main amplifier (Axopatch B200, Axon CNS, Molecular Divices, Germany) and passed through the built-in Low-pass filters (3 kHz). The analogue-digital (AD) converter then digitized the measured data, which was displayed on the computer.

The pClamp-Software (Version 10.2, Axon™ pCLAMP™, Molecular Devices, Sunnyvale, CA) was used for data acquisition and Clampfit (Version 10.4, Axon™ pCLAMP™, Molecular Devices, Sunnyvale, CA) for data analysis. For imaging, an inverted microscope unit coupled with a Video camera was used for screen monitoring allowing for better view for cell patching and monitoring of a seal formation and also actively observing the entire experiment. For fast perfusion of cells with different compounds or drugs, a rapid-solution exchange system was used.

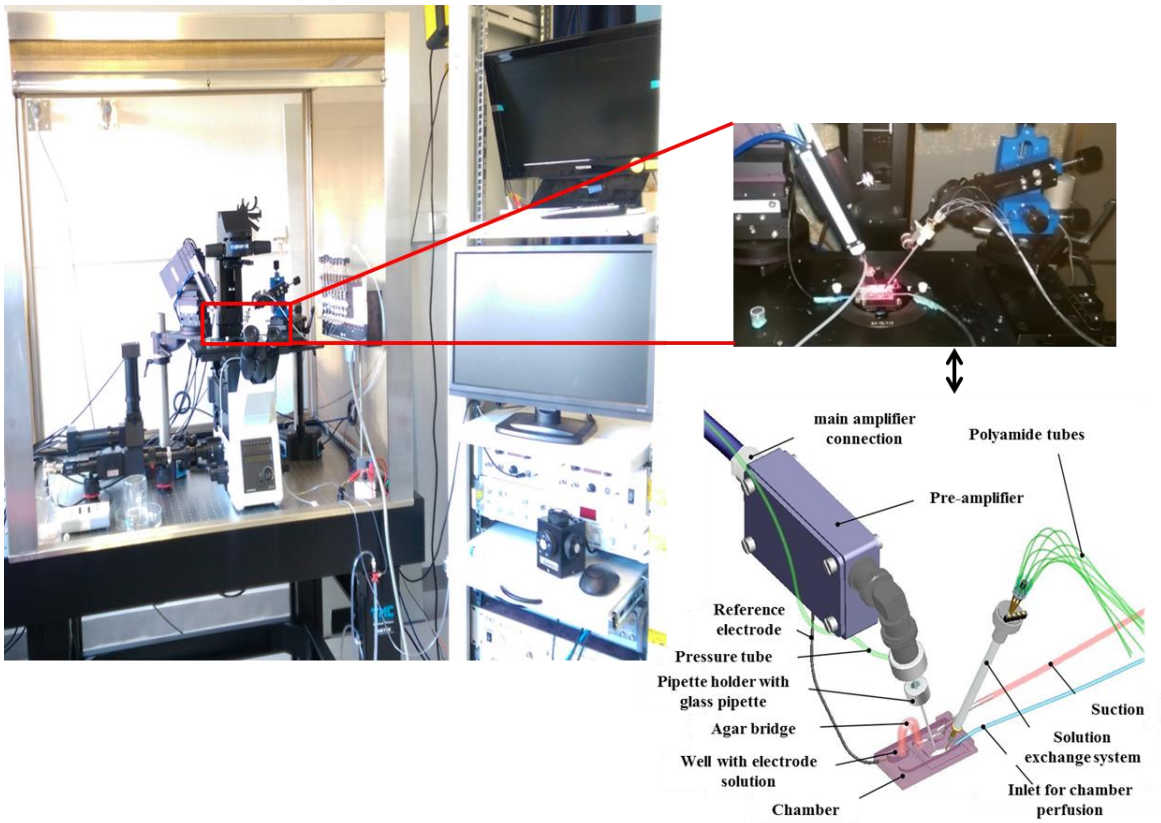

Figure 16: Patch-clamp setup.

Left: Setup of the measurement with Faraday's cage, vibration-damped table, a perfusion system, an inverse microscope and micromanipulator outside. Right: measuring chamber setup.

Table 5: Instruments for patch-clamp setup.

Instrument	Company
Microscope	IX73, Olympus
Filters	Olympus
Computer and monitor	hp and Prolite E2280HS iiyama
DAD-VM superfusion system	ALA Scientific Instruments
Camera	WAT-902 Hz Supreme,
CV 203BU Headstage	Axon CNS, Molecular Divices CNS,
Axopatch B200 amplifier	Molecular Devices
Rapid-solution exchange system	ALA Scientific Instruments

3.2.4 Pipette tip preparation for patch-clamp recordings

For whole-cell patch-clamp applications, the resistance of a pipette tip when filled with pipette solution was 2-5 Mega-ohms (MΩ). To achieve this morphology, medium-hard thin walled borosilicate glass capillaries (1.5 mm outer diameter) with filaments were used (World Precision Instruments GmbH, Germany). They were pulled with a DMZ - Universal puller (Zeitz instruments GmbH, Munich, Germany) and kept protected from dust particles under a glass beaker. Capillaries with filaments have a small thin rod of glass adhered to the inner wall, which facilitate the capillary action of drawing the solution to the tip of the pipette without interfering with the forming of a GΩ seal. This might help reduce development of air bubbles when filling the pipette with pipette solution. These capillaries were first reduced by cutting with the help of a diamond tipped pen to 7 cm. Pipettes with a resistance of 2.5 - 5 MΩ were made with the help of a DMZ–Universal puller program, which is basically hot slide-polishing steps as detailed below. From each capillary, the pipette puller pulled two pipettes apart and polished them. The pipettes were then stored under a glass beaker to prevent blockage of pipette tips by dust, ready for use.

The pulling procedure and the detailed pulling program were adapted from pre-existing programs on the DMZ-Universal puller manual. The P (A) is the first pulling phase and P (B) is the final pull phase including polishing. To achieve smaller tip diameters P (B) t(F1) is decreased and simultaneously P (B) F1 and F2 increased.

Pipette DMZ-Universal Puller Program

P (A)

H	900	Heat for glass softening
F(TH)	020	Preliminary pull, force for glass elongation
s(TH)	017	Distance threshold for elongation (H and F(TH) terminated when reached)
t(H)	072	Position of right-hand electrode for polishing
s(H)	042	Position of left-hand electrode for polishing
t(F1)	050	Delay before starting main pull F1; starts at s(TH)
F1	015	Force, first phase of main pull
AD	020	Low heat range for main pull

P (B)

H	040	Heat strength for main pull (see AD above)
F(TH)	030	Sensing pull, force for sensing glass stiffness
s(TH)	010	Distance threshold for elongation (F(TH) terminates)
t(H)	030	Delay before heat is terminated; starts at s(TH)
s(H)	000	Distance threshold for termination of heat.
t(F1)	000	Delay before starting main pull F1; starts at s(TH)
F1	170	Force, first phase of main pull
s(F2)	002	Distance threshold for start of second force phase, main pull F2. Distance measured from s(TH)
F2	185	Force for second phase of main pull
AD	207	Polishing program heat strength activated, 2s duration

3.2.5 Reference electrode

The reference electrode was a siver/silver chloride electrode placed into a 50 mM KCl solution. This solution was filled in the well and connected by the agar bridge to the bath solution. This KCl concentration was chosen to minimize the offset potential between patch pipette and the reference electrode as much as possible. It was used for all patch-clamp experiments. The chloride concentration in the reference well should be the same as in the recording electrode.

3.2.6 Experimental design of different patch-clamp configurations

After cardiomyocyte isolation, cells were suspended in 1 mL Tyrode solution. Cells were transferred into the measuring chamber using 100 µL pipettes. For each experiment, about 70 µL of cell suspension was transferred into the measuring chamber and cells were allowed to settle for approximately 5 min. A suitable cell based on the criteria of cell morphology (clear striations, intact membrane or membrane integrity), cell size and also position of the cell in the measuring chamber (suitably in the middle of the chamber) was selected for measurement (**Figure 17**).

Figure 17: A picture of a representative human atrial cardiomyocyte.

Atrial cardiomyocyte showing clear striation, intact membrane thus appearing suitable for current recording.

Next, the mouth of the rapid-solution exchange system is placed at a distance of about 200 µm to the examined cell, to quickly supply the desired target concentration of a test compound to the cell and monitor the effects. The pipette filled with pipette solution was then immersed in the chamber while carefully avoiding breaking of the pipette tip. To avoid clogging of the pipette with dirt, a slight overpressure was produced using a syringe. Once the pipette touched the surface of the solution in the chamber (bath solution), the resistance of the pipette could be determined by a test pulse and was observed as an offset potential of the pipette on the measurement protocol. This was adjusted by manually tuning on the amplifier. The resistance of the filled pipette with the electrode solution was between 2-5 MΩ, corresponding to the diameter of the pipette orifice of about 1 µm which is important for both a very strong sealing resistance (GΩ-seal) as well as to obtain a sufficiently good access (series resistance < 10 MΩ)

3.2.6.1 Creation of the cell-attached configuration

After the set-up, the pipette tip was gently lowered onto the cell membrane with the help of the micromanipulator. As the pipette approached the cell, it was observed on the monitor as a characteristic reflection of light and a slight increase of the pipette resistance till a clear appearance of the pipette pointing the cell membrane. It was then lowered enough to pin the

cell immobile during chamber perfusion. The overpressure was removed by releasing the syringe to the open mode. A slight negative pressure was applied through the syringe to obtain a stable seal of about 1-2 GΩ between the pipette and the cell membrane (usually within 30 seconds **Figure 18)**.

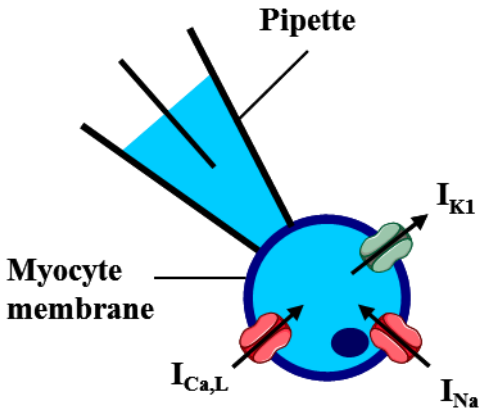

Figure 18: Cell-attached configuration.

3.2.6.2 Creation of the whole-cell configuration

In order to access the whole-cell configuration from the cell-attached configuration, the cell membrane was broken by suction to the pipette with a slight negative pressure applied using a syringe (ruptured patch; **Figure 19**). The ruptured patch of the membrane inside the tip of the pipette with electrode allows the intracellular space to be in contiguous with the internal pipette solution. This could be confirmed through the formation of the capacitive discharge current that was observed compared to the rectangular pulse test at the beginning and the end of each pulse. The cell membrane capacitance (C_M), as well as the series resistance is compensated to some degree (up to ~70%) by manual tunings on the amplifier. At this point, measurements according to protocols of interest were performed. For this work, the protocols allowed for measurement of whole-cell membrane currents (I_M).

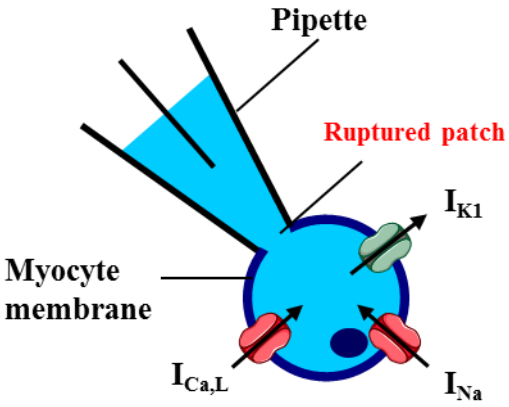

Figure 19: Whole-cell configuration.

3.2.7 Determination of the membrane capacitance as cell size index

At the beginning of each experiment the capacitance (C_M) of the cell was determined as surrogate of cell size assuming a constant specific membrane capacity of 1 µF/cm^2. The capacitance (C in farads), is the amount of charge (Q in Coulomb), which an object can hold at a certain electric potential (U in volts). It is expressed as: C = dQ/dV. The C_M of the cell is directly proportional to the surface area of the cell (1 pF/1 µm^2; Gentet et al. 2000). The C_M was determined through a standard voltage protocol, expressed as: dV/dt = (dQ/dt)/C_M where t, is time. Since the current capacitance I_C is also valid as dQ/dt, the membrane capacitance can be expressed as C_M = I_C / (dV/dt). To measure the membrane capacitance with the standard voltage protocol, dV/dt was kept constant at a potential -80 mV close to membrane potential to have a resulting current in pA, close to the membrane capacitance in pF. Since cells with different sizes (capacitance) have different current amplitudes, the total current amplitude (I in pA) is divided through the membrane capacitance (C_M in pF) of the cell to yield the normalized membrane current density (pA/pF).

3.3 Whole-cell patch-clamp recording of I_{K1} and $I_{K,ACh}$

In the cell isolation procedure for the measurement of inward-rectifier K^+ currents, Ethylene glycol-bis (β-aminoethyl ether)-N,N,N',N'-tetraacetic acid (EGTA, 10 mM, a Ca^{2+} buffer) was added to the Feng medium. During cell isolation EGTA binds to intracellular Ca^{2+}, thereby reducing cell contraction.

3.3.1 Voltage-clamp protocol for I_{K1} and $I_{K,ACh}$ recordings

I_{K1} was activated by means of a voltage-ramp protocol at 0.5 Hz and room temperature (RT; **Figure 20**). The holding potential was -80 mV. The protocol began with a short voltage step to -100 mV for 50 ms, after which the cells were then depolarized with a voltage ramp within 1250 ms from -100 mV to +40 mV. The subsequent voltage jump to -50 mV for 50 ms allows for the assessment of possible leak current. Under ideal conditions at this potential, no current flows. The cell is clamped at a holding potential of -80 mV, until a new protocol starts again. This ramp protocol allows for activation of inward-rectifier K^+ currents only because with the slow change in voltage inward currents like I_{Na} and $I_{Ca,L}$ that activate during depolarization then quickly inactivate without causing any significant inward currents.

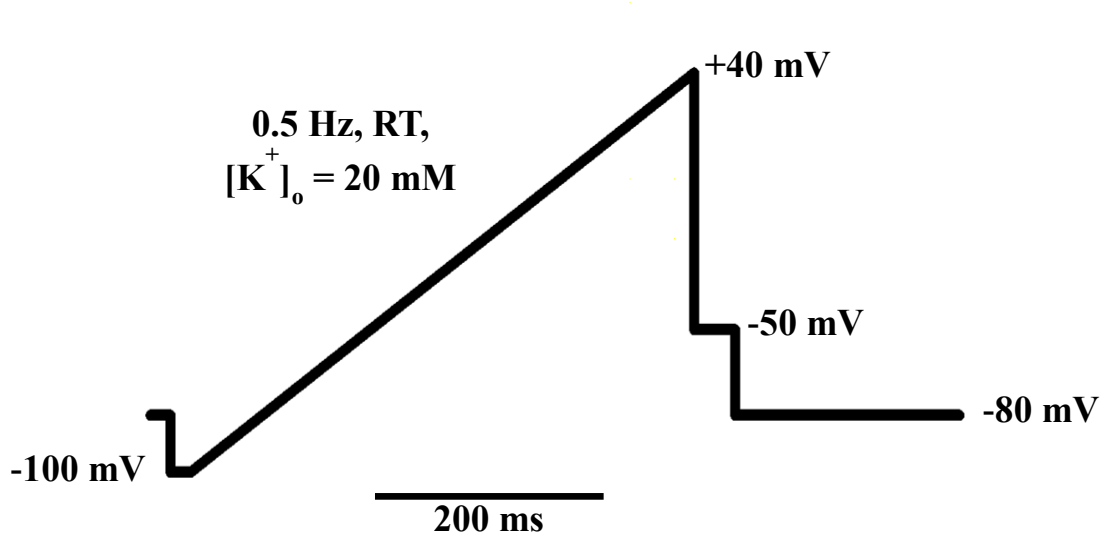

Figure 20: Voltage-ramp protocol for I_{K1} and $I_{K,ACh}$ measurements.

3.3.2 Working solutions for I_{K1} and $I_{K,ACh}$ recordings

After allowing the cells to settle in the measuring chamber for about 5 min, the cells were continuously perfused with bath solution. The bath solution (also known as Tyrode's solution) contained glucose as energy source and roughly reflects interstitial fluid. Adjustments can be made to this solution for various purposes depending on experimental interest e.g. to test the effect of drugs. The bath solution here contained 120 mM NaCl, 20 mM KCl, 1 mM $MgCl_2$. H_2O, 10 mM HEPES, 2 mM $CaCl_2$, and 10 mM glucose. It was prepared in stock volumes of 1 L and the pH adjusted to 7.4 with 1 M NaOH and kept at 8°C. $CaCl_2$ and glucose were only added on the experimental day.

The physiological equilibrium potential of K^+ is about -80 mV. The high extracellular KCL concentration (20 mM) shifts the reversal Nernst potential of K^+ (E_K) to about -50 mV and allows to record reliable larger amplitude I_{K1} and $I_{K,ACh}$.

The Nernst potential:

$$EK^+ = \frac{R \cdot T}{F \cdot z} \cdot ln \frac{[K^+]_\alpha}{[K^+]_i} = \frac{8{,}314\,J \cdot 293{,}15\,K}{96487\,C} \cdot ln \frac{20\ mM}{150\ mM} = -51\ mV$$

(Where R is the universal gas constant, T is the absolute temperature, F is the Faraday`s constant and z is the valence of the ion)

$I_{K,ACh}$ was activated with the non-selective muscarinic-receptor agonist carbachol (CCh) at a concentration of 2 µM as described in (Dobrev et al. 2001). Identity of recorded currents as inward-rectifier K^+ currents was achieved by inhibition with 1 mM $BaCl_2$ (Alagem et al. 2001). Stock solutions of 1 mM CCh and 1 M $BaCl_2$ were prepared and stored at -20°C.

On the experimental day, 500 mL of the working bath solution (Tyrode's solution) was prepared accordingly: 450 mL of aqua desk, 50 mL of bath stock solution, 1 g of glucose, 1 mL of $CaCl_2$. Subsequent solutions were prepared from this bath working solution (Tyrode's solution). CCh working solution was prepared as 10 mL Tyrode's working solution plus 20 µL of 1 mM CCh to have an end concentration of 2 µM CCh. Ba^{2+} working solution was prepared as 10 mL Tyrode's working solution plus 10 µL of 1 M $BaCl_2$ to have an end concentration of 1 mM Ba^{2+}. All substances were purchased from Sigma Aldrich and all solutions were made using aqua desk from B. Braun Melsungen AG.

The effects of the I_{K1} blocker PA-6 (kind gift from the Lab of Dr. Van de Hayden, Utrecht) on basal inward-rectifier K^+ currents were tested by acute application through the rapid-solution exchange system.

3.3.3 "27 A" pipette solution

The "27 A" pipette solution contained 5 mM EGTA, 0.1 mM GTP-Tris, 10 mM HEPES, 80 mM K-aspartate, 40 mM KCl, 5 mM Mg-ATP, 8 mM NaCl, 2 mM $CaCl_2$. The pipette solution was adjusted to pH of 7.4 with 1 M KOH. EGTA buffers Ca^{2+} and Mg^{2+}, minimizing cell contractions which hamper seal formation (Wang et al. 2004). ATP served as energy source for the cell. Its Mg^{2+} salt was used because pure ATP would bind strongly to Mg^{2+} and build a Mg^{2+}-complex with all Mg^{2+} ions of the cell. The GTP-Tris is assumed to trigger the G-proteins associated membrane signal transduction systems. All substances were purchased from Sigma Aldrich except Fluo-3 from Invitrogen. Pipette solutions were prepared stored in 1 ml Eppendorf tubes at -20°C. On experimental day, pipette solution was kept cool on ice.

3.4 Whole-cell patch-clamp recording of $I_{Ca,L}$ and Ca^{2+}-induced $[Ca^{2+}]_i$

Unlike for I_{K1} measurement, cells were first loaded with a Ca^{2+} indicator (Fluo-3, Invitrogen, Germany) for 10 min to allow for simultaneous measurement of $I_{Ca,L}$ and Ca^{2+}-induced $[Ca^{2+}]_i$. All experiments were performed at 37°C.

3.4.1 Voltage-clamp protocol for $I_{Ca,L}$ recordings

$I_{Ca,L}$ was measured with a standard voltage-clamp protocol at 0.5 Hz (**Figure 21**), as described (Voigt et al. 2012). From a holding potential of -80 mV a ramp pulse until -40 mV for 100 ms was used to inactivate Na^{2+} channels. A subsequent step to +10 mV activated the $I_{Ca,L}$ thereby triggering a corresponding $[Ca^{2+}]_I$ transient (CaT).

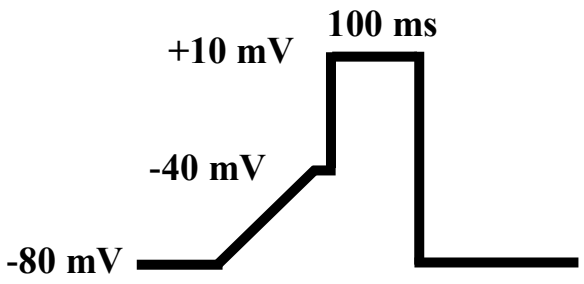

Figure 21: Standard voltage protocol for $I_{Ca,L}$ measurement.

3.4.2 Bath solutions for $I_{Ca,L}$ and Ca^{2+}-induced $[Ca^{2+}]_i$ measurement

The bath solution for these measurements contained 2 mM $CaCl_2$, 10 mM glucose, 10 mM HEPES, 48 mM KCl, 1 mM $MgCl_2$, 140 mM NaCl, and 2 mM probenecid. The solution was adjusted to a pH of about 7.4. K^+-currents were blocked by adding 4-aminopyridine (5 mM) and $BaCl_2$ (0.1 mM) to the bath solution and caffeine (10 mM) for almost complete depletion of Ca^{2+} from the SR. The bath solution was prepared in volumes of 1 L and stored at 8°C as stocks. On the experimental day, glucose and $CaCl_2$ were then added to the working solution of 100 mL to minimize bacterial growth. All substances were purchased from Sigma Aldrich. The effect of IL-1β (40 ng/mL from Thermo Fisher Scientific / Gibco) on $I_{Ca,L}$ and Ca^{2+}-induced $[Ca^{2+}]_i$ were tested by acute application through the rapid-solution exchange system.

3.4.3 Pipette solution for $I_{Ca,L}$ and Ca^{2+}-induced $[Ca^{2+}]_i$

This pipette solution compared to "27 A" pipette solution contained 0.02 mM EGTA, 0.1 mM Fluo-3, 0.1 mM GTP-Tris, 10 mM HEPES, 92 mM K-aspartate, 8 mM KCl, 1 mM Mg-ATP, 4 mM Na_2-ATP. The pipette solution was adjusted to pH of 7.2 with 1 M KOH. Pipette solutions were prepared and stored in 1 ml Eppendorf tubes at -20°C. Fluo-3 from 1 mM stock solution was added to the pipette solution prior to begin of each experiment and stored on ice. All substances were purchased from Sigma Aldrich except Fluo-3 from Invitrogen.

3.4.4 Epifluorescence imaging for Ca^{2+} measurements

Epifluorescence imaging is a technique used to optically investigate intracellular Ca^{2+} in living animals, allowing studies of Ca^{2+} signaling in a wide variety of cell types. It makes use of Ca^{2+} indicators (fluorescent molecules) that react to the binding of Ca^{2+} ions by changing their fluorescence properties. In this work, Fluo-3 was used. The absorption and emission peaks of Fluo-3 are 506 and 526 nm, respectively. It is excited with an argon ion laser at 488 nm, and its emitted fluorescence (at 500 nm, **Figure 22**) rises with increasing [Ca^{2+}] (Takahashi et al. 1999). **Table 6** lists the instruments of the epifluorescence setup.

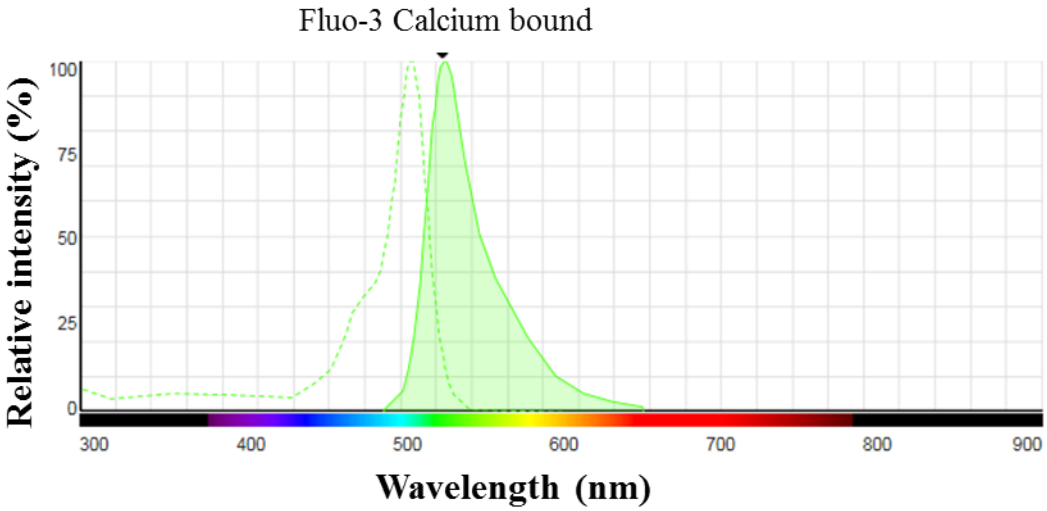

Figure 22: Fluorescence spectrum.

The fluorescence spectrum shows the emission fluorescence of Fluo-3 at 500 nm. Adapted from Fluorescence SpectraViewer. (n.d.). *Thermo Scientific™ Web site*.

Table 6: Instruments for epifluorescence setup.

Instruments	Company
Opto Lite	Cairn Research
High intensity arch lamp	Cairn Research
Optoscan	Cairn Research
Optoscan Monochromator	Cairn Research

3.4.4.1 Loading of human atrial cardiomyocytes with Ca^{2+} indicator

Human atrial cardiomyocytes were loaded with Ca^{2+} indicator Fluo-3AM as described (**Figure 23;** Voigt et al. 2013). Briefly, 1.5 ml of cell suspension was transferred into a 2 ml micro centrifuge Eppendorf tube and 15 µL of Ca^{2+} indicator Fluo-3 solution was carefully

added. This Ca^{2+} indicator Fluo-3 solution contained 50 µg of the membrane permeable acetoxymethyl ester derivative of Fluo-3 (Fluo-3AM, **Table 7**) dissolved in 44 µL of the Pluronic F-127 (**Table 7**) stock solution (20% w/v in anhydrous DMSO) to get a 1 mM Fluo-3AM stock solution, which could be stored at -20 °C for about 1 week. The micro centrifuge Eppendorf tube containing 1.5 ml of cell suspension and 15 µL of Fluo-3AM stock solution were incubated for 10 min in an optically opaque box or black box, after which it is centrifuged, considering sensitivity of Fluo-3AM to light at about 6,000 rpm. After centrifugation, the supernatant was discarded and pellets re-suspended in 1.5 ml of bath solution. The cell suspension was kept for 30 min in a dark box for de-esterification before used to perform experiments.

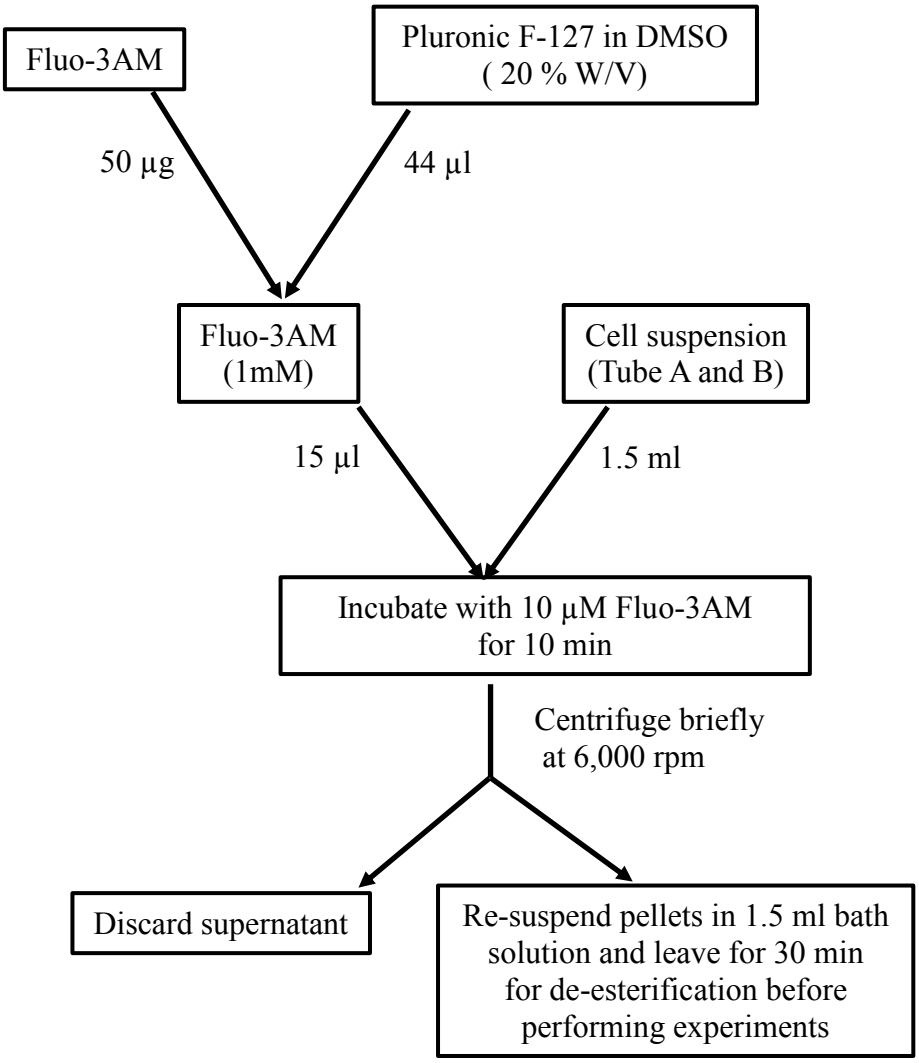

Figure 23: Flow chart for loading of human atrial cardiomyocytes with Fluo-3.
m/v, mass/volume. Adapted from Voigt et al. 2013.

Table 7: Fluo-3AM solution for loading human atrial cardiomyocytes.

Substances	Company
Dimethyl-sulphoxide	Sigma Aldrich
Fluo-3AM	Invitrogen
Pluronic F-127	Invitrogen

3.5 Western blotting

Western blotting, also called immunoblotting, is a semi-quantitative technique for protein detection (Towbin et al. 1979). It makes use of antibodies to identify specific protein targets bound to a membrane. The specificity of the antibody-antigen interaction allows a target protein to be identified amidst a complex protein mixture. The principle of Western blotting is based on separation of proteins in a sample by size using denaturing gel electrophoresis (i.e., sodium dodecyl sulfate polyacrylamide gel electrophoresis, SDS-PAGE). After electrophoresis, the separated proteins are transferred or "blotted" onto a solid matrix or membrane (e.g., a nitrocellulose membrane). The membrane is blocked with blocking buffer to prevent nonspecific binding of antibody probes to the membrane surface. The transferred protein is incubated consecutively with a primary antibody specific for the target protein and a secondary antibody/detection probe aimed at the primary antibody (e.g., enzyme, fluorophore). Depending on the detection probe used, an appropriate method is chosen to detect the immobilized probe. Using a marker with known molecular weight, the size of the protein is determined and its relative level is calculated with Image Studio Lite 5.2 software from LICOR Biosciences.

3.5.1 Protein isolation

Tissue samples were weighed (~100 mg) and stored in cryo-tubes in liquid nitrogen prior to protein isolation. The tissue sample was pulverized to a most fine form possible, using a mortar and pestle chilled in liquid nitrogen. According to the weight of the sample a 5-fold amount of Western blot buffer (**Table 8**) was added.

Table 8: Composition of Western blot buffer.

Substances	Company	Concentrations
EDTA	SIGMA	5 mM
Glycerol	ROTH	10 %
NaF	NUNCHRITZ	30 mM
Natrium dodecyl sulfate (SDS)	SERVA	3 %
Tris-(hydroxymethyl)-aminomethane (Tris)	ROTH	30 mM

Western blot buffer was supplemented with a protease-inhibitor-cocktail ("CompleteMini", ROCHE) in a ratio of 1:25 and a phosphatase-inhibitor-cocktail ("PhosSTOP", ROCHE) in a ratio of 1:10 to prevent degradation of proteins. After tissue homogenization with a homogenizer (IKA T10 basic Ultra Turrax, Sigma Aldrich) and subsequent centrifugation at 900 g for 10-15 min, the resulting supernatant was transferred into a new Eppendorf tube and stored at -80˚C. The remaining coarse cell fragments (pellets) contained in the tubes was discarded.

3.5.2 Protein determination

Pierce™ BCA Protein Assay Kit (23225) from Thermo Scientific was used to determine total protein content. Bicinchoninic acid assay (BCA assay) is a colorimetric method for the detection and quantification of total protein based on BCA reaction with protein. For reference values, a dilution series is performed using Bovine serum albumin (BSA) as standards (~ standard included in the Thermo-Scientific Pierce-kit). This kit contained: 1.) 1000 mL BCA reagent A, made of sodium carbonate, sodium bicarbonate, bicinchoninic acid and sodium tartrate in 0.1 M sodium hydroxide, 2.) 25 mL BCA reagent B, made of 4 % cupric acid sulfate and 3.) Albumin standard ampules, 2 mg/mL in 0.9 % sodium azide. The working solution contained 50 mL of Reagent A (containing sodium carbonate, sodium bicarbonate, bicinchoninic acid and sodium tartrate in 0.1 M sodium hydroxide) mixed with 1 mL of Solution B (containing 4 % cupric sulfate). BCA standards were prepared in the range 2 mg/mL to 0.08 mg/mL with a dilution in aqua dest. (dil factor of 0.5), for at least 7 points. 20 µL of these standards were transferred per well in a transparent flat-bottom multiwell plate (96 well, Greiner bio-one). 20 µL of Western blot buffer were taken for blank determinations. 20 µL of the supernatant of the test sample previously collected were then incubated with 200 µL of working solution for 30 min at 37°C. Depending on the expected amount of protein, a dilution of blank and sample is used in the assay to ensure that the protein results keep within the linear range of the BCA-assay. We used a 1:20 dilution of sample. Absorbance was then measured at 562 nm with a spectrophotometer (Infinite M200 PRO, TECAN) at RT. With the desired concentration, the test samples were first diluted in a ratio 1:6 with 6-fold Laemmli sample buffer (for composition see **Table 9**) and then boiled for 5 -10 min at 95°C.

Table 9: Composition of Laemmli buffer.

Substance	Company	Concentrations
Bromophenol blue	FLUKA	1 mM
Dithiothreitol	SIGMA	603 mM
Glycerol	ROTH	652 mM
Natrium dodecyl sulfate (SDS)	SERVA	12 %
Tris-(hydroxymethyl)-aminomethane (Tris)	ROTH	60 mM

The protein in the samples reduces Cu^{2+} to Cu^{1+} in an alkaline medium (the biuret reaction) giving rise to a water soluble chelate complex of two BCA molecules with one cupper cation (Pierce BCA Protein Assay Kit, **Figure 22**). The formation of a purple chelate complex with an absorbance at 562 nm is linear to the protein concentration over a broad concentration range (20 - 2000 µg/mL). The macromolecular structure of the protein, the number of peptide bonds and the presence of four particular amino acids (cysteine, cystine, tryptophan and tyrosine) all contribute to the color of the BCA chelate complex (Wiechelman et al. 1988). Therefore, protein concentrations are generally determined and reported with reference to standards of a common protein as BSA.

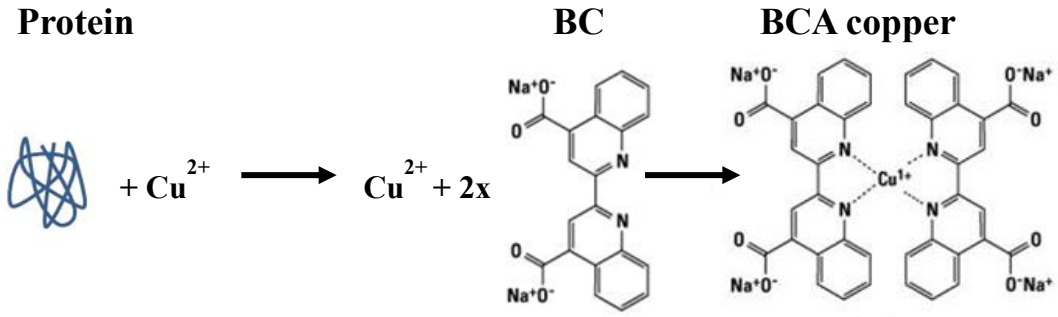

Figure 24: Schematic description of the BCA Protein Assay.

Proteins (especially cystein, cystine, tyrosin and tryptophan) reduce Cu^{2+} to Cu^{1+}. The cupper cation and two BCA molecules form the purple chelate complex which has an absorbance at 562 nm. Adapted from (Chemistry of Protein Assays. (n.d). *Thermo Scientific™ Web site*).

3.5.3 Preparation for gel electrophoresis

Gels at appropriate acrylamide-concentrations were freshly poured either at the beginning prior to the Western blot electrophoretic run or a day before and stored at 4°C. To accomplish this, a chamber was assembled, comprising of glass plates and a spacer clamped into the chamber holder provided (Bio-Rad). Separating gels, as well as stacking gels were mixed separately. The detergent SDS in the gel mixture allows protein separation according to size by giving the proteins a uniform negative charge. The amount of acrylamide determines the pore size of the gel and thus the strength of the protein separation.

The separating gel (**Table 10**) was filled up to 6 cm into the prepared chamber and a smooth finishing was achieved by overlaying with isopropanol. The stacking gel (**Table 10**) was then poured after 15 min. A comb with teeth of 0.75 mm width was inserted in the stacking gel to obtain pockets or wells. On a gel up to 10 pockets were created for protein loading. After 45 min the comb was removed and the gel was ready for use.

Table 10: Gel preparation for Western blot.

Substance	Company	Separating gel	Starking gel
Acrylamide	ROTH	8 %	8 %
10 % Ammoniumpersulfate (APS)	Bio-Rad	0.1 %	0.1 %
Tetramethylethylendiamin (TEMED)	Bio-Rad	0.1 %	0.1 %
10 % Natrium dodecyl sulfate (SDS)	SERVA	0.1 %	0.1 %
Tris-(hydroxymethyl)-aminomethane (Tris)	ROTH	0.4 mM	0.1 mM

3.5.4 General protocol for Western blotting

To run the test samples, the prepared gels were clamped in an electrophoresis chamber and placed in a buffer tank (mini PROTEAN System, Bio-Rad, **Figure 23**). This tank and the buffer-reservoir of the electrophoresis chamber were then filled with electrophoresis buffer (**Table 11**). The gels were loaded each with molecular weight markers "Precision Plus Protein Dual Xtra standard" (Bio-Rad) or ”Hi Mark pre-stained HMW protein standard” (Invitrogen) and with 50 µg protein of the test samples. By applying a voltage using the “PowerPac HC Power Supply” (Bio-Rad) initially at 80 V for 15 min, the test samples were compressed in the stacking and then at 110 V for 75 min. This time depends on the percentage of the gel and the size of the protein aimed at. 75 min would be quite long for a low percentage gel because small to mid-sized protein might be lost. The proteins move to the anode due to their negative charge and are being separated according to size. After electrophoresis run completion, the gel was carefully removed for protein transfer onto a nitrocellulose blotting membrane (pore size 0.2 µm, PeQlab). The nitrocellulose membrane was placed on the backside of the gel and both were positioned in the middle of a “sandwich” with two layers of blotting paper (GB003, 15 x 20 cm, Oehmen) and a fiber sponge on each side, all of this held by a gel holder cassette. The gel holder cassette was subsequently fixed into the cassette holder and inserted into a buffer tank filled with blotting buffer and ice cooling bags and a magnetic rod (Mini Trans-Blot cell, Bio-RAD) to stir and placed on a stirrer (**Figure 25**).

Figure 25: Electrophoresis setup.

Adapted from Mini Trans-Blot® Cell. (n.d.). *Bio-Rad Web site*.

Table 11: Electrophoresis buffer.

Substance	Company	Electrophoresis buffer	Blot buffer
Tris	ROTH	25 mM	25 mM
Glycin	Roth	192 mM	192 mM
SDS	SERVA	0.1 %	--
Methanol	VWR PROLABO	--	20 %

The electrophoretic transfer of the proteins on the membrane was conducted at 4°C under a constant voltage of 130 V for 90 min. Then, the membrane was checked for successful transfer by staining with Ponceau S (ROTH) for 5 -10 min. After this, the membrane was trimmed and then incubated with different antibodies for detection of specific proteins of interest and TBST buffer (**Table 12**) is used to un-stain the membrane. Before application of antibodies to the membrane, the remaining protein binding sites on the membrane were blocked with a blocking buffer (LI-COR®), diluted 1:1 in aqua desk for 1 hr. As such the amount of non-specific binding and therefore background staining was minimized. After the washing step with TBST, the membrane was first incubated with primary antibody at 4˚C overnight. The antibodies used are listed in **Table 13**.

Table 12: TBST buffer.

Substance	Company	Concentration
Tris	ROTH	150 mM
NaCl	MERCK	100 mM
Tween 20	SERVA	10^{-3} %

*The pH was adjusted to 7.5 with ~ 40 % HCl.

Table 13: Primary antibodies.

Primary antibodies	Company	Species	Dilution
PLB-Ser16	Abcam	rabbit	1:1000
PLB-Thr17	Badrilla	rabbit	1:2500
PLB-total 2D12	Abcam	mouse	1:2000
Serca 2 N-19	Santa Cruz	Goat	1:2000
RyR2-Ser2808	Badrilla	rabbit	1:1000
RyR2-Ser2814	Badrilla	rabbit	1:2000
RyR2-total Ma3-925	Dr. Wehrens Lab	rabbit	1:1000
Junctin/ASPH	Life Science	mouse	1:1000
PLB-total 2D12	Abcam	mouse	1:2000
$^{+}$JPH2 H-250	Santa Cruz	rabbit	1:1000
Calsequestrin	Thermo Fischer	rabbit	1:2000
Triadin	Thermo Fischer	mouse	1:1000
*GAPDH	HyTest	rabbit	1:2000

* GAPDH, Glycerinaldehyd-3-phosphatdehydrogenase $^{+}$ JPH2, Junctophilin-2

On the next day, unbound antibodies were removed by washing the membrane 3 times with TBST buffer and followed by incubating the membrane with a secondary infra-red fluorescence-labelled antibody (**Table 14**) for 1 hr at RT.

Table 14: Secondary antibodies.

Secondary antibody	Company	Dilution
Anti- Mouse (GAM)	Merck millipore	1:5000
Anti-Goat (DAG)	Santa cruz	1:5000
Anti-Rabbit (DAR)	Ge healthcare	1:5000

The Infrared fluorescence detection of the proteins was then possible with an infrared imager (Odyssey CLx, LI-COR®).

3.6 Other equipment's used

Small samples were mixed using a vortexer (IKA® VORTEX, SIGMA ALDRICH). For cell suspension preparation, centrifugation steps were performed on a SIGMA 4-10 centrifuge. Solutions were warmed in a water bath by B BRAUN. Cell sonication was performed on a sonicator (SONOREX DIGITEC, BANDELIN). Samples and chemicals were weighed on an analytical balance (ABS-N/ABJ-NM, KERN).

3.7 Statistical analysis

The results are expressed as mean ± standard error of the mean (mean±SEM). For functional experiments the number of cells studied per patient are indicated (n = number of myocytes/patients). The statistical analysis was performed using the computer software program Prism (Version 6, GraphPAD Software, Inc, San Diego, USA). Differences between groups were analyzed by independent Student's t-tests for normally distributed data or Mann-Whitney tests for data not following a normal distribution. For multiple comparisons, one-way ANOVA, followed by Dunnett's post-hoc test was performed. Significant difference was considered if the p-value was less than 0.05 (*p <0.05; **P <0.01; ***P <0.001).

4 Results

4.1 $I_{Ca,L}$-triggered Ca^{2+} transients (CaT) in human atrial cardiomyocytes of patients with poAF

To determine whether poAF was associated with preoperative cellular Ca^{2+}-handing abnormalities, cardiomyocyte electrophysiology ($I_{Ca,L}$ and $I_{Ca,L}$-triggered CaT) from patients with no history of preoperative AF was analyzed based on the occurrence of poAF during the in-hospital postoperative recovery period (1 – 10 days) compared to control (Ctl) patients that did not develop poAF. **Table 15** lists the clinical characteristics of Ctl and poAF patients. About 50 % of the surgical patients developed poAF. With the exception of age, no further significant differences were observed in the clinical parameters between Ctl and poAF patient groups.

Table 15: Characteristics of patients used for functional studies in poAF.

	Ctl	poAF
Patient, n	37	31
Gender, m/f	25/12	17/14
Age, y	69±1.9	73±1.4*
Body mass index, kg/m^2	32±1.6	28±0.9
CAD, n	15	10
MVD/AVD, n	11	12
CAD + MVD/AVD, n	8	8
Hypertension, n	23	24
Diabetes, n	7	10
Hyperlipidemia, n	13	12
LVEF, %	53±2.6	59±2.1
Digitalis	0	0
ACE inhibitors, n	17	14
α_1-blockers, n	0	2
AT_1-blockers, n	3	7
β-blockers, n	20	18
Ca^{2+}-antagonists, n	7	5
Dihydropyridines, n	0	0
Diuretics, n	19	10
Nitrates, n	0	3
Lipid-lowering drugs, n	0	0

Values are presented as mean±SEM or number of patients. CAD, coronary artery disease; MVD/AVD, mitral/aortic valve disease; LVEF, left ventricular ejection fraction; ACE, angiotensin-II-converting enzyme. AT_1, angiotensin-II receptor type-1. *P<0.05 vs control.

The C_M is proportionate to the cell surface area and together with the membrane resistance it determines the membrane time constant, which determines how fast the membrane potential responds to the ion currents. To correct for cell-to-cell differences in C_M, recorded currents were divided by C_M. The C_M did not differ between the groups (**Figure 26**).

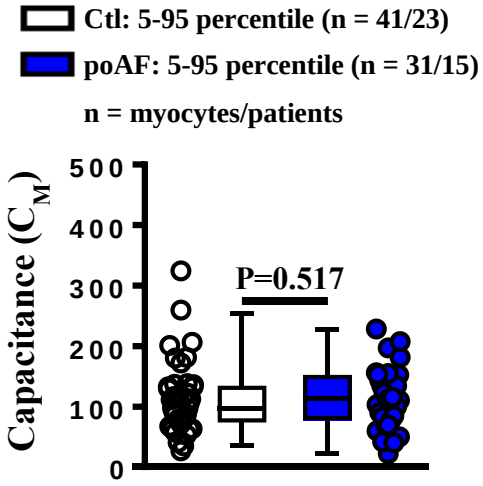

Figure 26: Cell capacitance in Control (Ctl) and poAF patients.
Numbers indicate number of myocytes/patients.

Membrane currents were measured under voltage-clamp conditions simultaneously with $[Ca^{2+}]_i$ (Fluo-3) to assess CaT properties in atrial cardiomyocytes. **Figure 27** shows representative current recordings and the peak current density-voltage relation of $I_{Ca,L}$ with corresponding $I_{Ca,L}$-triggered CaT for Ctl and poAF patients. Their mean±SEM are further shown in quantitative analysis.

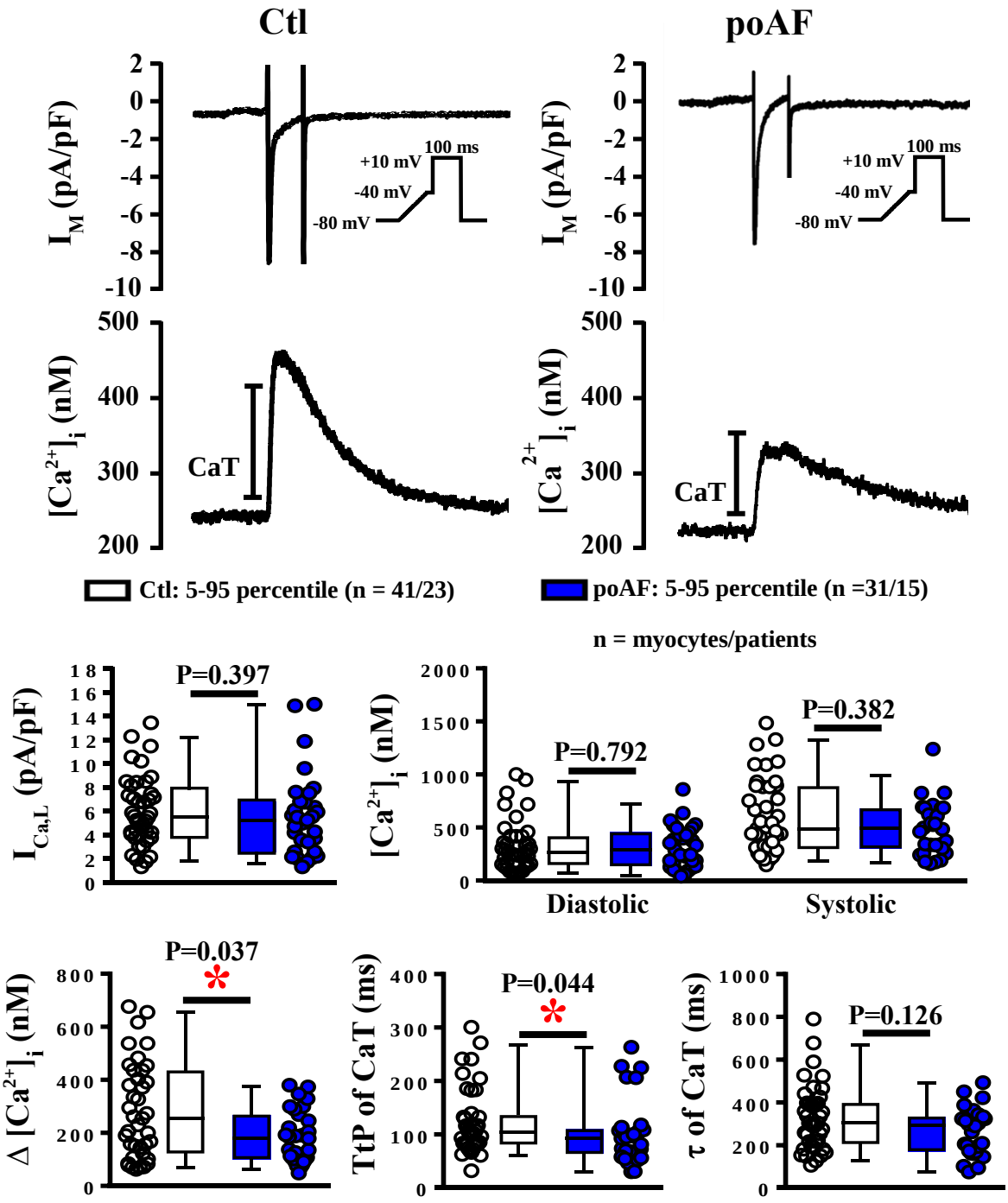

Figure 27: L-type Ca^{2+} current ($I_{Ca,L}$) and triggered Ca^{2+}-transients (CaT) in poAF.

Representative recordings of simultaneous $I_{Ca,L}$ and $I_{Ca,L}$-triggered CaT in patients who stay in sinus rhythm (Ctl) and those who develop atrial fibrillation post-surgery (poAF). Voltage-clamp protocol (inset), applied at 0.5 Hz. Quantitative analysis show peak $I_{Ca,L}$ amplitude, diastolic and systolic ($I_{Ca,L}$-triggered) Ca^{2+} levels and corresponding Ca^{2+} transient amplitude ($\Delta[Ca^{2+}]_i$), the time to peak (TtP) and the decay (τ) of the systolic CaT.*P<0.05 vs Ctl. Numbers in brackets indicate myocytes/patients.

$I_{Ca,L}$ amplitude was not different between Ctl and poAF (**Figure 27**). Similarly, diastolic and systolic Ca^{2+} levels were unchanged, whereas CaT amplitude was significantly decreased by

~35%. Finally, there was no difference in the time-constant of CaT decay (a measure of Ca^{2+} removal by SERCA, NCX and PMCA).

Inactivation of Ca^{2+} channels can be estimated by the decay of current during continuous depolarization (Kubalová 2003). Cardiac L-type Ca^{2+} channels are known to inactivate through voltage- and Ca^{2+}-dependent mechanisms. This inactivation process is a key mechanism by which cells are able to tightly control intracellular Ca^{2+} levels to regulate cellular excitability. Pure voltage-dependent inactivation has a much slower time course of development than Ca^{2+}-dependent inactivation and plays only a minor role by the control of Ca^{2+} influx into the cell. Thus, the major determinants of the inactivation kinetics of $I_{Ca,L}$ during depolarization are Ca^{2+}-dependent mechanisms (Kubalová 2003). Two phases in the kinetics of Ca^{2+}-dependent $I_{Ca,L}$ inactivation exist: a fast phase (τ f) that depends on Ca^{2+} released from the SR (Ca^{2+} release-dependent inactivation) and a slow phase (τ s) that depends on Ca^{2+} flow through the channels itself (Ca^{2+} current-dependent inactivation), although SR Ca^{2+} release-dependent inactivation plays the predominant role (Kubalová 2003). We analyzed both time constants of $I_{Ca,L}$ inactivation in Ctl and poAF patients. Despite significant differences in CaT amplitude between Ctl and poAF (**Figure 27**), the fast or the slow components of $I_{Ca,L}$ inactivation were comparable in both groups (**Figure 28**).

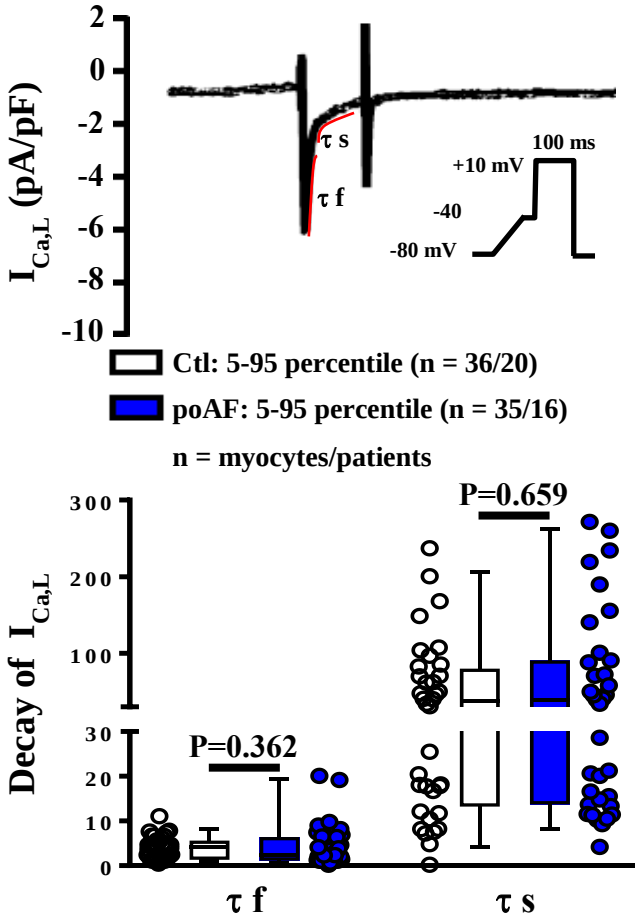

Figure 28: Kinetics of voltage and Ca^{2+}-dependent inactivation of $I_{Ca,L}$.

Representative $I_{Ca,L}$ showing the decay kinetics of the current, the fast component (τ f) and the slow component (τ s). The quantitative analysis of all recordings in Ctl and poAF patients is shown below. Numbers in brackets indicate myocytes/patients.

The AF-associated reduction in CaT amplitudes, which we also observed in poAF patients (**Figure 27**), may contribute to impaired preoperative atrial contractility (Verdejo et al. 2015). To test whether reduced CaT amplitude contributes to impaired cellular shortening, we employed a video-edge detection software to measure cell shortening simultaneously with $I_{Ca,L}$ and $[Ca^{2+}]_i$ (video edge-detector [IonOptix], frame rate acquisition frequency: 200 Hz), as shown in **Figure 29**.

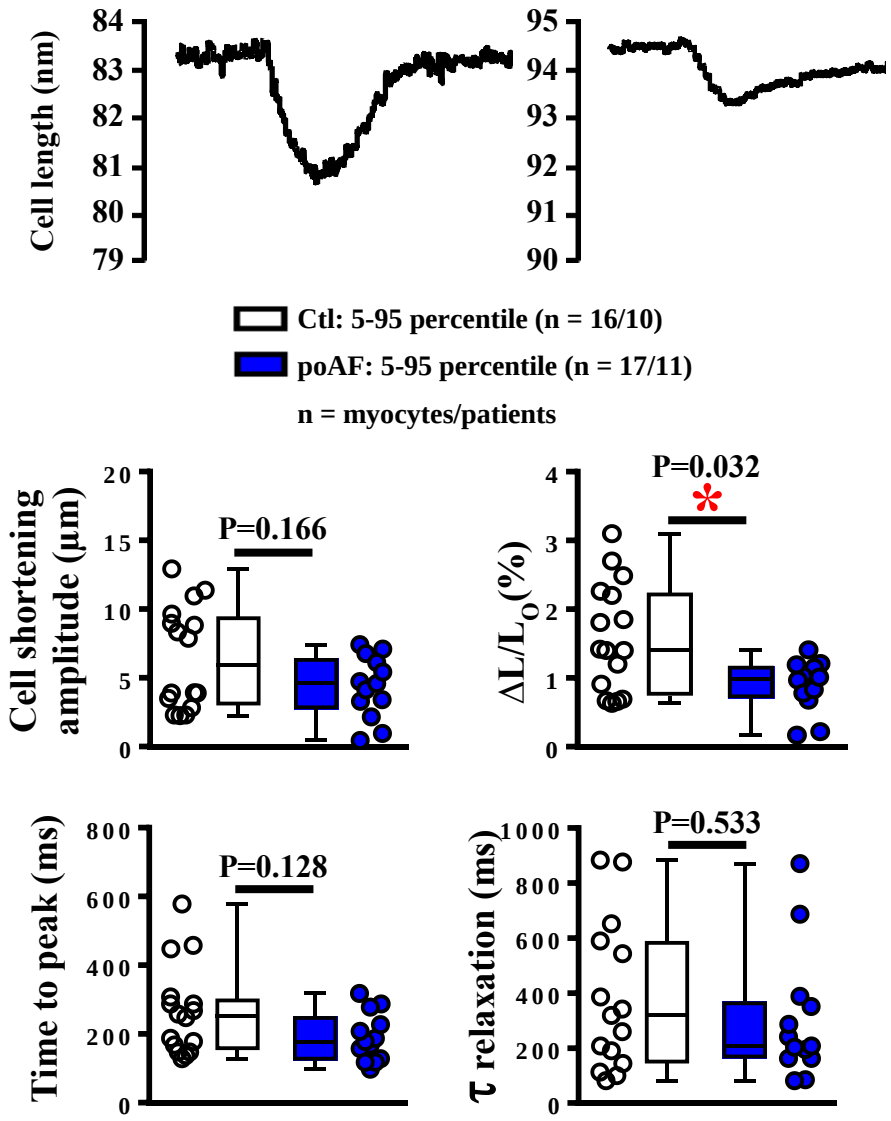

Figure 29: Ca^{2+} transient-triggered cell shortening.

Representative recordings from an atrial cardiomyocyte from a Ctl and a poAF patient (top). Amplitude of cell shortening and fractional shortening ($\Delta L/L_O$), expressed as cell shortening amplitude (ΔL) relative to diastolic (resting) cell length (L_O), middle). Time to peak of shortening and relaxation time constant (τ, bottom). *P<0.05 vs. Ctl. Numbers in brackets indicate myocytes/patients.

Figure 29 shows representative recordings together with the quantification of cell shortening. The difference in the amplitude of cell shortening between Ctl and poAF groups did not reach statistical significance. However, there was a significant 44% reduction of the fractional cell shortening in the poAF compared to Ctl group. The time to peak of shortening showed a non-significant 28% reduction in the poAF group. There was no difference in the time constant (τ) of relaxation in the poAF vs Ctl group. These *in vitro* data suggest that impaired Ca^{2+} handling affects cellular contractility in poAF likely contributing to the impaired mechanical function of the atria in poAF patients *in vivo*.

The decreased CaT amplitude in poAF despite unaltered 'trigger' $I_{Ca,L}$ suggests either reduced SR Ca^{2+} load or impaired regulation of SR Ca^{2+}-release e.g. decreased gain of Ca^{2+}-induced Ca^{2+} release due to abnormal RyR2 function. In some experiments we therefore applied caffeine to open RyR2 channels to release all available Ca^{2+} from the SR and measured the caffeine-induced CaT and the transient-inward current generated through this process as indicators of SR Ca^{2+} load. Application of 10 mmol/L caffeine to cardiomyocytes voltage-clamped at -80 mV caused a rapid increase of $[Ca^{2+}]_i$ as a result of SR Ca^{2+} release. The subsequent decay of $[Ca^{2+}]_i$ results from Ca^{2+} extrusion across the sarcolemma, mainly through NCX with a minor contribution of PMCA. The extrusion of Ca^{2+} via NCX generates a transient-inward current (I_{NCX}), the amplitude and time course of which were monitored simultaneously with the caffeine-induced Ca^{2+} transient (**Figure 30**).

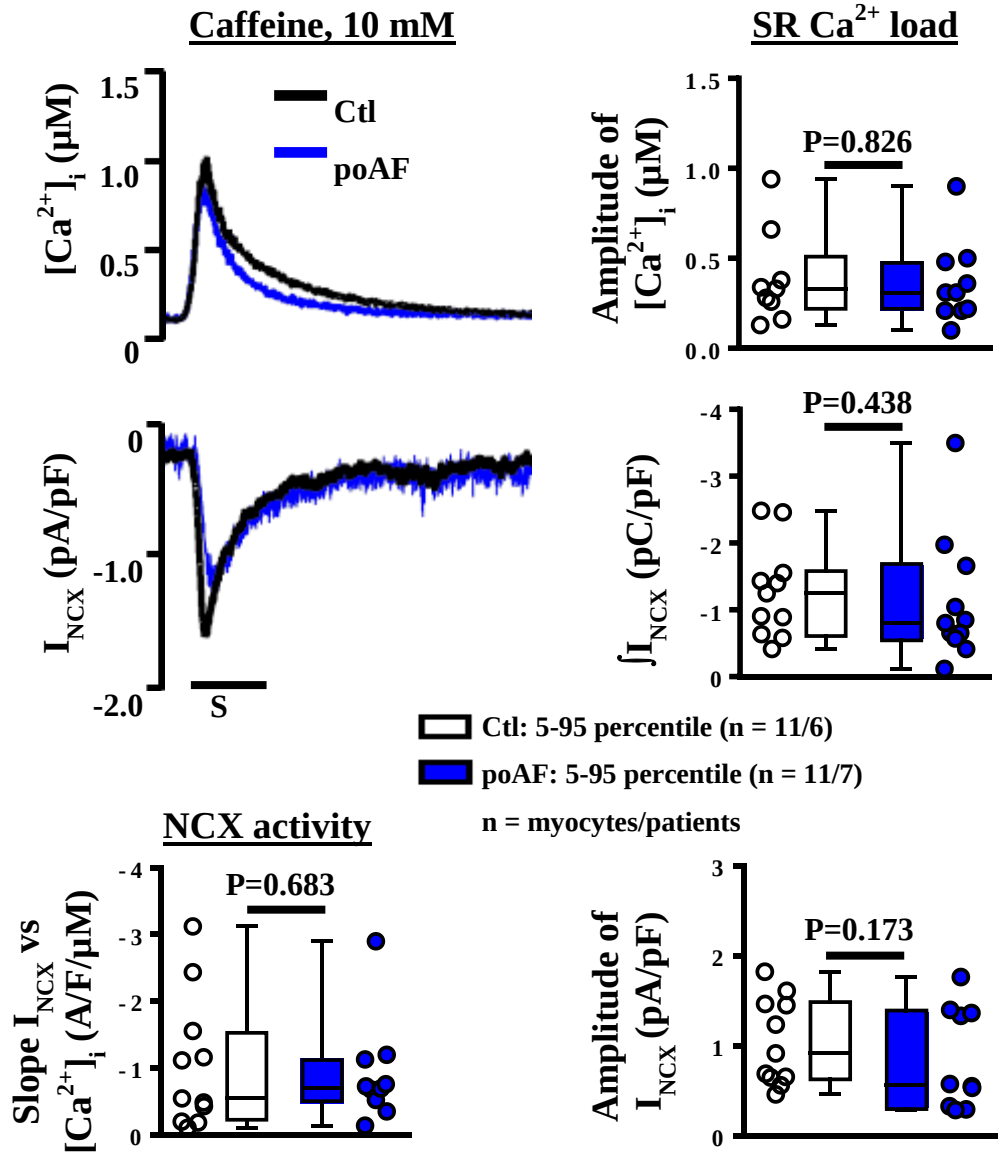

Figure 30: Caffeine-induced Ca^{2+} transients (cCaT) in Ctl and poAF patients: Functional NCX and SR Ca^{2+} load.

Representative recording of caffeine (10 mM)-induced release of SR Ca^{2+}-content and triggered I_M, predominantly mediated by I_{NCX} in atrial cardiomyocytes of Ctl and poAF patients. SR Ca^{2+}-load, quantified with cCaT amplitude and integrated membrane-current during caffeine application (reflecting Ca^{2+}-extrusion via NCX). NCX activity expressed as slope of I_{NCX} on cCaT which reflects Ca^{2+}-dependence of NCX. * $P<0.05$ vs. corresponding Ctl. Numbers in brackets indicate myocytes/patients.

The quantification of the amplitude of cCaT provides a semi-quantitative index of SR Ca^{2+} content, which can be sensitive to differences in Ca^{2+}-buffering properties and is therefore not quite a reliable measure of SR Ca^{2+} content (Voigt et al. 2012; Voigt et al. 2014). In **Figure 30**, no significant effect on the amplitude of caffeine-induced CaT was observed in poAF vs Ctl. The integral (the area under the curve) of the caffeine-induced I_{NCX}, a measure of the amount of Ca^{2+} extruded by NCX and a more reliable indicator of SR Ca^{2+} content, was also

analyzed. The mean integral of I_{NCX} in the poAF group was non-significantly lower by ~13 % compared to the Ctl group, likely contributing to the significantly reduced I_{CaL}-triggered CaT seen in **Figure 27**. The amplitude of I_{NCX} and the NCX activity expressed as slope of the I_{NCX} vs $[Ca^{2+}]_{i,}$ an indicator of the Ca^{2+} sensitivity of NCX, were similar in both groups. These results point to a potentially abnormal Ca^{2+} flux regulation at the SR level.

Uptake of Ca^{2+} via SERCA and extrusion of Ca^{2+} through NCX are the principal pathways for cytosolic Ca^{2+} removal in cardiomyocytes during diastole. In addition, PMCA may also have a minor contribution to this process (Bassani et al. 1994). Although the relative contributions of SERCA and NCX to $[Ca^{2+}]_i$ decline differ among species, in adult mammalian cardiomyocytes the relative contribution of SERCA to cytosolic Ca^{2+} removal is much greater than that of NCX (Bassani et al. 1994; Guo & Yang 2009).

To evaluate the relative contribution of SERCA, NCX and PMCA to cytosolic Ca^{2+} removal in atrial cardiomyocytes of poAF patients, the decay of the I_{CaL}-triggered CaT and the cCaT were analyzed using a mono-exponential function. The decay rate of cCaT was used as a measure of non-SERCA Ca^{2+} removal (NCX+PMCA). To estimate the fractional contribution of SERCA, we subtracted the decay rate of cCaT from the decay of the I_{CaL}-triggered CaT (representing all three Ca^{2+} removal processes). The fractions of the Ca^{2+} transport contributed by NCX+PMCA and SERCA were quantified and represented in pie charts. SERCA was responsible for ~80%, while NCX+PMCA responsible for ~20% of total Ca^{2+} removal and there were no significant differences between Ctl and poAF patients (**Figure 31**).

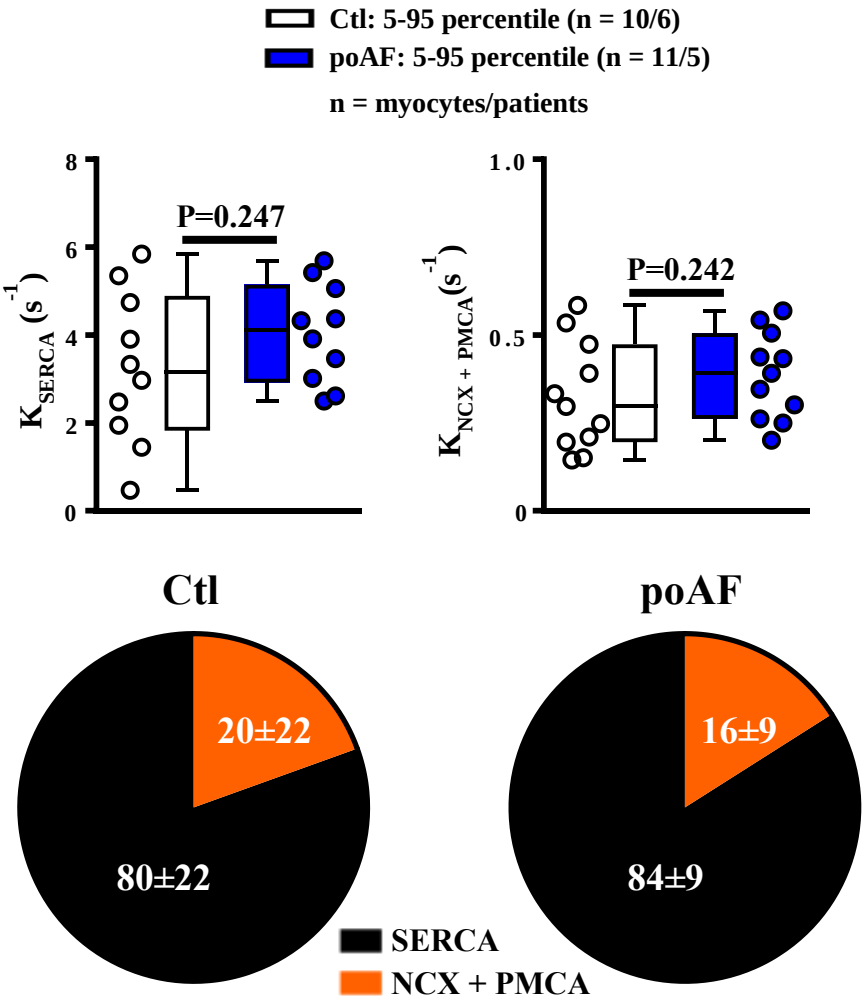

Figure 31: Contribution of SERCA, NCX, and PMCA to Ca^{2+} removal.

Mean±SEM of calculated rate constants of SERCA (K_{SERCA}) and NCX+PMCA ($K_{NCX+PMCA}$). Relative contributions of SERCA, NCX and PMCA to diastolic Ca^{2+} removal. Numbers in brackets indicate myocytes/patients.

Finally, we assessed the occurrence of SCaEs under voltage-clamp conditions in the presence of supra-physiological bath Ca^{2+} concentrations (5 mM) to increase cardiomyocyte Ca^{2+} loading and unmask potential differences in the regulation of SR Ca^{2+} fluxes. SCaEs were defined as unstimulated rises in $[Ca^{2+}]_i$ following a 1-minute of $I_{Ca,L}$-triggered CaTs at 0.5 Hz during application of the cytokine IL-1β (40 ng/mL) to mimic the proinflammatory state of the system in the postoperative period (**Figure 32**).

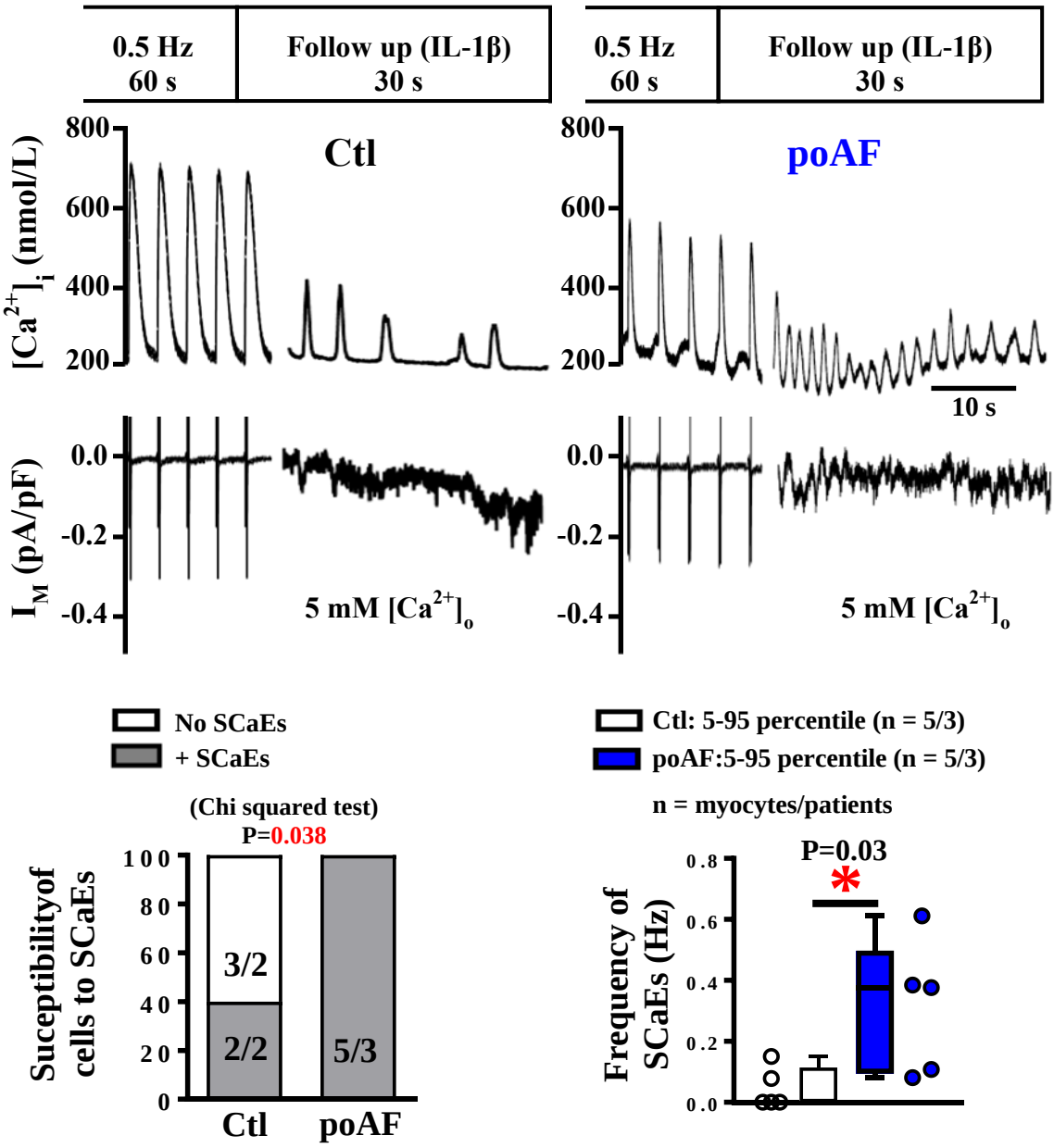

Figure 32: SCaEs following IL-1β application in Ctl and poAF patients.

Representative $[Ca^{2+}]_i$ (CaT and SCaEs, respectively) and corresponding I_M ($I_{Ca,L}$ and I_{NCX}, respectively) recording following 1 min of pacing at 0.5 Hz and 5 mM $[Ca^{2+}]_o$ and then voltage clamped at -80 mV and in the presence of IL-1β (40 ng/ml) showing SCaEs with corresponding I_{NCX} (top). Quantitative analysis showing susceptibility and frequency of SCaEs in Ctl compared to poAF group (bottom). *P<0.05 vs Ctl. Numbers indicate myocytes/patients.

Figure 32 shows CaT and membrane current in representative voltage-clamped atrial cardiomyocytes from a Ctl and poAF patients. Cardiomyocytes were first stimulated with depolarizing pulses at 0.5 Hz (5 mM $[Ca^{2+}]_o$), giving rise to $I_{Ca,L}$-triggered CaT, followed by a follow-up period at -80 mV in the presence of IL-1β (40 ng/ml), showing susceptibility of cells to SCaEs, thereby generating potentially proarrhythmic I_{NCX}. The susceptibility to SCaEs was larger in poAF compared to Ctl and the frequency of SCaEs was significantly

higher in poAF vs Ctl cardiomyocytes. The increased incidence of SCaEs in response to IL-1β in poAF suggests that Ca^{2+}-handling abnormalities may contribute to the formation of preexisting substrate that is more sensitive to proinflammatory postoperative triggers, thereby supporting the induction of poAF. The potential molecular mechanisms underlying the poAF-associated Ca^{2+}-handling abnormalities will be discussed in **Section 5**. However, to validate the present findings, we first investigated $I_{Ca,L}$ and $I_{Ca,L}$-triggered CaT in atrial cardiomyocytes from cAF patients as a positive control (**Section 4.1.1**). To investigate the molecular basis of potential RyR2 and SERCA2a dysregulations in poAF patients, we studied expression levels and fractional phosphorylation of SR-located proteins with immunoblots and specific antibodies in Ctl compared to poAF patients (**Section 4.1.2**).

4.1.1 $I_{Ca,L}$-triggered Ca^{2+} transients (CaT) in human atrial cardiomyocytes of cAF patients

Consistent with our previous publication (Voigt et al. 2012), new measurements in an independent patient cohort showed both decreased $I_{Ca,L}$ and $I_{Ca,L}$-triggered CaT in cAF vs Ctl group (here defined as patients who stay in sinus rhythm post-surgery, similar to the previous section). We used these data (**Figure 31**) as internal control and compared them to poAF using the same voltage-clamp protocols. In effect, this result is a confident control supporting the validity of the results of the present work with poAF. Patients' characteristics are shown in **Table 16.**

Table 16: Characteristics of patients used for functional studies in cAF.

	Ctl	poAF	cAF
Patient, n	37	31	4
Gender, m/f	25/(12)	17/14	4
Age, y	69±1.9	73±1.4*	77±2.3*
Body mass index, kg/m^2	32±1.6	28±0.9	23±2.6
CAD, n	15	10	1
MVD/AVD, n	11	12	2
CAD + MVD/AVD, n	8	8	1
Hypertension, n	23	24	3
Diabetes, n	7	10	0
Hyperlipidemia, n	13	12	1
LVEF, %	53±2.6	59±2.1	50±2.3
Digitalis	0	0	1
ACE inhibitors, n	17	14	1
α_1-blockers, n	0	2	0
AT_1-blockers, n	3	7	0
β-blockers, n	20	18	2
Ca^{2+}-antagonists, n	7	5	2
Dihydropyridines, n	0	0	1
Diuretics, n	19	10	3
Nitrates, n	0	3	0
Lipid-lowering drugs, n	0	0	1

Values are presented as mean±SEM or number of patients. CAD, coronary artery disease; MVD/AVD, mitral/aortic valve disease; LVEF, left ventricular ejection fraction; ACE, angiotensin-II-converting enzyme; AT_1, angiotensin-II receptor type-1. *P<0.05 vs control.

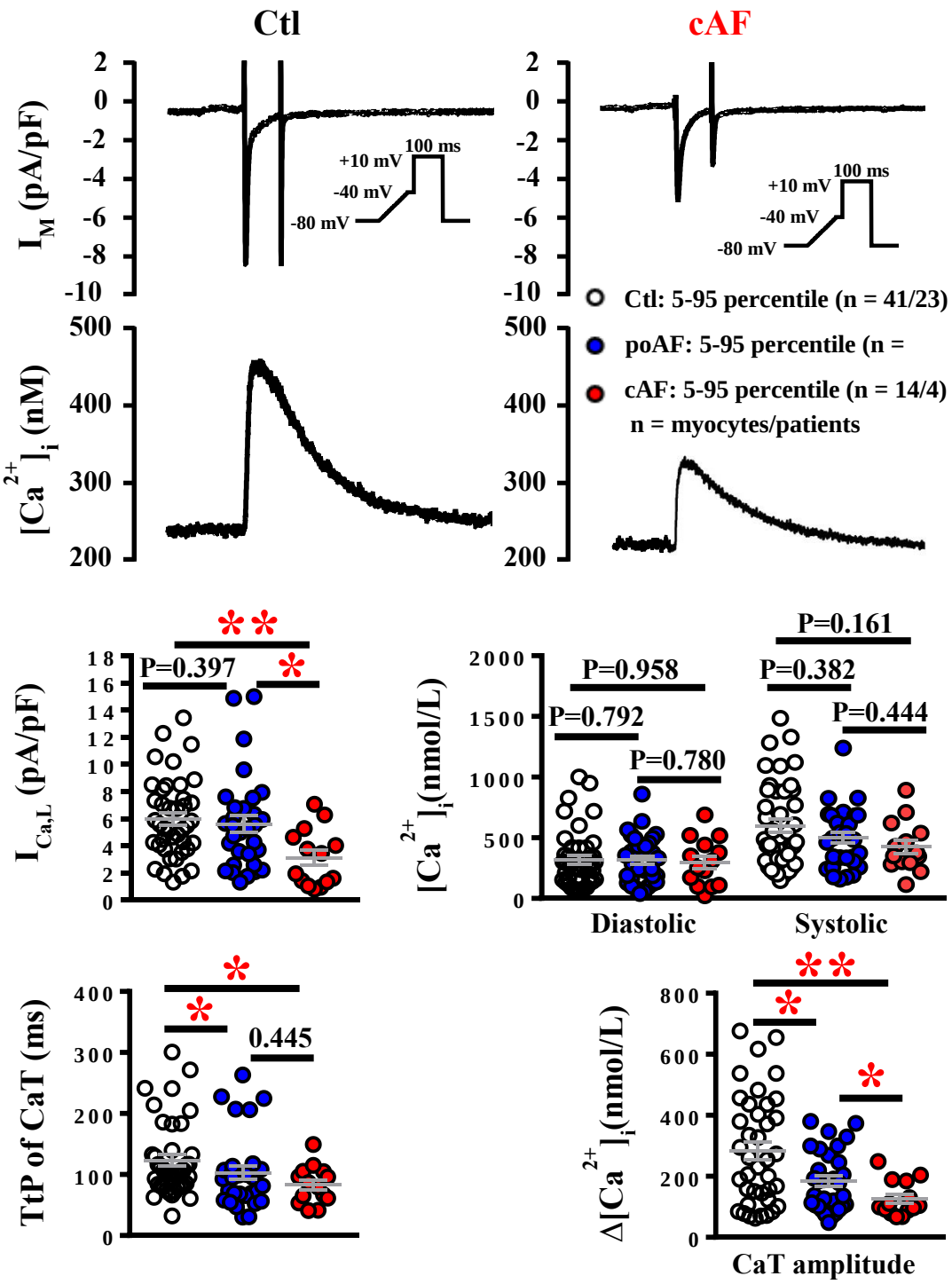

Figure 33: L-type Ca^{2+} current ($I_{Ca,L}$) and triggered Ca^{2+}-transients (CaT) in cAF.

Representative $I_{Ca,L}$ and corresponding CaT recordings in Ctl and cAF patients and quantitative analysis showing peak $I_{Ca,L}$ amplitude, diastolic and systolic ($I_{Ca,L}$-triggered) Ca^{2+} levels, the time to peak (TtP) and amplitude of systolic CaT in patients with cAF compared to patients who stay in sinus rhythm post-surgery (Ctl) and to those who develop post-operative AF (poAF). *P<0.05 vs Ctl. *P<0.05 and **P<0.05 vs Ctl or poAF. Numbers in brackets indicate myocytes/patients.

4.1.2 Protein expression and phosphorylation in Ctl and poAF patients

In order to test whether changes in protein expression and/or phosphorylation underlie functional abnormalities we performed Western-blot experiments of major Ca^{2+}-handling proteins. The characteristics of the patients are listed in **Table 17**.

Table 17: Characteristics of patients used for biochemistry.

	Ctl	poAF
Patient, n	16	16
Gender, m/f	15/1	15/1
Age, y	64±3.8	70±3.2*
Body mass index, kg/m^2	28±0.9	27±1.0
CAD, n	7	5
MVD/AVD, n	6	7
CAD+ MVD/AVD, n	3	4
Hypertension, n	6	4
Diabetes, n	6	4
Hyperlipidemia, n	8	7
LVEF, %	51±3.6	60±2.7
Digitalis, n	0	0
ACE inhibitors, n	9	4
α_1-blockers, n	0	2
AT_1 -blockers, n	1	3
β-blockers, n	10	5
Ca^{2+}-antagonists, n	4	6
Dihydropyridines, n	0	0
Diuretics, n	7	3
Nitrates, n	1	1
Lipid-lowering drugs, n	11	5

Values are presented as mean±SEM or number of patients. CAD, coronary artery disease; MVD/AVD, mitral/aortic valve disease; LVEF, left ventricular ejection fraction; ACE, angiotensin-II-converting enzyme; AT_1, angiotensin-II receptor type-1. *P<0.05 vs control.

Protein isolation from whole-tissue lysates and immunoblot experiments were performed as described in **section 3.5.** We focused on the SR Ca^{2+}-handling proteins Serca2a, PLB, RyR2 and the RyR2-associated regulators triadin, junctin, junctophilin-2, and calsequestrin.

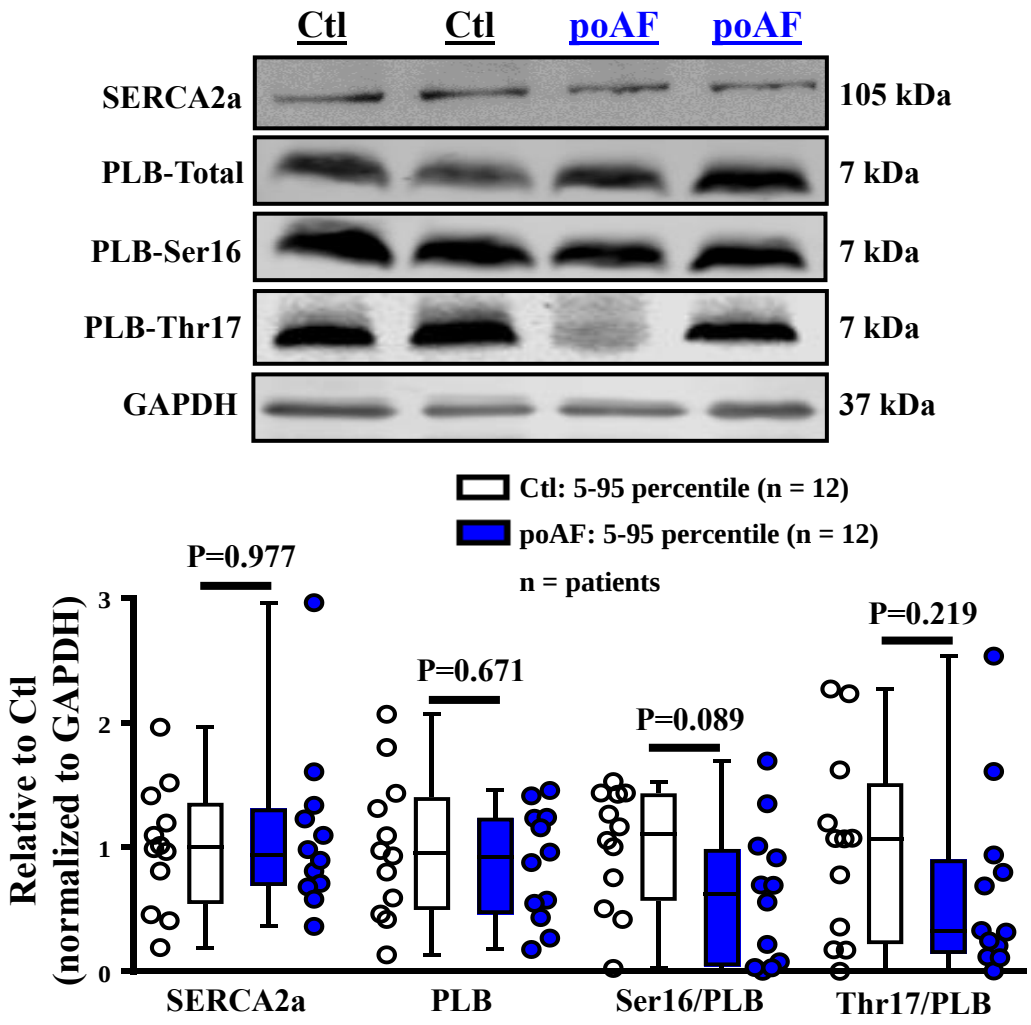

Figure 34: SERCA2a and PLB protein expression and phosphorylation state of PLB at Ser16 and Thr17.

Representative immunoblots and quantitative analysis showing SERCA2a, phospholamban (PLB) protein expression and its phosphorylation levels in Ctl and poAF group. Numbers indicate patients.

Figure 34 shows that SERCA2a and PLB protein expression were unchanged in poAF vs Ctl. There was a nonsignificant reduction of the phosphorylation state of PLB at Ser16 (PKA site) and Thr17 (CaMKII site) in poAF.

We showed in **Section 4.1** that cardiomyocytes from poAF patients have an increased frequency of SCaEs. To investigate the potential relationship between SCaEs and dysfunctional RyR2, we measured the expression levels of RyR2 including its phosphorylation states (**Figure 35**).

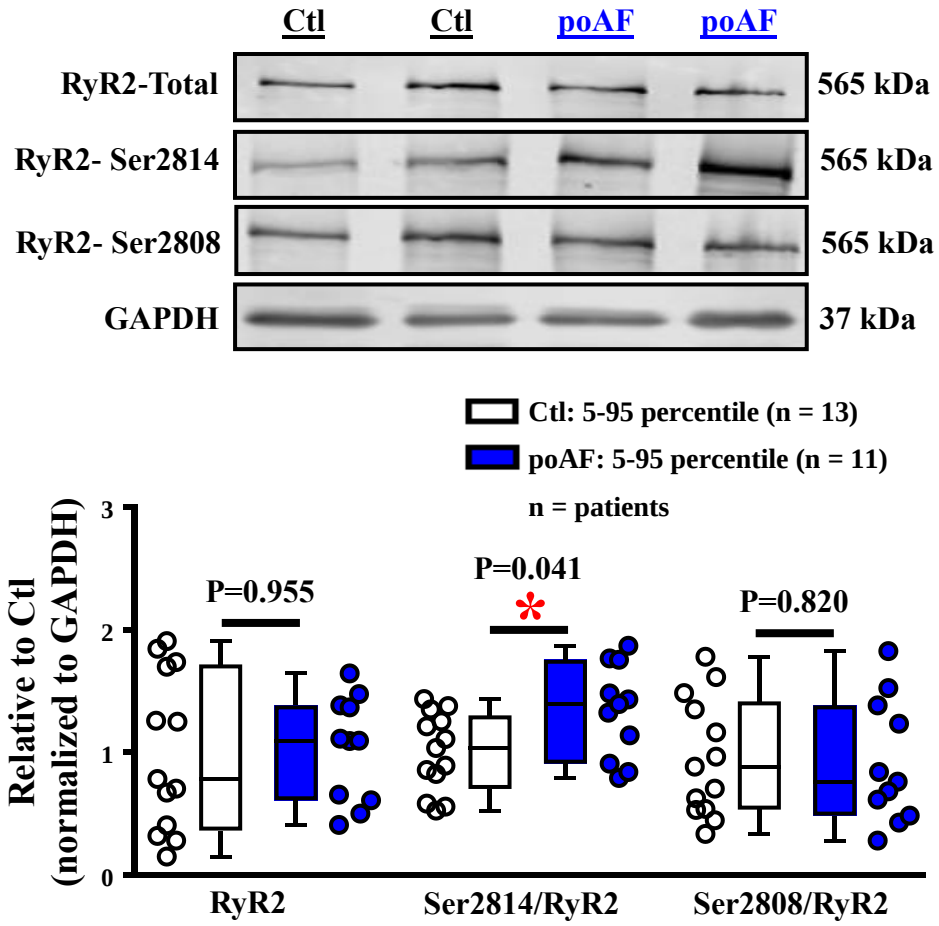

Figure 35: RyR2 protein expression and phosphorylation state of RyR2 at Ser2808 and Ser2814.

Representative immunoblots and quantitative analysis showing RyR2 protein expression and its phosphorylation levels in Ctl and in poAF group. *P<0.05 vs Ctl. Numbers indicate patients.

Figure 35 shows that the protein expression level of RyR2 in poAF and its phosphorylation at Ser2808 are comparable to Ctl patients. However, RyR2-phosphorylation at Ser2814 was significantly higher (~36 %) in poAF compared to Ctl patients. Protein levels of the RyR2-associated regulators triadin, junctin, junctophilin-2 and calsequestrin were similar in the poAF and Ctl groups (**Figure 36**).

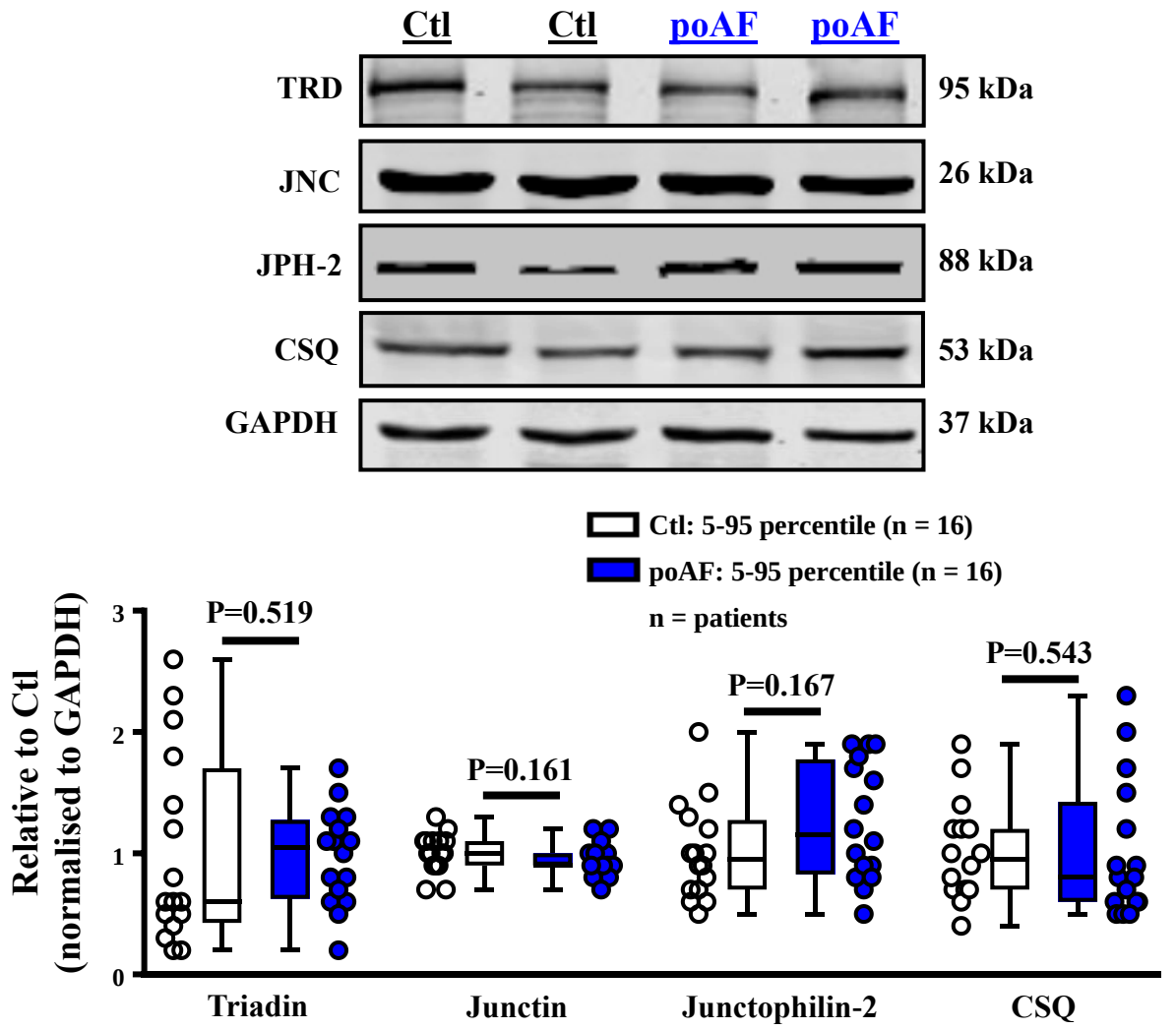

Figure 36: Triadin, junctin, junctophilin-2 and calsequestrin protein expression.

Representative immunoblots and quantitative analysis showing triadin (TRD), junctin (JNC), juntophilin-2 (JPH-2) and calsequestrin (CSQ) protein expression levels in Ctl and poAF groups. Numbers indicate patients.

4.2 Inward-rectifier K^+ currents I_{K1} and $I_{K,ACh}$ in cAF compared to Ctl patients

Stimulation of M-receptors with CCh activates the G-protein-coupled $I_{K,ACh}$ through dissociation of the βγ subunit from the G-protein complex, which then binds to $I_{K,ACh}$ channels to activate them (Dobrev et al. 2005). **Figure 37** is a schematic of basal inward-rectifier K^+ currents usually considered to be represented by I_{K1} only and G-protein-activated $I_{K,ACh}$ on the membrane of a cardiomyocyte.

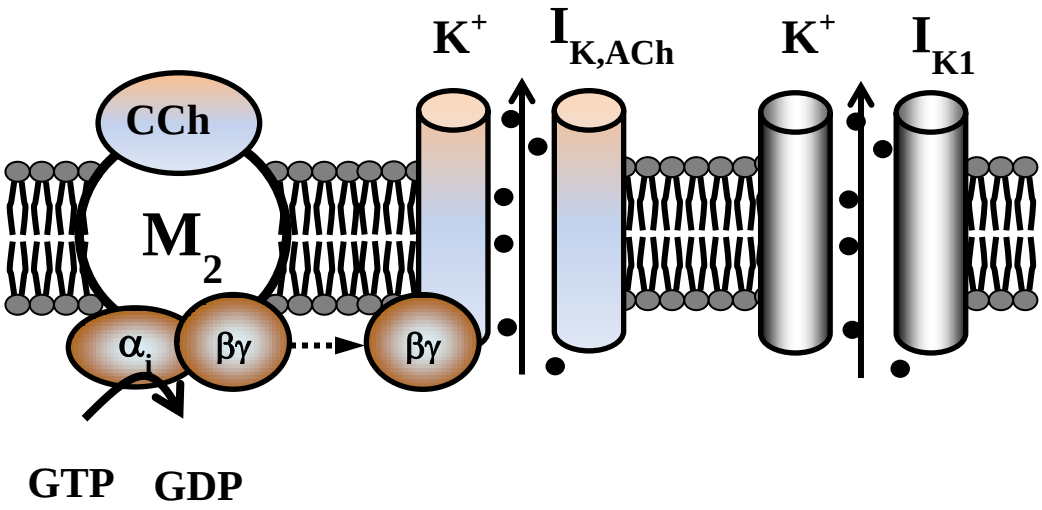

Figure 37: Basal and G-protein activated inward rectifier K^+ currents (I_{K1} and $I_{K,ACh}$, respectively).

Type-2 muscarinic (M_2)-receptor stimulation leads to G-protein-mediated activation of $I_{K,ACh}$ via βγ-subunits.

4.2.1 The ramp pulse protocol and the definition of current density

In this work cardiomyocytes were isolated from right atrial appendages of patients in SR before surgery, here defined as control (Ctl) patients, or patients with cAF. Freshly isolated cells lasted an average of 6 hrs for measurements. Of these isolations, measurements of cells that showed an unacceptable large leak current, unstable access resistance or even loss of access resistance were excluded.

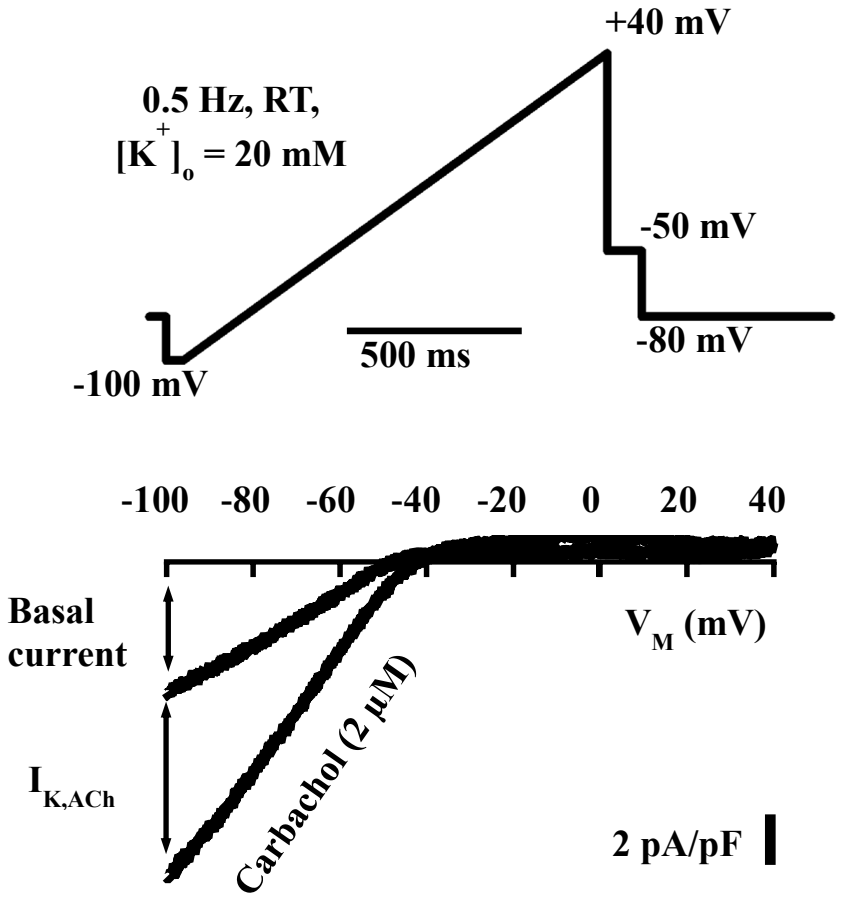

Figure 38: Representative recording of the current voltage relationships of basal current and $I_{K,ACh}$ in a human atrial cardiomyocyte.

Voltage-clamp protocol (0.5 Hz) for activation of basal current and carbachol-mediated activation of $I_{K,ACh}$ (**top**). Original recording showing Ba^{2+}-sensitive inward-rectifier K^+ current recorded from a right atrial cardiomyocyte of a control (Ctl) patient with SR under basal conditions and after application of 2 µM carbachol to activate $I_{K,ACh}$ (**bottom**).

Under control conditions, a characteristic current-voltage relationship of the basal inward-rectifier K^+ current was registered. After application of a maximal concentration (2 µM) of CCh, the total membrane current rapidly increased due to additional activation of $I_{K,ACh}$. The CCh-sensitive component of the total current is defined as $I_{K,ACh}$ (**Figure 38**).

4.2.2 Time course for $I_{K,ACh}$ activation using the M-receptor agonist carbachol

For $I_{K,ACh}$ activation, a saturating concentration of CCh (2 µM) was used. The ramp protocol described in **section 4.3.1** was repeated every 2 s. **Figure 39** shows the current density at -100 mV as a function of time before, during and after two min of CCh application. After CCh wash out, $I_{K,ACh}$ is rapidly deactivated due to the GTPase of the G_{α} subunit. $I_{K,ACh}$ has a biphasic time course: it reaches a peak (Peak-$I_{K,ACh}$) then falls back to a Quasi-Steady-State level (QSS-$I_{K,ACh}$, **Figure 39**). This is due to desensitization of the $I_{K,ACh}$ current (Dobrev et al. 2005).

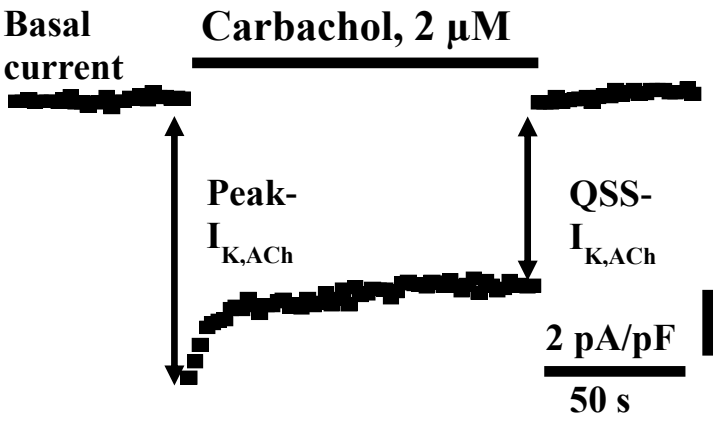

Figure 39: Time course for $I_{K,ACh}$ activation at -100 mV in a Ctl patient.

The current density (pA/pF) is shown here as a function of time (s) before, during and after activation of $I_{K,ACh}$ with 2 µM carbachol application at -100 mV from a ramp pulse applied at 0.5 Hz. The current reaches a maximum (Peak-$I_{K,ACh}$) and then runs back despite the presence of the agonist to a "Quasi-Steady-State level" (QSS-$I_{K,ACh}$).

4.2.3 Basal current and $I_{K,ACh}$ in atrial cardiomyocytes of Ctl and cAF patients

For this study, the characteristics of the patients used are listed on **Table 18.**

Table 18: Patients characteristics used for studies of I_{K1} and $I_{K,ACh}$ in cAF.

	Ctl	cAF
Patient, n	6	2
Gender, m/f	4/2	17/1
Age, y	77±1.5	81
Body mass index, kg/m^2	29±1.5	27
CAD, n	2	0
MVD/AVD, n	3	1
CAD + MVD/AVD, n	1	1
Hypertension, n	3	2
Diabetes, n	3	2
Hyperlipidemia, n	3	0
LVEF, %	0	0
Digitalis, n	0	1
ACE inhibitors, n	1	1
α_1-blockers, n	0	2
AT_1 -blockers, n	0	0
β-blockers, n	1	1
Ca^{2+}-antagonists, n	1	0
Dihydropyridines, n	0	0
Diuretics, n	0	0
Nitrates, n	0	3
Lipid-lowering drugs, n	2	2

Values are presented as mean±SEM, median (range), or number of patients. CAD, coronary artery disease; MVD/AVD, mitral/aortic valve disease; LVEF, left ventricular ejection fraction; ACE, angiotensin-II-converting enzyme. AT_1, angiotensin-II receptor type-1. *P<0.05 vs control.

Atrial cardiomyocytes from Ctl or cAF patients were voltage-clamped under control conditions in the presence of Tyrode's solution. In both groups, the basal current and the CCh-mediated activation and desensitization of $I_{K,ACh}$ at the first stimulation (S1) and the second stimulation (S2) can be clearly observed (**Figure 40**). The desensitization of $I_{K,ACh}$ from the peak to QSS despite continuous presence of CCh is described in more detail in the work of (Voigt et al. 2007).

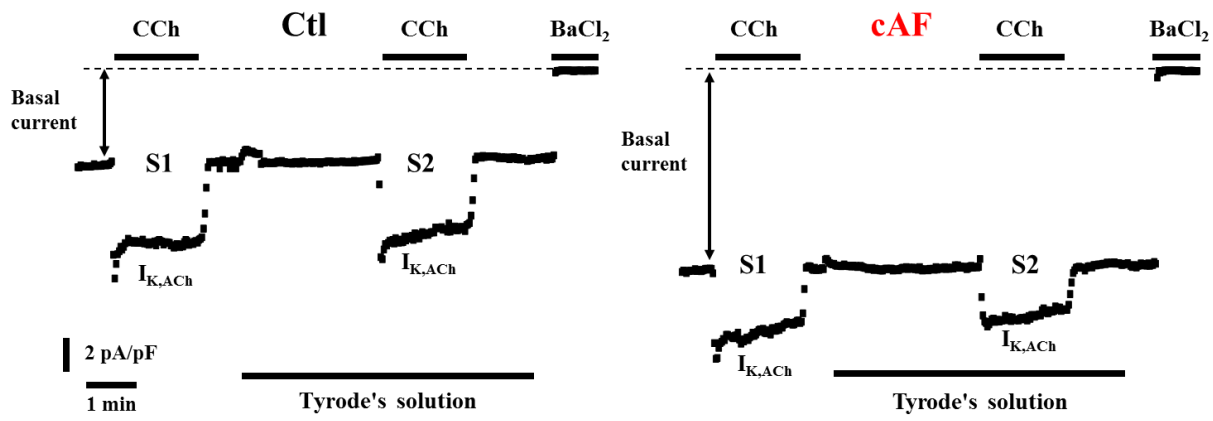

Figure 40: Time course of basal current and CCh-activated $I_{K,ACh}$ at -100 mV in cardiomyocytes of Ctl and cAF patients.

Activation of $I_{K,ACh}$ during two successive carbachol (CCh, 2 µM) applications (S1, S2, 3 min apart) in Ctl and cAF. The current density I_m (pA/pF) is shown here as a function of time. CCh was washed out for 1 minute after S2. At the end of the experiment $BaCl_2$ (1 mM) was used to establish the identity of the currents as inward-rectifiers.

The example recording in **Figure 40** show increase of the basal current in cAF compared to Ctl group (Dobrev et al. 2001; Dobrev et al. 2005). More of these recordings were quantified as shown on **Figure 41**.

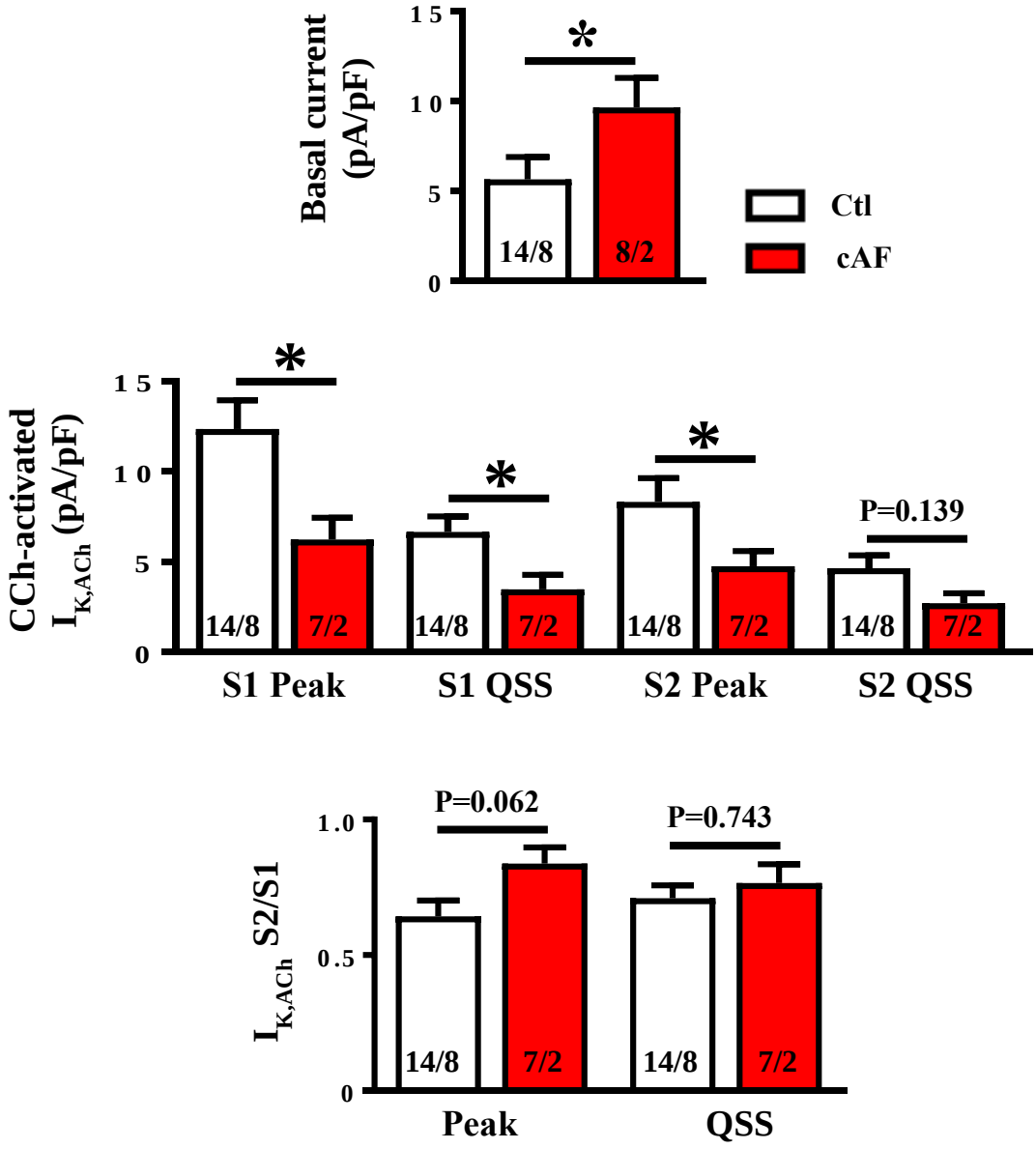

Figure 41: Voltage-clamp recordings of basal current and CCh-activated $I_{K,ACh}$ at -100 mV.

Mean±SEM of basal current (top) and activation of $I_{K,ACh}$ at peak (S1 and S2) and at QSS (S1 and S2, middle) during two successive CCh (2 µM) applications (3 min apart) and the ratio of S2/S1 in SR and cAF patients. *P<0.05 vs. Ctl. Numbers indicate myocytes/patients.

The basal current in the absence of M-receptor agonists was confirmed to be larger in cAF, whereas CCh-activated $I_{K,ACh}$ was smaller in both successive CCh (2 µM) applications (**Figure 41;** Dobrev et al. 2001; Dobrev et al. 2005). The ratio of $I_{K,ACh}$ during both stimulation steps (S2/S1) in SR and cAF patients showed no significant difference (**Figure**

41) confirming the similar degree of $I_{K,ACh}$ desensitization between cardiomyocytes from SR and cAF patients (Dobrev et al. 2001; Dobrev et al. 2005).

The increased basal inward-rectifier K^+ current (**Figure 41**) has been suggested to contribute to the shortening of atrial APD in cAF, supporting arrhythmia maintenance (Dobrev et al. 2001; Voigt et al. 2010). However, the exact contribution of Kir2.1-2.3-carried I_{K1} to the function of basal inward-rectifier K^+-current is unknown due to lack of selective I_{K1} inhibitors. Indeed, previous work has suggested that the constitutive $I_{K,ACh}$, small-conductance Ca^{2+}-activated K^+ (SK) current (Heijman et al. 2015) and/or two-pore 'background' K^+ currents (Schmidt et al. 2015) may all contribute to the basal inward-rectifier K^+-current.
Recently, PA-6 an analogue of the old anti-protozoal drug pentamidin has been shown to selectively block I_{K1} currents in expression systems and animal models, providing a new tool to study I_{K1} in humans (Boer et al. 2010; Takanari et al. 2013; Varkevisser et al. 2013). Exploiting the I_{K1} selectivity of PA-6, we investigated the inhibitory effect of PA-6 on I_{K1} in human atrial cardiomyocytes.

4.2.4 Effect of pentamidine analogue-6 (PA-6) on basal current and $I_{K,ACh}$

To assess whether PA-6 is specific for $I_{K1,}$ Takanari et al (Takanari et al. 2013) measured $I_{Na1.5}$, $I_{Ca,L}$, $I_{Kv4.3}$, $I_{Kv11.1}$, and $I_{Kv7.1/minK}$ by whole-cell patch-clamp experiments and tested the effects of 200 nM PA-6. They measured $I_{Nav1.5}$ (representing cardiac I_{Na}) in HEK-Nav1.5 cells, $I_{Ca,L}$ measured in adult dog cardiomyocytes, $I_{Kv4.3}$ (representing cardiac I_{to}) measured in COS7 cells, $I_{Kv11.1}$ (representing cardiac I_{Kr}) measured in HEK-hERG cells and $I_{Kv7.1/mink}$ (representing cardiac I_{Ks}) measured inHEK-293 cells. They showed that PA-6 did not block $I_{Na1.5}$, $I_{Ca,L}$, I_{to}, I_{Kr}, nor I_{Ks} and suggested that the preserved presence of especially I_{Kr} and I_{Ks} could compensate I_{K1} block and maintain the repolarization phase of cardiac action potential (Takanari et al. 2013). Therefore, we further used this concentration to test the effects of PA-6 in atrial cardiomyocytes of patients with SR or cAF.

Figure 42 shows the time course of the basal current and CCh-activated $I_{K,ACh}$ in voltage-clamped atrial cardiomyocytes at -100 mV during 3 min of PA-6 application. Before the application of the I_{K1} inhibitor, the basal current and $I_{K,ACh}$-S1 was recorded through stimulation using the ramp protocol. The inhibitor was then applied before, during and after $I_{K,ACh}$-S2, whereas the $I_{K,ACh}$-S1 served as an internal control. This protocol allowed us to discriminate between the contribution of I_{K1} and $I_{K,ACh}$ to the enhanced basal inward-rectifier

currents in Ctl and cAF patients and also to explore the effect of PA-6 on both groups using Tyrode's solution (Ty) as control conditions of the voltage-clamped atrial cardiomyocytes.

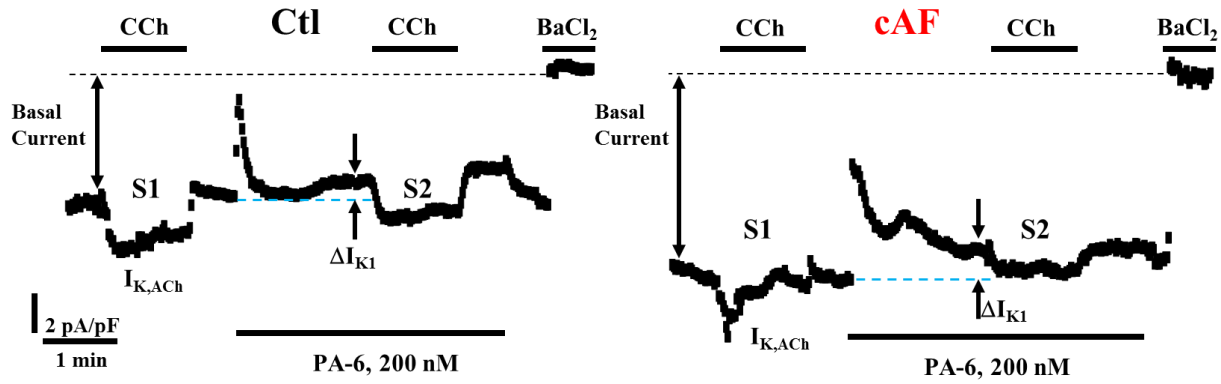

Figure 42: Time course of basal current and CCh-activated $I_{K,ACh}$ at -100 mV in the presence of PA-6 (200 nM) in a Ctl and cAF patient.

PA-6 applied during S2 only and S1 serving as internal control.

A representative recording of membrane current at -100 mV in atrial cardiomyocytes in the presence of PA-6 is shown for the control (Ctl) and cAF groups. The amplitudes of the basal inward-rectifier K^+ current at -100 mV were larger in cAF patients compared to Ctl patients, as expected. The inhibitory effect of PA-6 similarly appears slightly larger in cAF than in Ctl.

4.2.4.1 Effect of pentamidine analogue-6 (PA-6, 200 nM) on basal current in Ctl and cAF patients

We quantitatively analyzed the PA-6 sensitive current, representing I_{K1}, as a difference in basal inward-rectifier K^+ current amplitude before and after application of PA-6 before the second CCh application in SR and in cAF patients (**Figure 43**).

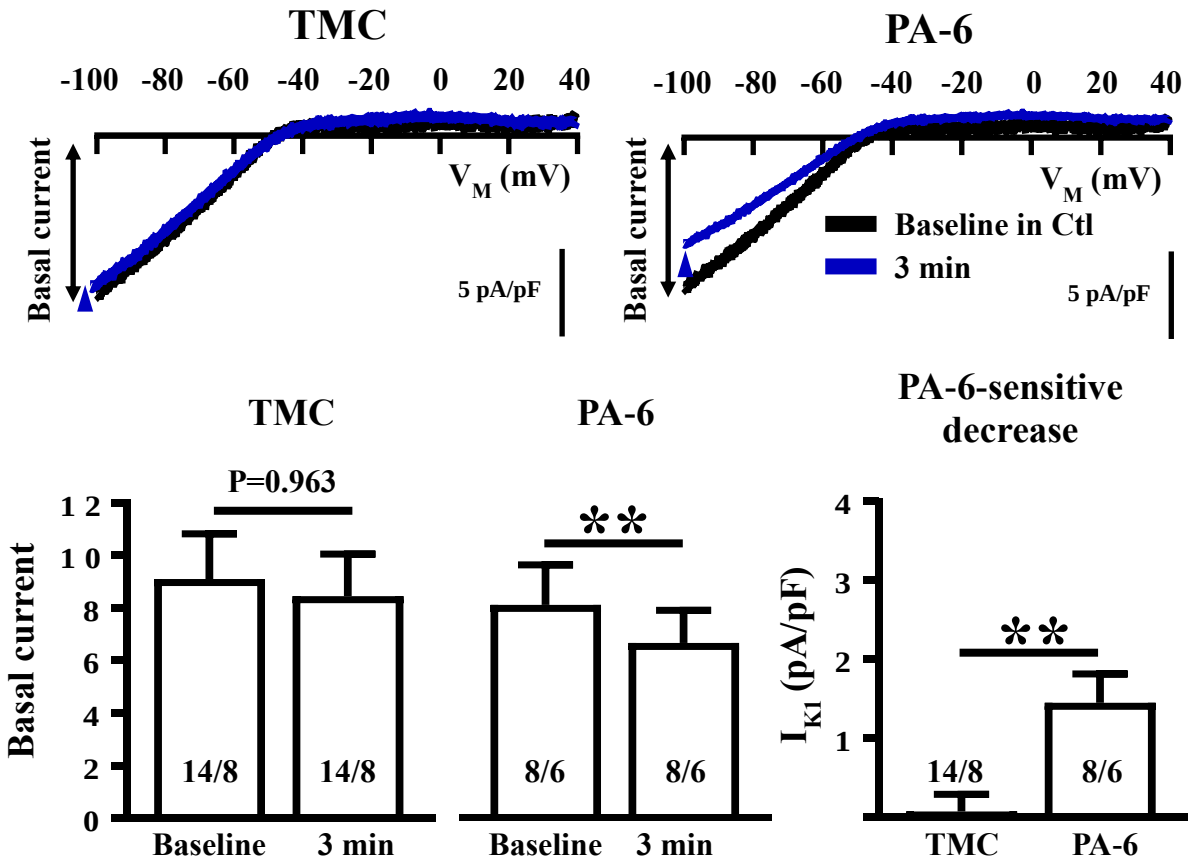

Figure 43: Effect of PA-6 (200 nM) on basal current in human atrial cardiomyocytes of Ctl patients.

Representative current-voltage relationship in time-matched control (TMC; Tyrode`s solution application only) and during PA-6 application for 3 min versus corresponding baseline. Mean±SEM of basal current before (baseline) and after 3 min of Tyrode`s solution or 3 min of PA-6 application and the PA-6-sensitive decrease of $I_{K1.}$ **P<0.05 vs. baseline or TMC, respectively. Numbers in columns indicates myocytes/patients.

Quantitative analyses showed that during 3 min of PA-6 application, there is a clear reduction of the basal inward-rectifier K^+ current in cardiomyocytes of Ctl patients. In order to exclude that this reduction was not due to time-dependent run-down of the current, we performed time-matched control (TMC) experiments, which show that the current amplitude remained stable during 3 min under control conditions. Accordingly, the decrease in the current due to

PA-6 was significantly larger than time-dependent change in TMC, with the PA-6 sensitive decrease unmasking I_{K1}.

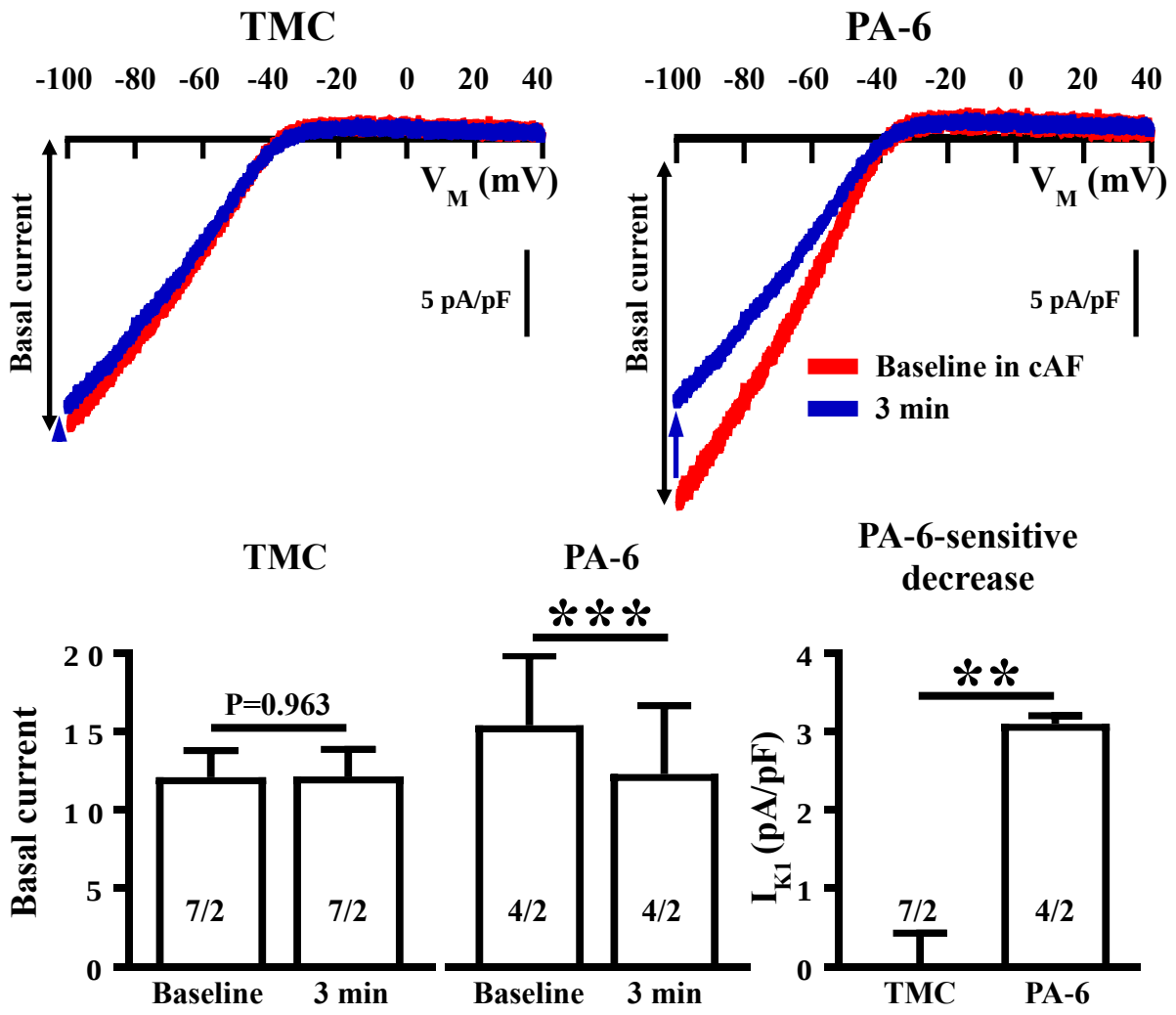

Figure 44: Effect of PA-6 (200 nM) on basal current in human atrial cardiomyocytes of cAF patients.

Representative current voltage relationship in time matched control (TMC; Tyrode`s solution application only, was the baseline) and under PA-6 application. Mean ± SEM difference of basal current during 3 min of Tyrode`s solution and during 3 min of PA-6 application and the PA-6 sensitize decrease of I_{K1}. **P < 0.05 and ***P<0.05 vs. TMC and baseline, respectively. Numbers in columns indicates myocytes/patients.

Figure 44 shows quantitative analyses during 3 min of PA-6 application in patients with cAF, there is a significant reduction of the basal current amplitude. There was no time-dependent effect on the basal current amplitude and the decrease in current due to PA-6 was significantly larger than the time-dependent current change in TMC. We then compared the decrease in basal current due to PA-6 effect in the Ctl and cAF group (**Figure 41**).

4.2.4.2 The PA-6-sensitive decrease of basal current in Ctl and cAF patients

To explore the PA-6 sensitivity to the basal current between Ctl and cAF patients, the relative reduction of the basal current was calculated from the basal current before PA-6 and I_{K1} as the PA-6-sensitive decrease of basal current in both groups (**Figure 45**).

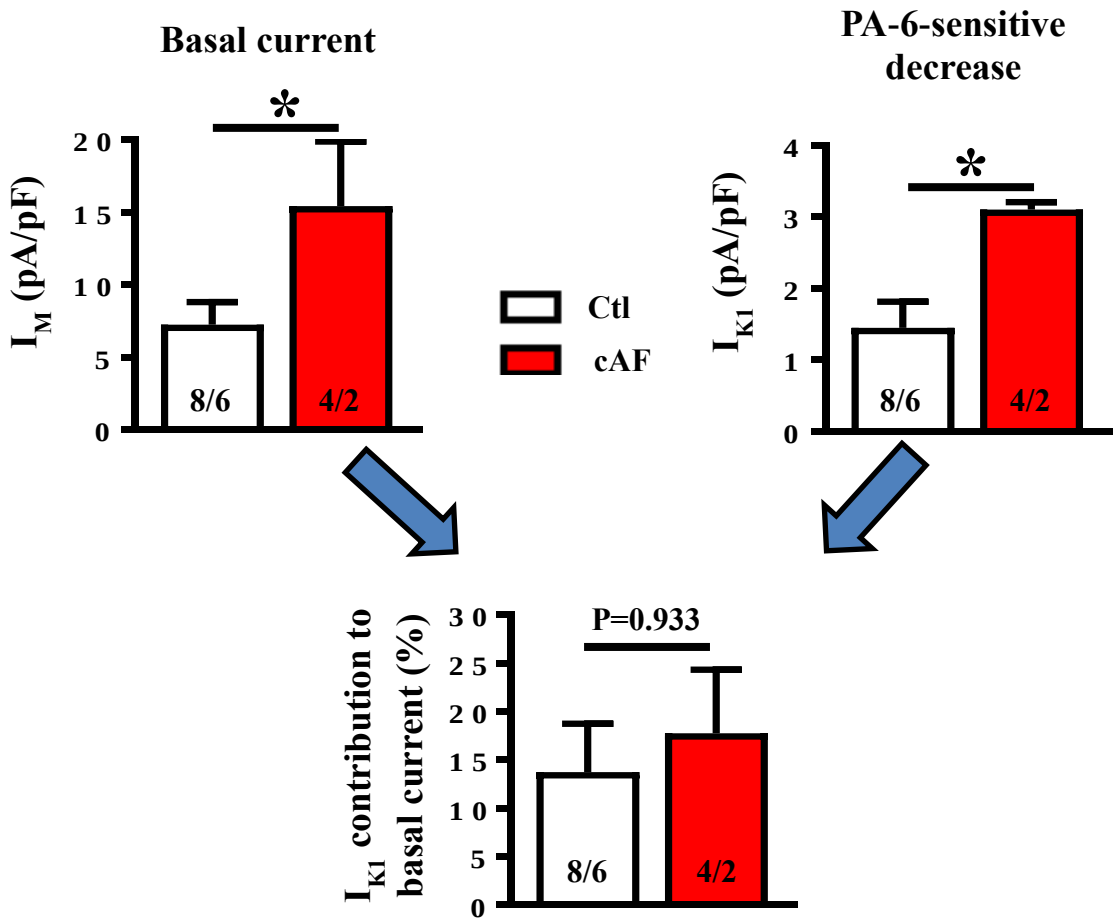

Figure 45: PA-6-sensitive decrease of basal current in Ctl and cAF patients.

Mean±SEM of basal current, PA-6-sensitive decrease representing I_{K1} and the relative reduction of basal current in Ctl vs cAF patients. *P<0.05 vs SR. Numbers in columns indicate myocytes/patients.

These data confirm previous findings showing increased I_{K1} in cAF vs Ctl patients (Dobrev et al. 2001; Dobrev et al. 2005). It also shows the sensitivity of I_{K1} to PA-6. The relative current decrease in response to PA-6 was calculated as the ratio of the I_{K1} to the PA-6-sensitive decrease of the currents, showing that PA-6 blocks a comparable fraction (~15%) of basal inward rectifier in SR and cAF. It points to a comparable affinity of the PA-6 drug for I_{K1} in both groups. This relatively low contribution could either be due to the fact that the concentration of PA-6 used (200 nM) may be too low for completely blocked I_{K1} in the

deceased human atrium or that other K^+ currents (e.g., I_{SK}, I_{K2P}) may also contribute and compensate as least it part the inhibition of I_{K1}. Future work is needed to validate this hypothesis.

4.2.4.3 Effects of PA-6 on $I_{K,ACh}$ in Ctl and cAF patients

The effect of PA-6 on CCh-activated $I_{K,ACh}$ was investigated by analyzing its effects on the ratio between the two consecutive applications of CCh. The ratio of the peak and QSS of both stimulation steps in the absence or presence of PA-6 was employed to check for potential modulation of $I_{K,ACh}$ by PA-6. This was performed in both Ctl and cAF patient groups comparing them to their corresponding TMC, but no effect of PA-6 could be detected (**Figure 46**).

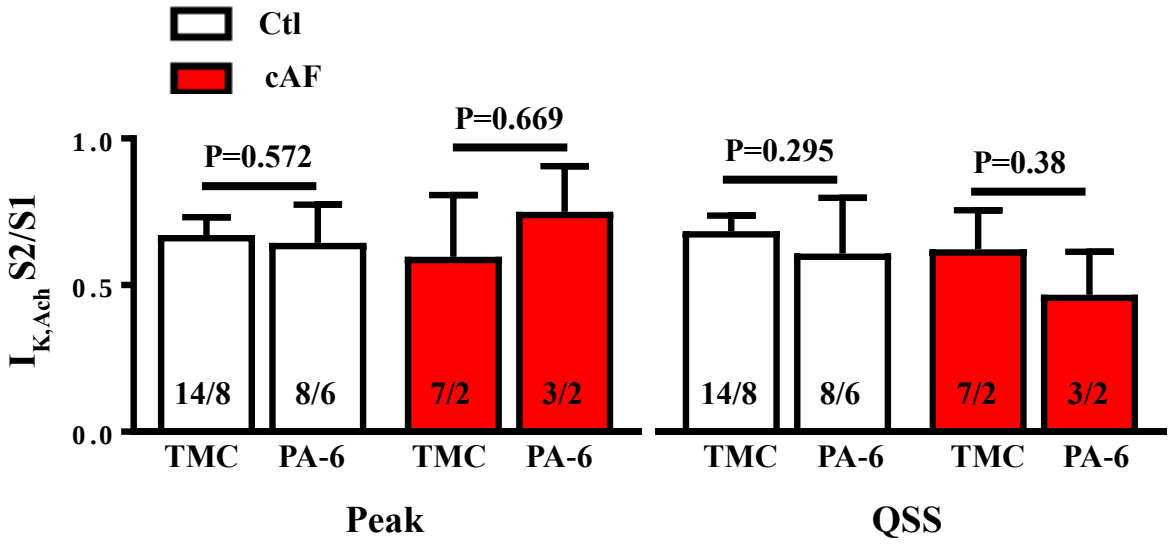

Figure 46: Effect of PA-6 on $I_{K,ACh}$ in Ctl and cAF patients.

Mean±SEM of CCh-activated $I_{K,ACh}$ at S2/S1 of Peak and Quasi-Steady-State (QSS) under PA-6 (200 nM) application and in time matched controls (TMC). Numbers indicates myocytes/patients.

Thus, PA-6 (200 nM) selectively blocks I_{K1} current in human atrial cardiomyocytes from SR and cAF patients without effects on CCh-activated $I_{K,ACh}$. PA-6 may provide an important tool to discover additional non-I_{K1} contributors to increased basal current in cAF. By prolonging APD in patients with cAF, it might also help to reduce the persistence of AF.

5 Discussion

The study presented in this thesis is divided in two parts. In the first part, the underlying pathophysiology and mechanisms of poAF were investigated. In particular, the as intrinsic arrhythmogenic substrate and potential triggers for poAF were studied in isolated atrial cardiomyocytes from patients undergoing open-heart surgery. Our findings identify a number of key differences in intracellular Ca^{2+} handling and the expression of Ca^{2+}-handling proteins in atrial cardiomyocytes from poAF patients. The major findings are: I) unchanged $I_{Ca,L}$ amplitude, II) smaller amplitudes of the systolic Ca^{2+} transient, III) markedly reduced fractional shortening, IV) preserved SR Ca^{2+} load reflected by the unchanged integral of $I_{NCX,}$ and V) increased CaMKII-phosphorylation of RyR2 at Ser2814 along with a higher incidence of potentially proarrhythmic SCaEs in poAF vs Ctl patients.

In the second part of this study, the selective I_{K1} inhibitor PA-6 was employed to evaluate the contribution of I_{K1} to the basal inward-rectifier K^+ current in cAF patients. The major findings of this part include: I) basal inward-rectifier K^+ current and PA-6-sensitive current defined as I_{K1} are increased in cAF, II) reduced muscarinic-receptor activated $I_{K,ACh}$ in cAF, III) lack of effect of PA-6 on $I_{K,ACh}$ validating the selective inhibition of I_{K1} by PA-6 in the human atrium.

For the functional experiments in the first study, analyses were performed in a blinded manner, without knowledge of patient´s post-operative rhythm status and poAF substratification usually performed several weeks after completion of the experiments. During the post-operative period, the patients rhythm was monitored during their in hospital stay with continuous 3-lead ECG-recording in the intensive care unit by clinicians for 3 to 5 days, then once daily. These are saved on a central monitoring system (Medico) accessible for clinical characterization of patients' postoperative status. The ECGs were analyzed by experienced clinicians from the cardiac-surgery team. PoAF status was assigned to patients with any documented AF episode lasting longer than 30 s (Frendl et al. 2014), while the control group consisted of patients without any AF episodes.

Based on the data collected from patients enrolled in this study, about ~46 % developed poAF, which is in accordance with previous published estimates of surgical patients that develop poAF (Mathew et al. 2004; Ozawa et al. 2015). Our data also shows that poAF patients were older than Ctl patients, which suggests that age-dependent alterations in atrial Ca^{2+}-handling might also contribute to the poAF- associated remodeling. There were no differences in type and frequency of medication or other selected clinical parameters between the groups.

5.1 Changes in cellular Ca^{2+} handling in poAF

Conceptually, triggered activity and reentry are the main mechanisms for the initiation and maintenance of AF and they require both a pre-existing substrate and acute initiators ("triggers") (Heijman et al. 2014). In the case of poAF, the triggers are likely caused by the surgical interventions, which unmask pre-existing susceptibility to AF. Based on the data in this work, abnormal intracellular Ca^{2+}-handling and subsequent impairment of atrial contractility is hypothesized to contribute to the pre-existing substrate, since it can be detected in atrial samples taken during surgery, before the occurrence of poAF. Additionally, since inflammation is an accepted trigger of AF (Maesen et al. 2012), further investigations were conducted to determine the cellular mechanisms by which inflammation may trigger poAF by acting on remodeled atrial Ca^{2+}-handling, thereby contributing to the initiation and maintenance of poAF. Based on our data we hypothesized that atrial cardiomyocytes from poAF patients would be more susceptible to inflammatory cytokines induced SCaEs-mediated triggered activity.

To investigate the possible alterations in cellular electrophysiology, the methodology previously established for simultaneous recording of CaT and membrane currents in our laboratory (Voigt et al. 2012) was extended with parallel recording of cellular shortening to investigate cytosolic Ca^{2+} handling and cellular contractility predisposing to the development of poAF. IL-1β was acutely applied to cells to study the effects of inflammation as a post-operative trigger of Ca^{2+}-handling abnormalities that promote poAF induction. Experiments were performed on freshly isolated right-atrial cardiomyocytes from patients with sinus rhythm undergoing open-heart surgery. In addition, tissue samples for biochemistry experiments were frozen in liquid-nitrogen prior to collection from the operation room and stored in a liquid nitrogen storage tank until post-operative rhythm status was established. Atrial cardiomyocytes were isolated according to a previously published protocol (described in **section 3)** using EGTA-free solutions to prevent $[Ca^{2+}]_i$ buffering (Voigt et al. 2012). $I_{Ca,L}$ was activated through a standard voltage-clamp protocol at 0.5 Hz simultaneously with systolic CaTs, which were quantified using Fluo-3 AM as a Ca^{2+} indicator.

In the present study we detected unchanged amplitude of $I_{Ca,L}$, but a ~35% decrease CaT amplitude in poAF vs Ctl (**Figure 27**), which contrasts data on pAF, where we observed similar $I_{Ca,L}$ in both Ctl and pAF groups, but increased $I_{Ca,L}$-triggered CaT amplitude (Voigt et al. 2014). This underscores that distinct mechanisms contribute to AF in different forms of AF. In addition, simultaneously recorded single-cell contractions in the poAF group showed a lower absolute cell-shortening amplitude, reduced time-to peak, markedly smaller fractional

shortening with no change in the decay-time constant (**Figure 29)**. In the atrium, $I_{Ca,L}$ and RyR2 channels are not necessarily in close proximity to each other because of the lack of fully developed T-tubule systems (Smyrnias et al. 2010). This could explain why the lower CaT amplitude does not associate with a corresponding slowing of $I_{Ca,L}$ inactivation. The reduced CaT amplitude could however, contribute to the reduction in cellular shortening and may underlie the impaired atrial contraction in patients developing poAF (present study).

The reduced CaT amplitude may result from either a reduced SR Ca^{2+} load and/or an intrinsic dysregulation of Ca^{2+}-induced Ca^{2+} release through RyR2. We found that the amplitude of cCaT and the integrated I_{NCX} in response to caffeine, which is the most reliable index of SR Ca^{2+} load, were both unchanged in poAF vs Ctl (**Figure 30**). This suggests that SR Ca^{2+} load is an unlike cause of the reduced CaT amplitude in poAF. We calculated the rate constant of SERCA (K_{SERCA}) to estimate SERCA function and found comparable rate constants of SERCA in poAF and Ctl group (**Figure 31**), confirming previous finding which demonstrated that SERCA removes ~80%, whereas NCX+PMCA extrude only ~20% of cytosolic Ca^{2+} in the atria (Walden et al. 2009). In our previous publications we showed that SERCA contribution to Ca^{2+} removal was ~66% in Ctl, ~46% in cAF and ~62% in pAF patients (Voigt et al. 2012; Voigt et al. 2014), which are lower than the values we obtained in the present work. The reason for the quantitative differences is unknown and further work is needed to validate the contribution of SERCA, NCX, and PMCA to Ca^{2+} removal.

The elevation of extracellular Ca^{2+} increases the risk of atrial arrhythmias (Passini et al. 2014) and pro-inflammatory cytokines have been associated with the onset and maintenance of AF (Issac et al. 2007). For instance the levels of IL-1 and IL-6, two key cytokines mediating inflammatory responses, were elevated in patients with persistent AF (Cheng et al. 2012) and IL-1β has been suggested to reduce $I_{Ca,L}$ (Prabhu 2004). Therefore we increased extracellular Ca^{2+} from 2 mM to 5 mM to enhance the susceptibility to SCaEs by overloading the cells with Ca^{2+} and applied IL-1β to simulate the proinflammatory state in the postoperative period, with the expectation that these manipulations will increase SR Ca^{2+} leak through RyR2 channels and unmask a higher susceptibility to SCaEs, particularly in poAF patients. In this study, we identify for the first time an increased IL-1β-mediated susceptibility to SCaEs along with a higher frequency of SCaEs in the poAF group, which points to postoperative inflammation as a potential trigger of atrial arrhythmogenesis in poAF patients. In addition, our current data suggest that increased incidence of SCaEs and related triggered activity is a common denominator of the cellular pathophysiology of pAF, cAF and poAF patients (Voigt et al., 2012; Voigt et al., 2014; present study).

In order to test whether changes in protein expression and/or phosphorylation underlie the observed functional abnormalities, we performed Western-blot experiments of major Ca^{2+}-handling proteins. There were no significant differences in the protein expression levels of SERCA2a, PLB, RyR2, triadin, junctin, JPH-2 calsequestrin and the phosphorylation states of PLB at Ser16 and Thr17 and of RyR2 at Ser2808. However, CaMKII-mediated Ser2814-phosphorylation of RyR2 was ~34% higher in poAF vs Ctl group, which is expected to increase the Ca^{2+} sensitivity of RyR2 to cytosolic Ca^{2+} (Voigt et al. 2012), thereby increasing the diastolic RyR2-mediated SR Ca^{2+} leak and contributing to the increased incidence of SCaEs in poAF compared to Ctl patients. Altogether, our functional and biochemistry data provide novel insights into the preexisting cellular substrate, which predisposes patients to the development of poAF by open heart surgery related triggers like proinflammatory cytokins.

5.1.1 Comparison with previous findings of poAF

Postoperative AF is a frequent condition but the underlying causes are poorly understood. A reasonable hypothesis to explain the occurrence of poAF is that patients with predisposing ionic-current abnormalities respond to the atrial trauma associated with cardiac surgery by developing AF in the postoperative setting (Nattel 2006). Until now, only very few studies have attempted to address this hypothesis and the available data are partially inconsistent (**Table 1**). Density of I_{K1} and $I_{K,ACh}$ (Dobrev et al. 2002) and I_{to} and I_{Kur} (Brandt et al. 2000) were comparable in poAF and Ctl patients. By contrast, a significantly larger $I_{Ca,L}$ was related to the occurrence of poAF, contrasting the reduced $I_{Ca,L}$ density that is typical of cAF (Van Wagoner et al. 1999; Christ et al. 2004). A more recent study provided a more detailed analysis of the cellular electrophysiological properties including ionic currents and AP properties related to poAF occurrence. However, they found no significant changes in the ionic currents I_{to}, $I_{K1,}$ $I_{Ca,L}$ or in the AP properties (APD, upstroke velocity, and ERP) between poAF and Ctl patients, suggesting that there are no major preexisting electrophysiological properties that predispose to the development of poAF. Prolonged atrial electrograms along with reduced mRNA levels of SERCA2a (but not protein expression levels) and sarcolipin and decreased protein expression of sarcolipin and the myosin heavy chain were reported in poAF patients (Zaman et al. 2016). However, our data showed no differences in the density of $I_{Ca,L}$ in poAF vs Ctl and are consistent with observations showing no major changes in APD of multicellular atrial trabeculae of poAF patients (Khan et al. 2016), although the APD of the latter was slightly but significantly prolonged at 90% of repolarization (Khan et al. 2016).

In the present study we identified significant Ca^{2+}-handling abnormalities and contractile dysfunction, which may underlie the occurrence of poAF by increasing the susceptibility

SCaEs. Increased incidence of SCaEs is also typical for the cellular pathophysiology of pAF and cAF patients, although SCaEs appear to have distinct molecular bases in each form of AF. For instance, the activity of CaMKII is increased in patients with cAF, resulting in hyperphosphorylation of RyR2 and increases in RyR2 channel open probability, promoting SR Ca^{2+} leak and SCaEs (Voigt et al. 2012). In pAF, there was no increase in RyR2 phosphorylation, however, increased single-channel RyR2 open probability was observed, possibly resulting from other posttranslational modifications of RyR2 (e.g., oxidation, S-nitrosylation) (Voigt et al. 2014) or changes in the composition of the RyR2 macromolecular complex. For example, RyR2 expression was upregulated in pAF, but certain RyR2-stabilizing subunits like JPH-2 were unchanged (Beavers et al. 2013). The increase in RyR2 without change in the associated regulator protein JPH-2 would cause a relative depletion of inhibitory JPH-2 in the RyR2 complex, potentially enhancing channel activity (Beavers et al. 2013). SR Ca^{2+} uptake was increased in pAF (vs. decreased in cAF), and the consequent enhancement in SR Ca^{2+} load also promoted greater SR Ca^{2+} leak and a higher frequency of SCaEs and DADs (Voigt et al. 2014). In cAF, NCX1 expression was increased, producing a larger depolarizing inward current for a given amount of free intracellular Ca^{2+} (Voigt et al. 2012). In contrast, NCX1 expression and its Ca^{2+}-dependent activation were unaltered in pAF (Voigt et al. 2014). The molecular basis of increased incidence of SCaEs in poAF patients likely results from Ser2814-hyperphosphorylation (activation) of RyR2 during diastole, a phenotype similar to cAF patients, where RyR2 was also hyperphosphorylated at Ser2814. In contrast, increased Ser2808 phosphorylation of RyR2 and protein expression NCX1 along with a strong decrease in $I_{Ca,L}$ are typical findings in cAF patients (Schotten et al. 2001; Schotten et al. 2002; El-Armouche et al. 2006; Voigt et al. 2012), whereas these changes could not be observed in patients with pAF and poAF (Voigt et al. 2014; present study). The differences in Ca^{2+}-handling abnormalities between the distinct forms of AF highlight the clear need for novel AF-type-tailored therapeutic strategies (Heijman et al. 2015).

5.2 Contribution of I_{K1} to basal inward-rectifier K^+ current in cAF

In the cardiac AP, the basal inward-rectifier current is usually considered to be exclusively carried by I_{K1}, contributing strongly to the final repolarization phase-3 (Anumonwo & Lopatin 2010; Lopatin & Nichols 2001; Takanari et al. 2013). Loss- or gain-of-function of I_{K1} in patients have been associated with Andersen-Tawil Syndrome type 1, congenital AF, and catecholamine polymorphic ventricular fibrillation (Takanari et al. 2013), highlighting the

clinical importance of this current. AF is associated with an abbreviation of the APD, which creates an arrhythmogenic substrate for reentry and maintenance of AF (Dobrev et al. 2001; Dobrev et al. 2005; Voigt et al. 2010). Although the basal inward-rectifier K^+ current is often considered equal to $I_{K1,}$ multiple currents including agonist-independent "constitutive" $I_{K,ACh}$, I_{K2P} currents and SK currents are likely to contribute (Anumonwo & Lopatin 2010; Dobrev et al. 2005; Schmidt et al. 2015). The current study defines for the first time the magnitude of I_{K1} with a putatively selective I_{K1}-inhibitor. Typically, barium ions are often used during *in vitro* or *ex vivo* experiments to block the inward-rectifier K^+ currents; however, barium cannot be used in vivo (De Boer et al. 2010). The goal of this study was to employ the I_{K1}-inhibitor PA-6 and to quantify the contribution of I_{K1} to basal inward-rectifier K^+ current in Ctl and cAF patients. PA-6 has been shown to inhibit I_{K1} with low nanomolar IC_{50} values (with 200 nM producing a maximal block of I_{K1}), without affecting trafficking and/or expression of $K_{IR}2.x$ and other ionic channel proteins, and no direct block of additional cardiac ion channels (Takanari et al. 2013).

In this part of the study, the identity of basal inward-rectifier K^+ current and $I_{K,ACh}$ was proven with Ba^{2+}. The amplitude of the basal inward-rectifier K^+ current was larger in cAF vs Ctl (**Figure 41**), confirming previous findings of our laboratory (Dobrev et al. 2001; Dobrev et al., 2005; Voigt et al., 2010). Application of the M-receptor agonist CCh led to an increase in the total current density due to activation of $I_{K,ACh}$. Consistent with previous studies the M-receptor-mediated activation of $I_{K,ACh}$ was lower in cAF (Dobrev et al. 2001; Dobrev et al. 2005; Voigt et al. 2010).

Contribution of I_{K1} to basal current was assessed by comparing basal inward-rectifier K^+ currents in the presence of PA-6 with corresponding TMCs (**Figure 43 and 44**). The PA-6 sensitive decrease in basal current was larger in cAF than in Ctl, although the relative contribution of I_{K1} to basal current was smaller than expected in both Ctl and cAF group (**Figure 45**), likely because of differences in affinity of the drug to I_{K1} in the diseased human atrium than in the expression system or compensation of block by other K^+ conductance like I_{K2P} and/or SK channels. Future studies should directly test this hypothesis. There was no change in the density of $I_{K,ACh}$ in the presence of PA-6 (**Figure 46**), validating the selective nature of the drug for $I_{K1.}$ Taken together, these data suggest that PA-6 may be a potent and specific I_{K1}-blocker and a potential antiarrhythmic drug for patients with cAF, although its selectivity and potency for I_{K1} in the human atrium need further exploration.

5.2.1 Comparison with previous findings of inward-rectifier K^+ currents

Many studies have supported the hypothesis that AF is maintained by high-frequency reentrant mechanisms resulting from alterations in different repolarizing K^+ currents including I_{K1} and $I_{K,ACh}$ (Heijman et al. 2014). Accordingly, inhibition of repolarizing K^+ currents may prevent the maintenance of AF in the atrium. On the contrary, inhibition of ventricular repolarizing K^+ channels may lead to extensive AP prolongation supporting the occurrence of "torsades de pointes" type of ventricular arrhythmias (Qu et al. 2013; Voigt & Dobrev 2016).

The study of Pandit et al, (Pandit et al. 2005) on ionic determinants of functional reentry in a 2-D model of human atrial cardiomyocytes clearly showed that doubling the magnitude of the I_{K1} increased rotor frequency and reduced tip meander, thereby causing a shortening of the APD and an enhanced cardiac excitability and leading to rotor stabilization. The enhanced cardiac excitability was due to the hyperpolarization of the resting membrane potential, which increased availability of the I_{Na}. In addition they showed that a reduction of the maximum conductance (by 90%) of the atrial-selective current I_{Kur} (and I_{to}), but not the I_{Kr} or I_{Ks} also terminated the rotors and demonstrated that blockade of I_{Kur} and I_{to} prolonged the atrial AP at the plateau, but not at the terminal phase of repolarization, which led to random tip meander and wave break resulting in rotor termination (Pandit et al. 2005). Therefore, atrial-selective inhibition of cardiac repolarizing K^+ currents is still a major goal in development of novel anti-AF K^+ channel modulators (Voigt & Dobrev 2016).

We confirm our previous studies of increased basal inward-rectifier K^+ current and decreased M-receptor-mediated activation of $I_{K,ACh}$ (Dobrev et al. 2001; Dobrev et al. 2005; Voigt et al. 2010; Voigt & Dobrev 2016). However, agonist-independent (constitutive) activity of $I_{K,ACh}$ has been suggested to contribute to the increased total basal inward-rectifier K^+ current in cAF (Dobrev et al. 2005). Previous work in different cell models showed that PA-6 does not block $I_{Na1.5}$, $I_{Ca,L}$, I_{to}, I_{Kr}, whereas $K_{ir}2.1$-2.3-carried I_{K1} was almost completely inhibited with 200 nM PA-6 in HEK 293 cells (De Boer et al. 2010; Varkevisser et al. 2013; Takanari et al. 2013). Therefore, we have used 200 nM PA-6 to determine the contribution of I_{K1} to the total inward-rectifier K^+ current and in agreement, our data in human atrial cardiomyocytes also showed that PA-6 is selective for I_{K1} and do not inhibit $I_{K,ACh}$. The relative contribution of I_{K1} to basal current was small (15-20%) and it is therefore likely that other K^+ channels like the I_{K2P} and SK channels, which have been recently implicated in APD shortening in cAF (Schmidt et al. 2015; Heijman et al. 2015), partially compensated the PA-6 induced I_{K1} block.

In the work of Schmidt et al (Schmidt et al. 2015), $K_{2P}3.1$ subunits exhibited predominant atrial expression and transcription levels were highest among functional K_{2P} channels. Furthermore, $K_{2P}3.1$ mRNA and protein levels were increased in cAF with enhancement of

corresponding currents in the right atrium which, resulted in shortened APD compared to Ctl patients. Further work is required to precisely dissect the individual contributions of I_{K1}, I_{K2P} and SK channels to the basal inward-rectifier K^+ current in Ctl and AF patients.

5.3 Potential clinical implications

AF is the most common clinically relevant arrhythmia (Kannel et al. 1998) and current treatment options remain inadequate. This is in part due to an incomplete understanding of the underlying mechanisms in an individual patient. As such it is of clinical importance to identify whether alterations of the cellular ion currents and Ca^{2+} homeostasis described in this work contribute to the arrhythmogenic substrate in poAF and allow pharmacological control of AF in cAF.

This work has identified abnormal Ca^{2+} handling in poAF as a potential contributor to cellular triggered activity and perhaps reentry, with the hope that it might foster the development of experimental compound to target these abnormalities. One potential target could be RyR2, since it is crucial for the development of SCaEs, which were shown to be more prominent in poAF patients. Besides these underlying molecular triggers, advanced age is an independent predictor of poAF and it will be important to identify how advanced age predisposes to poAF development.

Inward-rectifier K^+ currents abbreviate APD in cAF patients and more effective in promoting reentrant mechanisms than reduced $I_{Ca,L}$ that produce similar APD abbreviation (Voigt et al. 2010). With the I_{K1}-specific inhibitor PA-6 we uncovered a higher I_{K1} in cAF than in Ctl patients. Thus PA-6 may be a potential new pharmacological agent to reduce the upregulated basal inward-rectifier K^+ current through a specific inhibition of I_{K1}, thereby potentially prolonging the APD and preventing arrhythmia maintenance in cAF.

5.4 Study limitations

All tissue samples were collected from right-atrial appendages, which may not be fully representative for the rest of the right atrium or other regions of the atrium including the left atrium. Also, the subset of patients used in this study was selected because of the better tissue availability due to open heart surgery and may thus not represent the situation of the general AF population. In addition, although except age there were no differences in the clinical characteristics and medication between Ctl, poAF and cAF patients, the type of cardiac surgery, the diversity in underlying heart diseases and the accompanying medications are likely to influence the outcome of our studies.

Ionic currents were recorded from cardiomyocytes acutely isolated from human atrial samples and use of proteases during the isolation procedure might destroy key cellular proteins biasing the results. This also holds true for the biochemistry experiments, including the tissue handling during freezing in liquid nitrogen. Another limitation when working with human tissue is the substantial inter-patient and inter-cell variability, with some patients providing more cells to the mean values than other patients. Cell viability also differed between the cell isolations and was generally limited to ~6 hrs after isolation. The ability to reproduce the complex initiating factors for the poAF study was done using IL-1β only. Finally, whole tissue homogenates were used for the Western blot experiments under the assumption that the measured protein levels also reflect the abundance of the protein of interest in atrial cardiomyocytes.

6 Conclusions

In conclusion, we found that the development of poAF is likely due to a combination of factors, including preoperative predisposing atrial Ca^{2+}-handling abnormalities and cardiac surgery-induced stressors such as inflammatory cytokins, which act on the preexisiting proarrhythmogenic substrate as triggers to initiate poAF. We investigated the cellular substrate that predisposes patients to the development of poAF and the potential triggers that may promote the initiation of poAF. To the best of our knowledge, this is the first comprehensive study addressing both cellular electrophysiology and Ca^{2+} handling, two major determinants of triggered activity and reentry in patients with poAF. The enhanced susceptibility to cellular triggered activity could be one major mechanism of arrhythmogenesis in poAF patients. Our novel findings are clearly of clinical relevance for future considerations in drug development. In addition, we could demonstrate that PA-6 is a novel inhibitor of I_{K1} which allows for discrimination of I_{K1} among other basal currents contributing to the resting membrane potential, with I_{K1} constituting a promising therapeutic approach for cAF. Overall, the present study improves our understanding of atrial cellular arrhythmogenic mechanisms in AF in general and in poAF in particular, potentially facilitating the development of improved therapeutic strategies.

7 References

Alagem N, Dvir M, Reuveny E. Mechanism of Ba^{2+} block of a mouse inwardly rectifying K^+ channel: differential contribution by two discrete residues. *J Physiol*. 2001;534:381–593.

Andrade J, Khairy P, Dobrev D, Nattel S. The clinical profile and pathophysiology of atrial fibrillation: relationships among clinical features, epidemiology, and mechanisms. *Circ Res.* 2014;114:1453–1468.

Antzelevitch C, Burashnikov A. Overview of basic mechanism of cardiac arrhythmia. *Card Electrophysiol Clin*. 2011;3:23–45.

Anumonwo JMB, Lopatin AN. Cardiac strong inward rectifier potassium channels. *J Mol Cell Cardiol.* 2010;48:45–54.

Bassani JW, Bassani RA, Bers DM. Relaxation in rabbit and rat cardiac cells: species-dependent differences in cellular mechanisms. *J Physiol*. 1994;476:279–293.

Beavers DL, Wang W, Ather S, Voigt N, Garbino A, Dixit SS, Landstrom AP, Li N, Wang Q, Olivotto I, Dobrev D, Ackerman M, Wehrens XHT. Mutation E169K in junctophilin-2 causes atrial fibrillation due to impaired RyR2 stabilization. *J Am Coll Cardiol.* 2013;62:2010–2019.

Bers DM. Calcium cycling and signaling in cardiac myocytes. *Annu Rev Physiol*. 2008;70:23–49.

Bers DM. Cardiac excitation-contraction coupling. *Nature*. 2002;415:198–205.

Bosch RF, Zeng X, Grammer JB, Popovic K, Mewis C, Kühlkamp V. Ionic mechanisms of electrical remodeling in human atrial fibrillation. *Cardiovasc Res*. 1999;44:121–131.

Brandt MC, Priebe L, Böhle T, Südkamp M, Beuckelmann DJ. The ultrarapid and the transient outward K^+ current in human atrial fibrillation. Their possible role in postoperative atrial fibrillation. *J Mol Cell Cardiol*. 2000;32:1885–1896.

Brundel BJ, Van Gelder IC, Henning RH, Tieleman RG, Tuinenburg E, Wietses M, Grandjean JG, Van Gilst WH, Crijns HJGM. Ion channel remodeling is related to intraoperative atrial effective refractory periods in patients with paroxysmal and persistent atrial fibrillation. *Circulation*. 2001;103:684–690.

Caballero R, González de la Fuente M, Gomez R, Barana A, Amorós I, Dolz-Gaitón P, Osuna L, Almendral J, Atienza F, Fernández-Avilés F, Pita A, Rodríguez-Roda J, Pinto Á, Tamargo J, Delpón E. In humans, chronic atrial fibrillation decreases the transient outward current and ultrarapid component of the delayed rectifier current differentially on each atria and increases the slow component of the delayed rectifier current in both. *J Am Coll Cardiol*. 2010;55:2346–2354.

Camm AJ, Kirchhof P, Lip GYH, Schotten U, Savelieva I, Ernst S, Van Gelder IC, Al-Attar N, Hindricks G, Prendergast B, Heidbuchel H, Alfieri O, Angelini A, Atar D, Colonna P, De Caterina R, De Sutter J, Goette A, Gorenek B, Heldal M, Hohloser SH, Kolh P, Le Heuzey JY, Ponikowski P, Rutten FH. Guidelines for the management of atrial fibrillation. *Europace*. 2010;12:1360–1420.

Cheng T, Wang XF, Hou YT, Zhang L. Correlation between atrial fibrillation, serum amyloid protein A and other inflammatory cytokines. *Mol Med Rep*. 2012;6:581–584.

Chemistry of Protein Assays. (n.d). *Thermo Scientific™ Web site.* Retrieved January, 2016, from https://www.thermofisher.com/de/de/home/life-science/protein-biology/protein-biology-learning-center/protein-biology-resource-library/pierce-protein methods/chemistry-protein-assays.html.

Christ T, Boknik P, Wöhrl S, Wettwer E, Graf EM, Bosch RF, Knaut M, Schmitz W, Ravens U, Dobrev D.et al. L-type Ca^{2+} current downregulation in chronic human atrial fibrillation is associated with increased activity of protein phosphatases. *Circulation*. 2004;110:2651–2657.

Chugh SS, Havmoeller R, Narayanan K, Kim Y, Jr JHM, Zheng Z. Worldwide Epidemiology of Atrial Fibrillation: A global burden of disease 2010 study. *Circulation.* 2014;129:837–847.

Curtis HJ, Cole KS. Membrane resting and action potentials from the squid giant axon. *J Cell Comp Physiol.* 1942;19:135–144.

De Boer T, Nalos L, Stary A, Kok B, Houtman M, Antoons G, van Veen T, Beekman JDM, de Groot BL, Opthof T, Rook MB, Vos MA, van der Heyden MB. The anti-protozoal drug pentamidine blocks $K_{IR}2.x$-mediated inward rectifier current by entering the cytoplasmic pore region of the channel. Br J Pharmacol. 2010;159:1532–1541.

Dobrev D, Friedrich A, Voigt N, Jost N, Wettwer E, Christ T, Knaut M, Ravens U. The G protein-gated potassium current $I_{K,ACh}$ is constitutively active in patients with chronic atrial fibrillation. *Circulation.* 2005;112:3697–3706.

Dobrev D, Graf E, Wettwer E, Himmel HM, Hála O, Doerfel C, Christ T, Schüler S, Ravens U. Molecular basis of downregulation of G-protein-coupled inward rectifying K^+ current $I_{K,ACh}$ in chronic human atrial fibrillation: decrease in GIRK4 mRNA correlates with reduced $I_{K,ACh}$ and muscarinic receptor-mediated shortening of action potentials. *Circulation*. 200;104:2551–2557.

Dobrev D, Wettwer E, Kortner A, Knaut M, Schuler S, Ravens U. Human inward rectifier potassium channels in chronic and postoperative atrial fibrillation. *Circ Res.* 2002;54:397–404.

El Khoury N, Mathieu S, Fiset CE. Interleukin-1β reduces L-type Ca^{2+} current through protein kinase C Epsilon activation in mouse heart. *J Biol Chem*. 2014;289:21896–21908.

El-Armouche A, Boknik P, Eschenhagen T, Carrier L, Knaut M, Ravens U, Dobrev D. Molecular determinants of altered Ca^{2+} handling in human chronic atrial fibrillation. *Circulation.*2006;114:670–680.

Fabiato A. Calcium-induced release of calcium from the cardiac sarcoplasmic reticulum. *Am J Physiol.* 1983;245:C1–14.

Fabritz L, Guasch E, Antoniades C, Bardinet I, Benninger G, Betts TR, Brand E, Breithardt G, Bucklar-Suchankova G, Camm AJ, Cartlidge D, Casadei B, Chua WWL, Crijns HJGM, Deeks J, Hatem S, Hidden-Lucet F, Kääb S, Maniadakis N, Martin S, Mont L, Reinecke H, Sinner MF, Schotten U, Southwood T, Stoll M, Vardas P, Wakili R ,West A, Ziegler A, Kirchhof P. Defining the major health modifiers causing atrial fibrillation: a roadmap to underpin personalized prevention and treatment. *Nat Rev Cardiol* 2015;13:230–7.

Fluorescence SpectraViewer. (n.d.). *Thermo Scientific™. Web site.* Retrieved October, 2016, from https://www.thermofisher.com/de/de/home/life-science/cell-analysis/labeling-chemistry/fluorescence-spectraviewer.html.

Frendl G, Sodickson AC, Chung MK, Waldo AL, Gersh BJ, Tisdale JE, Calkins H, Aranki S, Kaneko T, Cassivi S, Smith SC, Darbar D, Wee JO, Waddell TK, Amar D, Adler D. 2014 AATS guidelines for the prevention and management of perioperative atrial fibrillation and flutter for thoracic surgical procedures. *J Thorac Cardiovasc Surg*. 2014;148:e153–e193.

Fye WB. A History of the origin, evolution, and impact of electrocardiography. *Am J Cardiol*. 1994;73:937–949.

Gentet LJ, Stuart GJ, Clements JD. Direct measurement of specific membrane capacitance in neurons. *Biophys J*. 2000;79:314–320.

Goette A, Kalman JM, Aguinaga L, Akar J, Cabrera JA, Chen SA, Chugh SS, Corradi D, D'Avila A, Dobrev D, Fenelon G, Gonzalez M, Hatem SN, Helm R, Hindricks G, Ho SY, Hoit B, Jalife J, Kim YH, Lip GYH, Ma CS, Marcus GM, Murray K, Nogami A, Sanders P, Uribe W, Van Wagoner DR, Nattel S.EHRA/HRS/APHRS/SOLAECE expert consensus on atrial cardiomyopathies: definition, characterization, and clinical implication. *Europace.* 2016;18:1455–1490.

Grant AO. Cardiac ion channels. *Circ Arrhythm Electrophysiol*. 2009;2:185–194.

Guo A, Yang H. Ca^{2+} removal mechanisms in mouse embryonic stem cell-derived cardiomyocytes. *Am J Physiol Cell Physiol*. 2009;297:C732– C741.

Hamill OP, Marty A, Neher E, Sakmann B, Sigworth FJ. Improved patch-clamp techniques for high-resolution current recording from cells and cell-free membrane patches. *Pflügers Arch Eur J Physiol*. 1981;391:85–100.

Heijman J, Algalarrondo V, Voigt N, Melka J, Wehrens XHT, Dobrev D, Nattel S. The value of basic research insights into atrial fibrillation mechanisms as a guide to therapeutic innovation: a critical analysis. *Cardiovasc Res*. 2016;109:467–479.

Heijman J, Dewenter M, El-Armouche A, Dobrev D. Function and regulation of serine/threonine phosphatases in the healthy and diseased heart. *J Mol Cell Cardiol*. 2013;64:90–8.

Heijman J, Voigt N, Dobrev D. New directions in antiarrhythmic drug therapy for atrial fibrillation. *Future Cardiol*. 2013;9:71–88.

Heijman J, Voigt N, Ghezelbash S, Schirmer I, Dobrev D. Calcium handling abnormalities as a target for atrial fibrillation therapeutics: how close to clinical implementation?. *J Cardiovasc Pharmacol.* 2015;66:515–522.

Heijman J, Voigt N, Nattel S, Dobrev D. Cellular and molecular electrophysiology of atrial fibrillation initiation, maintenance, and progression. *Circ Res*. 2014;114:1483–99.

Hodgkin AL, Huxley AF. Action potentials recorded from inside a nerve fibre. *Nature*. 1939;144:710–711.

Hodgkin AL, Huxley AF, Katz B. Measurement of current-voltage relations in the membrane of the giant axon of Loligo. *J Physiol*. 1952a;116:424–448.

Hodgkin AL, Huxley AF. Currents carried by sodium and potassium ions through the membrane of the giant axon of Loligo. *J Physiol*. 1952b;116:449–472.

Hodgkin AL, Huxley AF. The components of membrane counductance in the giant axon of Loligo. *J Physiol*. 1952c;116:473–496.

Hodgkin AL, Huxley AF. The dual effect of membrane potential on sodium conductance in the giant axon of Loligo. *J Physiol*. 1952d;116:497–506.

Hodgkin AL, Huxley AF. A quantitative description of membrane current and its application to conduction and excitation in nerve. *Bull Math Biol*. 1990;52:25–71.

Interpreting ECG. (n.d.). *The Biology Corner Web site.* Retrieved February, 2016, from https://www.biologycorner.com/anatomy/circulatory/ecg.html.

Issac TT, Dokainish H, Lakkis NM. Role of inflammation in initiation and perpetuation of atrial fibrillation. A systematic review of the published data. *J Am Coll Cardiol*. 2007;50:2021–2028.

Joshi KK, Tiru M, Chin T, Fox MT, Stefan MS. Postoperative atrial fibrillation in patients undergoing non-cardiac non-thoracic surgery: a practical approach for the hospitalist. *Hosp Pract (1995).* 2015;43:235–244.

Kannel WB, Wolf PA, Benjamin EJ, Levy D. Prevalence, incidence, prognosis, and predisposing conditions for atrial fibrillation: population-based estimates. *Am J Cardiol.* 1998;82:2N–9N.

Khan AP, Voigt N, Heijman J, Ravens U, Nattel S, Dobrev D. Cellular mechanisms underlying post-operative atrial fibrillation in patients. *Circulation*. 2016;134:A12646.

Kirchhof P, Benussi S, Kotecha D, Ahlsson A, Atar D, Casadei B, Castella M, Diener H-C, Heidbuchel H, Hendriks J, Hindricks G, Manolis AS, Oldgren J, Popescu BA, Schotten U, Van Putte B, Vardas P. 2016 ESC Guidelines for the management of atrial fibrillation developed in collaboration with EACTS. *Europace.* 2016;18:1609–1678.

Kornreich BG. The patch clamp technique: Principles and technical considerations. *J Vet Cardiol.* 2007;9:25–37.

Kubalová Z. Inactivation of L-type calcium channels in cardiomyocytes. Experimental and theoretical approaches. *Gen Physiol Biophys*. 2003;22:441–454.

Lopatin AN, Nichols CG. Inward rectifiers in the heart: an update on I_{K1}. *J Mol Cell Cardiol*. 2001;33:625–38.

Lu Z. Mechanism of rectification in inward-rectifier K^+ channels. *Annu Rev Physiol.* 2004;66:103–29.

Lüscher TF. Atrial fibrillation and stroke: risk factors, anticoagulation, and left atrial appendage occluders. *Eur Heart J*. 2016;37:2443–5.

Maesen B, Nijs J, Maessen J, Allessie M, Schotten U. Post-operative atrial fibrillation: a maze of mechanisms. *Europace.* 2012;14:159–74.

Mathew JP, Fontes ML, Tudor IC, Ramsay J, Duke P, Mazer CD, Barash PG, Hsu PH, Mangano DT. A multicenter risk index for atrial fibrillation after cardiac surgery. *JAMA*. 2004;291:1720–1729.

Min XP, Zhu TY, Han J, Li Y, Meng X. Left atrial appendage obliteration in atrial fibrillation patients undergoing bioprosthetic mitral valve replacement. *Herz*. 2015;7:1–7.

Mini Trans-Blot® Cell. (n.d.). *Bio-Rad Web site*. Retrieved February, 2016, from http://www.bio-rad.com/de-at/product/mini-trans-blot-cell.

Molina CE, Heijman J, Dobrev D. Differences in left versus right ventricular electrophysiological properties in cardiac dysfunction and arrhythmogenesis. *Arrhythmia Electrophysiol Rev*. 2016;5:14–19.

Naccarelli G V, Gonzalez MD. Atrial fibrillation and the expanding role of catheter ablation: do antiarrhythmic drugs have a future? *J Cardiovasc Pharmacol*. 2008;52:203–209.

Nattel S, Heijman J, Voigt N, Wehrens XHT, Dobrev D. The molecular pathophysiology of atrial fibrillation. *Cardiac Electrophysiology: From Cell to Bedside (Seventh Edition)*. 2016. PART VII.

Nattel S. Direct Effects of Activation and inhibition of the coagulation system on the atrial fibrillation substrate. *JACC Basic to Transl Sci*; 2016;1:340–343.

Nattel S. Preoperative atrial cardiomyocyte ionic currents and postoperative AF: important insights into what is not the mechanism. *J Cardiovasc Electrophysiol.* 2006;17:1239–1241.

Neher E, Sakmann B. Single-channel currents recorded from membrane of denervated frog muscle fibres. *Nature.* 1976;260:799–802.

Nishida K, Nattel S. Atrial fibrillation compendium: historical context and detailed translational perspective on an important clinical problem. *Circ Res.* 2014;114:1447–1452.

Ozawa M, Komatsu T, Sato Y, Kunugita F, Tachibana H, Tashiro A, Okabayashi H, Nakamura M. Comparison of the effects of bepridil and aprindine for the prevention of atrial fibrillation after cardiac and aortic surgery: A prospective randomized study. *J Arrhythmia*. 2015;31(5):302–306.

Pandit S V, Berenfeld O, Anumonwo JMB, Zaritski RM, Kneller J, Nattel S, Jalife J. Ionic determinants of functional reentry in a 2-D model of human atrial cells during simulated chronic atrial fibrillation. *Biophys J*. 2005;88:3806–3821.

Passini E, Genovesi S, Severi S. Human atrial cell models to analyse haemodialysis-related effects on cardiac electrophysiology: work in progress. *Comput Math Methods Med*. 2014;2014:1-18.

Prabhu SD. Cytokine-induced modulation of cardiac function. *Circ Res*. 2004;95:1140–1153.

Qu Z, Xie LH, Olcese R, Karagueuzian HS, Chen PS, Garfinkel A, Weiss JN. Early afterdepolarizations in cardiac myocytes: beyond reduced repolarization reserve. *Cardiovasc Res.* 2013;99(1):6–15.

Roden DM, Balser JR, George AL, Anderson ME. Cardiac ion channels. *Annu Rev Physiol.* 2002;64:431–375.

Schmidt C, Wiedmann F, Voigt N, Zhou X-B, Heijman J, Lang S, Albert Vi, Kallenberger S, Ruhparwar A, Szabó G, Kallenbach K, Karck M, Borggrefe M, Biliczki P, Ehrlich JR, Baczkó I, Lugenbiel P, Schweizer PA, Donner BC, Katus HA, Dobre, D, Thomas D. Upregulation of $K_{2P}3.1$ K^+ current causes action potential shortening in patients with chronic atrial fibrillation. *Circulation*. 2015;132:82–92.

Schotten U, Ausma J, Stellbrink C, Sabatschus I, Vogel M, Frechen D, Schoendube F, Hanrath P, Allessie MA. Cellular mechanisms of depressed atrial contractility in patients with chronic atrial fibrillation. *Circulation*. 2001;103:691–698.

Schotten U, Greiser M, Benke D, Buerkel K, Ehrenteidt B, Stellbrink C, Vazquez-Jimenez JF, Schoendube F, Hanrath P, Allessie M. Atrial fibrillation-induced atrial contractile dysfunction: a tachycardiomyopathy of a different sort. *Cardiovasc Res*. 2002;53:192–201.

Smyrnias I, Mair W, Harzheim D, Walker SA, Roderick HL, Bootman MD. Comparison of the T-tubule system in adult rat ventricular and atrial myocytes, and its role in excitation-contraction coupling and inotropic stimulation. *Cell Calcium.* 2010;47:210–223.

Sossalla S, Kallmeyer B, Wagner S, Mazur M, Maurer U, Toischer K, Schmitto JD, Seipelt Ralf, Schöndube FA, Hasenfuss G, Belardinelli L, Maier LS. Altered Na^+ currents in atrial fibrillation. Effects of ranolazine on arrhythmias and contractility in human atrial myocardium. *J Am Coll Cardiol*. 2010;55:2330–2342.

Takahashi A, Camacho P, Lechleiter JD, Herman B. Measurement of intracellular calcium. *Physiol. Rev*. 1999;79:1089–1125.

Takanari H, Nalos L, Stary-Weinzinger A, de Git KCG, Varkevisser R, Linder T, Houtman MJC, Peschar M, de Boer TP, Tidwell RR, Rook MB, Vos MA, van der Heyden MAG. Efficient and specific cardiac I_{K1} inhibition by a new pentamidine analogue. *Cardiovasc Res*. 2013;99:203–214.

Towbin H, Staehelin T, Gordon J. Electrophoretic transfer of proteins from polyacrylamide gels to nitrocellulose sheets: procedure and some applications. *Proc Natl Acad Sci U S A*. 1979;76:4350–4354.

Van Wagoner DR, Nerbonne JM. Molecular basis of electrical remodeling in atrial fibrillation. *J Mol Cell Cardiol*. 2000;32:1101–1107.

Van Wagoner DR, Pond AL, Lamorgese M, Rossie SS, McCarthy P atrick M, Nerbonne JM. Atrial L-type Ca^{2+} currents and human atrial fibrillation. *Circ Res*. 1999;85:428–436.

Van Wagoner DR, Pond AL, McCarthy PM, Trimmer JS, Nerbonne JM. Outward K^+ current densities and Kv1.5 expression are reduced in chronic human atrial fibrillation. *Circ Res*. 1997;80:772–781.

Varkevisser R, Houtman MJC, Linder T, de Git KCG, Beekman HDM, Tidwell RR, Ijzerman AP, Stary-Weinzinger A, Vos MA. Structure-activity relationships of pentamidine-affected ion channel trafficking and dofetilide mediated rescue. *Br J Pharmacol*. 2013;169:1322–1334.

Verdejo HE, Becerra E, Zalaquet R, Del Campo A, Garcia L, Troncoso R, Chiong M, Marin A, Castro PF, Lavandero S, Gabrielli L, Corbalán R. Atrial Function assessed by speckle tracking echocardiography is a good predictor of postoperative atrial fibrillation in elderly patients. *Echocardiography*. 2015;00:1–7.

Verkhratsky A, Krishtal OA, Petersen OH. From Galvani to patch clamp: the development of electrophysiology. *Pflugers Arch Eur J Physiol*. 2006;453:233–2347.

Voigt N, Dobrev D. Atrial-Selective Potassium Channel Blockers. *Card Electrophysiol Clin*. 2016;8:411–421.

Voigt N, Friedrich A, Bock M, Wettwer E, Christ T, Knaut M, Strasser RH, Ravens U, Dobrev D. Differential phosphorylation-dependent regulation of constitutively active and muscarinic receptor-activated $I_{K,ACh}$ channels in patients with chronic atrial fibrillation. *Cardiovasc Res.* 2007;74:426–437.

Voigt N, Heijman J, Wang Q, Chiang DY, Li N, Karck M, Wehrens XHT, Nattel S, Dobrev D. Cellular and molecular mechanisms of atrial arrhythmogenesis in patients with paroxysmal atrial fibrillation. *Circulation.* 2014;129:145–156.

Voigt N, Li N, Wang Q, Wang W, Trafford AW, Abu-Taha I, Sun Q, Wieland T, Ravens U, Nattel S, Wehrens XHT, Dobrev D. Enhanced sarcoplasmic reticulum Ca^{2+} leak and increased Na^{+}-Ca^{2+} exchanger function underlie delayed afterdepolarizations in patients with chronic atrial fibrillation. *Circulation.* 2012;125:2059–2070.

Voigt N, Pearman CM, Dobrev D, Dibb KM. Methods for isolating atrial cells from large mammals and humans. *J Mol Cell Cardiol*. 2015;86:187–198.

Voigt N, Trausch A, Knaut M, Matschke K, Varró A, Van Wagoner DR, Nattel S, Ravens U, Dobrev D. Left-to-right atrial inward rectifier potassium current gradients in patients with paroxysmal versus chronic atrial fibrillation. *Circ Arrhythm Electrophysiol.* 2010;3:472–480.

Voigt N, Zhou X-B, Dobrev D. Isolation of human atrial myocytes for simultaneous measurements of Ca^{2+} transients and membrane currents. *J Vis Exp*. 2013;77:e50235.

Walden AP, Dibb KM, Trafford AW. Differences in intracellular calcium homeostasis between atrial and ventricular myocytes. *J Mol Cell Cardiol*. 2009;46:463–473.

Wang SQ, Wei C, Zhao G, Brochet DXP, Shen J, Song LS, Wang W, Yang D, Cheng H. Imaging Microdomain Ca^{2+} in Muscle Cells. *Circ Res*. 2004;94:1011–1022.

Wettwer E, Christ T, Endig S, Rozmaritsa N, Matschke K, Lynch JJ, Pourrier M, Gibson JK, Fedida D, Knaut M, Ravens U. The new antiarrhythmic drug vernakalant: ex vivo study of human atrial tissue from sinus rhythm and chronic atrial fibrillation. *Cardiovasc Res*. 2013;98:145–154.

Wiechelman KJ, Braun RD, Fitzpatrick JD. Investigation of the bicinchoninic acid protein assay: identification of the groups responsible for color formation. *Anal Biochem.* 1988;175:231–237.

Wijffels MC, Kirchhof CJ, Dorland R, Allessie MA. Atrial fibrillation begets atrial fibrillation. A study in awake chronically instrumented goats. *Circulation.* 1995;92:1954–1968.

Wit AL, Boyden PA. Triggered activity and atrial fibrillation. *Hear Rhythm*. 2007;4:1–12.

Workman AJ, Kane KA, Rankin AC. The contribution of ionic currents to changes in refractoriness of human atrial myocytes associated with chronic atrial fibrillation. *Cardiovasc Res*. 2001;52:226–235.

Workman AJ, Pau D, Redpath CJ, Marshall GE, Russell JA, Kane KA, Norrie, J, Rankin, AC. Post-operative atrial fibrillation is influenced by beta-blocker therapy but not by pre-operative atrial cellular electrophysiology. *J Cardiovasc Electrophysiol*. 2006;17:1230–1238.

Zaman JAB, Harling L, Ashrafian H, Darzi A, Gooderham N, Athanasiou T, Peters NS. Post-operative atrial fibrillation is associated with a pre-existing structural and electrical substrate in human right atrial myocardium. *Int J Cardiol*. 2016;220:580–588.

8 Attachment

8.1 Publications and presentations

8.1.1 Original publication

1. Heckel T, Schmucki R, Berrera M, Ringshandl S, Badi S, Steiner G, Ravon M, Küng E, Kuhn B, Kratochwil N, Schmitt G, Kiialainen A, Nowaczyk C, **Khan AP**, Daff H, Lekolool I, Okoth E, Pelle R; Bishop R, Daubenberger C, Ebeling M, Certa U (2015) Functional analysis and transcriptional output of the Göttingen minipig genome. ***BMC Genomics***, 16:932. (*Impact factor 3.99*)

8.1.2 Published abstracts

1. Scientific Sessions of American Heart Associations. New Orleans, USA, 12-16.11.2016:
   Khan AP, Voigt N, Heijman J, Ravens U, Nattel S, Dobrev D (2016). Cellular mechanisms underlying post-operative atrial fibrillation in patients. ***Circulation,*** 134: A12646.

2. Scientific Sessions of the German Society for Pharmacology and Toxicology. Kiel, Germany, 10 – 12/03/2015:
   Khan AP, Voigt N, Herrlinger Y, Heijman J, Varkevisser R, Vos MA, van der Heyden MAG, Dobrev D (2015) The pentamidine analogue PA-6 selectively blocks inward rectifier potassium current I_{K1} in human atrial myocytes. ***Naunyn Schmiedebergs Arch Pharmacol,*** 388 (Suppl.1):18.

8.1.3 Congress presentations

1. Bayer Cardiovascular Research Workshop, Düsseldorf, Germany, 23-25.03.2017:
   Topic "Cellular mechanisms underlying post-operative atrial fibrillation in patients"

2. Annual retreat of the BIOME core "ischemia, reperfusion and angiogenesis", workshop in Xanthen (26.-28.11.15):
   Topic "The Pentamidine analogue PA-6, selectively blocks inward-rectifier potassium current I_{K1} in human atrial cardiomyocytes"

3. Annual Meeting of the European Working Group of Cardiac Cellular Electrophysiology.in Milan, Italy, 20 - 23.06.2015:
   Topic "The Pentamidine analogue PA-6, selectively blocks inward-rectifier potassium current I_{K1} in human atrial cardiomyocytes"

8.2 Acknowledgments

First and foremost, I want to thank my supervisor and mentor, Prof. Dr. Dobromir Dobrev for the opportunity to complete my PhD at the Institute of Pharmacology at the University Hospital in Essen. He consistently provided direction and motivation for me to try out new ideas, through which I have become a better scientist in the field of cardiovascular research. In addition, much appreciation goes to Prof. Dr. Niels Voigt for his great support in understanding the complex patch-clamp technique. Furthermore, I am very indebted to Ass. Prof. Dr. Jordi Heijman, for his continuous support and invaluable mentorship during my scientific adventure.

I am grateful to all my colleagues at the Institute of Pharmacology for their collaboration and support in both personal and professional capacities during my time at the institute. I would like to thank Monika Hagedorn for her work in cell isolation which was crucial for the completion of this scientific endeavor, as well as Barbara Langer for assisting in the process. Many thanks to Bettina Mausa for coaching me with the Western blot technique and particularly Simone Olesch and Ramona Nagel for their technical support in the Western blot data for this work. I would also like to sincerely thank Iris Weinbach for pertinent informative updates and especially Marina Schäfer for her general support in this work.

Furthermore, many thanks to the cardiac surgery team from Huttrop Heart Center for their collaboration in tissue procurement.

Finally, I would like to thank my family and friends for all their love, support and encouragement either in being present, or through calls and prayers. Thank you Ophilia for much laughter in my difficult times. Thank you Ngewi and my most valuable friends, especially Kai B for your relentless moral support and warmth. Thank you so much dad for finding smart ways to keep me on track. To you mum (RIP), thank you for grooming me in so much love, kindness and modesty. I truly remain your pride. Most of all, I thank my partner, Shu Fon for lovingly putting up with me during this time, making it all seem effortless and for patiently enduring when I speak only of ion channels ☺. Thank you for your unshakable confidence in my success.

8.3 Curriculum Vitae

"The biography is not included in the online version for reasons of data protection".

Erklärung:

Hiermit erkläre ich, gem. § 7 Abs. (2) d) + f) der Promotionsordnung der Fakultät für Biologie zur Erlangung des Dr. rer. nat., dass ich die vorliegende Dissertation selbständig verfasst und mich keiner anderen als der angegebenen Hilfsmittel bedient, bei der Abfassung der Dissertation nur die angegeben Hilfsmittel benutzt und alle wörtlich oder inhaltlich übernommenen Stellen als solche gekennzeichnet habe.

Essen, den 26.09.2017 Azinwi Phina Muna geb. Khan

Erklärung:

Hiermit erkläre ich, gem. § 7 Abs. (2) e) + g) der Promotionsordnung der Fakultät für Biologie zur Erlangung des Dr. rer. nat., dass ich keine anderen Promotionen bzw. Promotionsversuche in der Vergangenheit durchgeführt habe und dass diese Arbeit von keiner anderen Fakultät/Fachbereich abgelehnt worden ist.

Essen, den 26.09.2017 Azinwi Phina Muna geb. Khan

Erklärung:

Hiermit erkläre ich, gem. § 6 Abs. (2) g) der Promotionsordnung der Fakultät für Biologie zur Erlangung der Dr. rer. nat., dass ich das Arbeitsgebiet, dem das Thema „Alterations of cellular electrophysiology and Ca^{2+}-handling in patients with different forms of atrial fibrillation“ zuzuordnen ist, in Forschung und Lehre vertrete und den Antrag von Azinwi Phina Khan befürworte und die Betreuung auch im Falle eines Weggangs, wenn nicht wichtige Gründe dem entgegenstehen, weiterführen werde.

Essen, den 26.09.2017 Prof. Dr. Dobromir Dobrev